THESIS FOR THE DEGREE OF DOCTOR OF PHILOSOPHY

# Analysis of the Fatigue Characteristics of Mooring Lines and Power Cables for Floating Wave Energy Converters

SHUN-HAN YANG


Department of Mechanics and Maritime Sciences
CHALMERS UNIVERSITY OF TECHNOLOGY
Gothenburg, Sweden 2018

**Analysis of the Fatigue Characteristics of Mooring Lines and Power Cables for Floating Wave Energy Converters**

SHUN-HAN YANG

ISBN 978-91-7597-773-7



Doktorsavhandlingar vid Chalmers tekniska högskola
Ny serie nr 4454
ISSN 0346-718X

Department of Mechanics and Maritime Sciences
Division of Marine Technology
Chalmers University of Technology
SE-412 96, Gothenburg
Sweden
Telephone: + 46 (0)31-772 1000

Printed by Chalmers Reproservice
Gothenburg, Sweden 2018

**Analysis of the Fatigue Characteristics of Mooring Lines and Power Cables for Floating Wave Energy Converters**

SHUN-HAN YANG
Department of Mechanics and Maritime Sciences
Division of Marine Technology

# Abstract

To reduce greenhouse gas emissions and expand the energy mix, there is a pressing need for the exploitation of renewable sources of energy, such as biomass, hydropower, solar power, waves, and wind. This thesis focuses on ocean wave energy and its applications. Ocean wave energy is abundant and geographically widespread and has one of the highest energy densities among renewable energy sources, presenting a great opportunity for securing an emission-free energy supply. However, one challenge associated with existing wave energy technology is to ensure and verify the reliability and long-term performance of wave energy converter (WEC) systems; these aspects are fundamental to achieving wave energy at a cost that is commercially competitive in the long term.

The main objective of this thesis was to develop a complete numerical analysis procedure for assessing the fatigue characteristics of the mooring lines and power cables used in floating WEC systems. Both the moorings and cables must be designed to survive under cyclic loading and not fail due to fatigue, which would endanger the safety and functionality of the WEC system. However, due to the wide variety of WEC concepts that have been proposed, it remains challenging to identify which numerical methods are most appropriate for the reliable prediction of the mechanical service life of the moorings and cables. Starting from a hydrodynamic and structural response analysis of a WEC system or an array of WECs, the research presented herein contributes to a systems perspective in which the fatigue performance of moorings and cables is predicted, the power performance is estimated, and the levelised cost of energy is calculated with consideration of the interaction effects among WECs in an array.

It was found that a coupled analysis approach should be used to simulate the hydrodynamic and structural responses of WECs because it captures best the mechanical coupling and hydrodynamic interaction effects of WEC systems. A wave-height/wave-period matrix of fatigue was designed as a visualisation tool to illustrate the influence of environmental loads on fatigue damage accumulation in the moorings and cables. Numerical simulations of multi-WEC array farms showed that hydrodynamic interactions among WECs in an array farm strongly affect fatigue damage in moorings, which in turn influence the related cost assessment of a WEC system. Compared with a biofouling-free condition, it was shown that the presence of biofouling on the WEC system not only reduces the power absorption of WECs but also decreases the fatigue life of the moorings and cables. The results obtained from the numerical simulation were validated against a model-scale ocean basin laboratory experiment and compared with measurement data from a full-scale WEC installation. The findings showed that the simulation model can satisfactorily predict the dynamic motion response of a WEC system under moderate sea state conditions and under non-resonant conditions.

**Keywords:** computational modelling, coupled analysis, experiment, fatigue, heaving point absorber, marine biofouling effect on fatigue, mooring line, power absorption, power cable, wave energy converter.

# Preface

This thesis comprises work conducted between 2013 and 2017 in the Department of Shipping and Marine Technology and between 2017 and 2018 in the Department of Mechanics and Maritime Sciences at Chalmers University of Technology in Gothenburg, Sweden. The research was performed as part of three projects funded by the Swedish Energy Agency: "Ocean Energy Centre – Durability analysis of cables and moorings used in systems for harvesting renewable ocean energy", under contract No. 36357-1 between 2013 and 2015; "R&D of dynamic low voltage cables between the buoy and floating hub in a marine energy system", under contract No. 41240-1 between 2015 and 2018; and "Simulation model for operation and maintenance strategy of floating wave energy converters – analysis of fatigue, wear, and influence of biofouling for effective and profitable energy harvesting", under contract No. 36357-2 between 2016 and 2018.

First and foremost, I would like to express my sincere gratitude to my supervisor Professor Jonas Ringsberg and my co-supervisor Adjunct Professor Erland Johnson. Thank you for your outstanding guidance, dedicated support, infectious enthusiasm, and warm-hearted care. There are, of course, so many more ways in which you have helped me on the path, although I am not able to list them all here. I have had so much fun and have enjoyed a fruitful journey throughout my PhD career because of you—thank you. Huge thanks also go to Professor Lars Bergdahl. He spent countless hours with me, and his broad and deep knowledge have enabled me to develop as a researcher in various ways. I would like to further extend my appreciation to Dr. Zhiqiang Hu at Newcastle University for his valuable advice and discussions, which pushed me to have a critical eye towards my own work.

This thesis would also not have been possible without the kind support from many others. I would like to express my gratitude to the companies Waves4Power and NKT Cables, the RISE Research Institutes of Sweden, and Shanghai Jiao Tong University for providing me with an inspiring and supportive environment in which to explore my research topic. In no particular order, grateful acknowledgements are due to Mr. Ulf Lindelöf, Dr. Filip Alm, Dr. Magnus Rahm, and Mr. Lennart Claesson at Waves4Power for providing opportunities and sharing valuable insight based on their industrial experience; Mr. Ingvar Hagman at NKT Cables for sharing unique domain knowledge; Mr. Pierre Ingmarsson and Ass. Prof. Pär Johannesson at RISE for providing ideas and fruitful discussions; Dr. Göran Johansson, formerly of GVA-Consultants in Gothenburg, for advice on developing the numerical model; the research team at the Deepwater Offshore Basin at Shanghai Jiao Tong University for the tremendous support in performing the ocean basin laboratory test; and Dr. Helge Skåtun, Dr. J.K. Heo, and Mr. Chris Kubes for their assistance in exploring the DNV GL SESAM package. Regarding the development of my research, I would also like to express my gratitude to Associate Professor Claes Eskilsson at Aalborg University, Professor Carl-Erik Janson, Associate Professor Wengang Mao, Associate Professor Lena Granghag, Dr. Johannes Palm, Dr. Luis Felipe Sánchez-Heres, and Lic. Eng. Dinis Soares Reis de Oliveira at Chalmers University of Technology. Your advice and insight into various subjects helped me perform my research with a firm foundation. Special acknowledgement must be given to Dr. Duan Fei. Thank you for all the time, help, support, and valuable contributions you provided in the ocean basin experiment presented in this thesis.

I am also very grateful for the wonderful working environment and colleagues of the department. It is amazing going to work every day and always finding an inspiring and joyful environment. Among my colleagues, I particularly want to mention Per Hogström, Anna Hedén, Johan Cimbritz, Selma Brynolf, Henrik Pahlm, Lotta Sjögren, Carl Sjöberger, Ulrik

Larsen, Jan Skoog, Mats Isaksson, Artjoms Kuznecovs, and Xiao Lang. Thank you for helping me realise that I did not come to Chalmers just to do a PhD but also to develop and enjoy the professional part of my life.

Special thanks go to Nicole, Francesco, Josefin, Vanesa, Huong, Ting-Hua, Hiba, Sara, and Olga. I met all of you through Chalmers, but you have done so much more for me than I can imagine from a colleague. You have lit up my life in Sweden and have made Sweden feel like my second home.

I would also like to thank Professor Ya-Jung Lee at National Taiwan University and the big family at the Structure Lab in Taiwan. You have sparked my dream of doing research and continuously encouraged me to stick to my current research path. Thank you.

I deeply thank Diana for being my friend in all stages of my life. You have always made yourself available to me and reminded me that there is also an important part of life outside of work. You also deserve special thanks from me for being the chief designer of all my artwork throughout the years.

I wish to thank my fiancé Jeff for his company and for cheering up throughout the years. Thank you for always being there to listen, to support, and to keep life enjoyable. For all the laughs, all the love, and all the "what-to-do", I cannot thank you enough.

Finally, I would like to dedicate this thesis to my parents and my brother. Without your everlasting love and support, I would undoubtedly not be where I am today.

Gothenburg, July 2018
Shun-Han Yang

# Contents

# List of appended papers

For each of the five appended papers, the author of this thesis contributed to the ideas presented, planned the paper with the co-authors, performed the numerical simulations, and wrote the majority of the manuscript. For Paper IV, the author was also responsible for the design of the experiment and performed the experiment with assistance from the research team at Shanghai Jiao Tong University.

**Paper I** Yang, S.-H., Ringsberg, J. W., Johnson, E., Hu, Z., & Palm, J. (2016) A comparison of coupled and de-coupled simulation procedures for the fatigue analysis of wave energy converter mooring lines. Ocean Engineering 117, 332-345. doi:10.1016/j.oceaneng.2016.03.018.

**Paper II** Yang, S.-H., Ringsberg, J. W., & Johnson, E. (2018) Parametric study of the dynamic motions and mechanical characteristics of power cables for wave energy converters. Journal of Marine Science and Technology 23 (1), 10-29. doi:10.1007/s00773-017-0451-0.

**Paper III** Yang, S.-H., Ringsberg, J. W., Johnson, E., & Hu, Z. (2017) Biofouling on mooring lines and power cables used in wave energy converter systems—Analysis of fatigue life and energy performance. Applied Ocean Research 65, 166-177. doi:10.1016/j.apor.2017.04.002.

**Paper IV** Yang, S.-H., Ringsberg, J. W., Johnson, E., Hu, Z., Bergdahl, L., & Duan, F. (2018) Experimental and numerical investigation of a taut-moored wave energy converter: A validation of simulated buoy motions. Proceedings of the Institution of Mechanical Engineers, Part M: Journal of Engineering for the Maritime Environment 232 (1), 97-115. doi:10.1177/1475090217735954.

**Paper V** Yang, S.-H., Ringsberg, J. W., & Johnson, E. (2018) Wave energy converters in array configurations—Influence of interaction effects on the power performance and fatigue of mooring lines. (Submitted to *Renewable Energy.*)

# List of other published papers by the author

For Papers A to C listed below, the author of this thesis contributed to the ideas presented, planned the paper with the co-authors, performed the numerical simulations, and wrote the majority of the manuscript. For Paper D, the author of this thesis contributed to the ideas presented, the numerical simulations and the writing of the manuscript.

**Paper A** Yang, S.-H., Ringsberg, J. W., & Johnson, E. (2014) Analysis of mooring lines for wave energy converters – A comparison of de-coupled and coupled simulation procedures. In: *Proceedings of the ASME 2014 33rd International Conference on Ocean, Offshore and Arctic Engineering (OMAE2014), 8-13 June 2014, San Francisco, California, USA.* New York, NY, American Society of Mechanical Engineers. OMAE2014-23377, 11 pp. (Presenting author.)

**Paper B** Yang, S.-H., Ringsberg, J. W., & Johnson, E. (2015) Parametric study of the mechanical characteristics of power cable under dynamic motions. In: *Proceedings of the 11th European Wave and Tidal Energy Conference (EWTEC2015), 6-11 September 2015, Nantes, France.* pp. 09D5-5-1–09D5-5-11. (Presenting author.)

**Paper C** Yang, S.-H., Ringsberg, J. W., & Johnson, E. (2016) The influence of biofouling on power capture and the fatigue life of mooring lines and power cables used in wave energy converters. In: Guedes Soares, C. (ed.) *Progress in Renewable Energies Offshore—Proceedings of the 2nd International Conference on Renewable Energies Offshore (RENEW2016), 24-26 October 2016, Lisbon, Portugal.* London, Taylor & Francis Group. pp. 711-721. (Presenting author.)

**Paper D** Ringsberg, J. W., Jansson, H., Örgård, M., Yang, S.-H., & Johnson, E. (2018) Comparison of mooring solutions and array systems for point absorbing wave energy devices. In: *Proceedings of the ASME 2018 37th International Conference on Ocean, Offshore and Arctic Engineering (OMAE2018), 17-22 June 2018, Madrid, Spain.* New York, NY, American Society of Mechanical Engineers. OMAE2018-77062, 11 pp.

# Symbol and abbreviations

*Latin notations*

| | |
|---|---|
| $B_{\mathrm{PTO}}$ | PTO damping in the heave DoF of the WEC [Ns/m]. |
| $Dir_{\mathrm{curr}}$ | Direction of the incoming current [deg], defined as the angle of incidence relative to the *x*-axis of the coordinate system. |
| $Dir_{\mathrm{load}}$ | Direction of incoming loads [deg], defined as the angle of incidence relative to the *x*-axis of the coordinate system. The symbol is used when the loads of waves, winds, and current are all heading in the same direction. Otherwise, the incidences of the three loads are defined by $Dir_{\mathrm{curr}}$, $Dir_{\mathrm{wave}}$, and $Dir_{\mathrm{wave}}$. |
| $Dir_{\mathrm{wave}}$ | Direction of the incoming wave [deg], defined as the angle of incidence relative to the *x*-axis of the coordinate system. |
| $Dir_{\mathrm{wind}}$ | Direction of the incoming wind [deg], defined as the angle of incidence relative to the *x*-axis of the coordinate system. |
| $FD_{\mathrm{Cable}}$ | Accumulated fatigue damage of the power cable [-]. |
| $FD_{\mathrm{Moor}}$ | Accumulated fatigue damage of the mooring line [-]. |
| $H_{m_0}$ | Significant trough to crest response estimate from the response spectrum, also referred to in the text as significant motion or significant response. The value is calculated as $4\sqrt{m_0}$. |
| $H_{\mathrm{s}}$ | Significant wave height [m]. |
| $H_{\mathrm{w}}$ | Regular wave height [m]. |
| $I_{\mathrm{F}}$ | Interaction factor of fatigue damage [-]. The value indicates the ratio of fatigue damage of moorings with and without the hydrodynamic interaction effect. |
| $I_{\mathrm{P}}$ | Interaction factor of power absorption [-]. The value indicates the ratio of WEC's power absorption with and without the hydrodynamic interaction effect. |
| $m_0$ | Variance of a spectrum or zeroth moment of the spectrum. |
| $N_{\mathrm{A}}$ | Axial force [N]. |
| $P$ | Time-averaged power absorption of the WEC [W]. |
| $s_{\mathrm{Cable}}$ | Curvilinear coordinate system of the power cable [m]. The $s_{\mathrm{Cable}}$ coordinate runs along the length of the power cable, with a value of 0 at the connection point to the WEC (i.e., fairlead at the WEC) and a maximum value at the connection point to the hub (i.e., fairlead at the hub). |
| $s_{\mathrm{Moor}}$ | Curvilinear coordinate system of the mooring leg [m]. The $s_{\mathrm{Moor}}$ coordinate runs along the length of the mooring line, with a value of 0 at the connection point to the WEC (i.e., fairlead) and a maximum value at the connect point to the seabed (i.e., anchor point). |
| $t$ | Time [s]. |
| $T_{\mathrm{p}}$ | Peak wave period [s]. |
| $T_{\mathrm{w}}$ | Regular wave period [s]. |

*Latin notations* (*continued*)

| | |
|---|---|
| $T_z$ | Zero-up-crossing wave period [s]. |
| $V_{curr}$ | Current velocity [m/s]. |
| $V_{wind}$ | Wind velocity [m/s]. |
| $(x, y, z)$ | Position in Cartesian coordinate system [m]. |
| $x, y, z, xx, yy, zz$ | Modes of motion in six DoFs, consisting of surge [m], sway [m], heave [m], roll [deg], pitch [deg], and yaw [deg]. |

*Greek notations*

| | |
|---|---|
| $\gamma$ | Non-dimensional peak enhancement factor of JONSWAP spectrum [-]. |
| $\eta$ | Capture width ratio [-]. |
| $\eta_{Availability}$ | Non-dimensional coefficient for the availability [-], defined as the fraction of time that a particular operational site is available. |
| $\eta_{Transmission}$ | Non-dimensional coefficient for transmission efficiency [-]. The value represents the transmission efficiency of the energy generated by each WEC to the final electricity output to the end user. |
| $\sigma_A$ | Axial stress [Pa]. |
| $\sigma_{yc}, \sigma_{zc}$ | Bending stress [Pa]. |
| $\sigma_s$ | Total stress [Pa]. |
| $\omega$ | Angular frequency [rad/s]. |

*Abbreviations*

| | |
|---|---|
| AEP | Annual energy production. |
| CapEx | Capital expenditure. |
| CDF | Cumulative distribution function. |
| CoB | Centre of buoyancy. |
| CoG | Centre of gravity. |
| DoF | Degree of freedom. |
| FE | Finite element. |
| FLS | Fatigue limit state. |
| JONSWAP | Joint North Sea Wave Project |
| LCC | Life cycle cost. |
| LCoE | Levelised cost of energy. |
| NPD | Norwegian Petroleum Directorate |
| PTO | Power take-off. |
| RAO | Response amplitude operator. |
| R-N | Relative tension - number of cycles to failure. |
| S-N | Stress - number of cycles to failure. |
| WEC | Wave energy converter. |

# 1 Introduction

This chapter presents the research background and motivation for the thesis, followed by the objectives of the work and an outline of the thesis.

## 1.1 Background and motivation

Between 1971 and 2015, global energy consumption more than doubled from 61,900 TWh to 160,000 TWh (EIA, 2017; IEA, 2017a). Albeit at a decreasing pace, the projected global energy demand is expected to increase by another 30% before 2040 due to growth in the global economy and population (IEA, 2017b). Part of the total energy is consumed as electricity. Figure 1 presents the distribution of global electricity production by various energy alternatives in 2016. At that time, electricity production from renewable energy sources represented approximately 25% of the total electricity production.

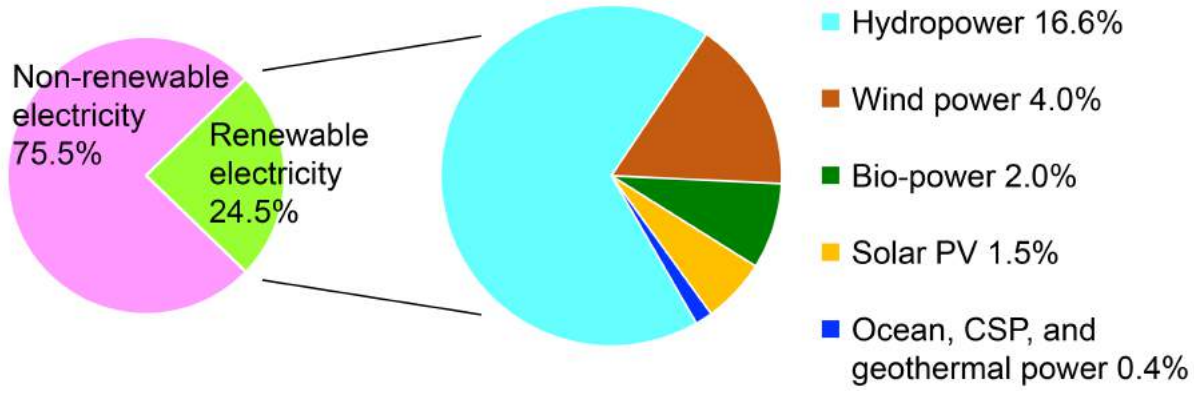


**Figure 1.** Estimated renewable energy share of global electricity production at the end of 2016; data extracted from REN21 (2017).

As part of the worldwide Sustainable Development Goals (UN, 2018), there is a goal to increase the share of renewable energy production by extending utilisation from all possible sources, such as bio-power, hydropower, solar power, wave power, and wind power. The work presented in this thesis relates to the wave energy resource and aims to contribute to enhancing the harnessing of wave energy from the oceans.

Figure 1 shows that the electricity production from wave energy in 2016 was modest (in the 0.4% group) compared with the total electricity production. According to IRENA (2017), the installed wave power generation capacity at the end of 2016 was less than 600 MW; by comparison, the installed generation power capacity from all renewable alternatives was 2.0 TW. Among the renewable energy sources, alternatives that allow for on-shore energy production have increased significantly over the past decades, while offshore installations such as those harnessing offshore wind, wave energy, and tidal energy are now progressing (IRENA, 2018). Increased knowledge on how to design technology and how to operate and maintain offshore installations has resulted in new opportunities and confidence in utilising offshore renewable energy sources.

Wave energy holds great potential for contributing to the global energy demand and reducing the need for energy production from non-renewable energy resources. Estimates suggest that the energy content in the oceans may be as large as 30,000 TWh/year (Lewis et al., 2011). By comparison, the annual electricity generation in the 28 countries composing the European Union is 3,000 TWh (Eurostat, 2018). The European Commission has therefore committed to supporting the research and development of wave energy technologies to enable full-scale implementation as soon as possible. The Ocean Energy Forum has outlined a road map that targets an installed power capacity of 100 GW from wave and tidal energy in Europe by 2050 (Ocean Energy Forum, 2016); this figure corresponds to approximately 10% of electricity demand projected for Europe by that time, or the daily electricity needs of 76 million households (EC, 2016; Ocean Energy Europe, 2018). In considering all these estimates and expectations, note that substantial wave energy is available in the oceans, but not all sites and areas are appropriate for installation due to, e.g., challenges in operability, maintenance, installation (such as water depth), and marine spatial planning, including shipping routes. Thus, the potential is greater than the amount of energy that is actually accessible with current knowledge and technology (Sims et al., 2007).

Harnessing wave energy requires a wave energy converter (WEC), or a device that converts wave power to electricity. A WEC typically consists of several sub-components, including (1) a main structure that captures the mechanical energy in waves, (2) foundation or mooring systems that keep the main structure in place, (3) a power take-off (PTO) system through which the mechanical energy of the main structure is converted to electrical energy, and (4) control systems to safeguard and optimise the performance of the WEC system (Falcão, 2010; Kempener & Neumann, 2014). State-of-the-art reviews on wave energy technology have been provided by Falcão (2010) and IEA-OES (2018) for an overall technology review and categorisation of WECs; Wang et al. (2018) for control strategies; and Fraunhofer & ECORYS (2017) and SI Ocean (2012) for the development path of the entire wave energy sector.

To increase the utilisation of marine renewable energy, international authorities have joined forces with industry, research institutes, and stakeholders to identify the challenges that have inhibited the development and deployment of wave energy; see, e.g., reports by Callaghan & Boud (2006), Fraunhofer & ECORYS (2017), MacGillivray et al. (2013), and Mofor et al. (2014). Multiple challenges related to technology, economics, environmental and social issues, and grid infrastructure have been identified. One of the challenges highlighted in these investigations has been how to ensure and verify the reliability and long-term performance of a WEC system, which are fundamental aspects of achieving a wave energy cost that is commercially competitive in the long term.

This thesis contributes to the design of reliable and safe WEC systems. The work emphasises the fatigue limit state (FLS) design of mooring lines and power cables for floating point-absorbing WECs. This type of WEC is suitable for large-scale offshore installations called wave farms, where WEC systems are clustered in arrays, forming a farm. The mooring system and the power cables are examples of components that must have high reliability in a WEC system. The moorings must be designed to survive a large number of cyclic loads and not fail due to fatigue, which would endanger the safety of the WEC, other nearby objects and the functionality of the system. The power cables also undergo a large number of load cycles and should never be allowed to fail due to fatigue. If failure were to occur, the functionality, i.e., energy production, would be interrupted. From a systems perspective, the moorings and power cables face the same challenge: reliable fatigue design and the question of how such a design should be achieved for various floating point-absorbing WEC system concepts.

Mooring lines and power cables have been developed over years in many other offshore structures (Isaacson & Nwogu, 1987; Worzyk, 2009). Both of these components are flexible and slender structures attached to the main floating structures. However, these two components for WECs entail multiple key differences from those used in general offshore applications. First, the WEC is typically designed to be in resonance with the dominating wave frequency in high-energy areas to maximise energy harvesting. Johanning et al. (2006) and Thies et al. (2012) recommended that the designs of moorings and cables for WECs should take into account these dynamic motions. Second, as observed in several studies (Casaubieilh et al., 2014; Fitzgerald & Bergdahl, 2007, 2008; Paredes et al., 2016), mooring configurations can affect WECs' dynamic motion and power performance and, consequently, the loads the moorings must withstand. Paredes et al. (2013) therefore concluded that the analysis of moorings should be coupled with that of the entire WEC system to properly assess PTO performance and structural responses with regard to their reliability and survivability. Third, because WECs are typically installed in relatively shallow water at depths of tens to hundreds of metres (Kempener & Neumann, 2014), the effects of currents, tides, and waves can be of greater significance than for other offshore floating structures, as observed by Harnois (2014).

In 2011, a national survey was conducted among several Swedish wave energy companies to identify obstacles limiting the commercial impact of their wave energy technologies. Two major obstacles were identified: (i) insufficient mechanical service life of mooring lines and power cables compared with the target service life of the WEC device itself and (ii) lack of an established methodology for making reliable predictions of the mechanical service life of the components used in WEC systems. The results of this survey were aligned with those reported in the aforementioned literature, serving as a motivation for the current thesis project, which began in 2013.

## 1.2 Objective

Because of the possibility of investigating a large number of variants at relatively low cost, numerical analyses and modelling have been widely adopted to assist in the development of ships and offshore structures. Without exception, the development of wave energy technology relies heavily on numerical analyses and modelling. However, due to the wide variety of WEC concepts that have been proposed, identifying which numerical models are most appropriate for a particular WEC concept and what method should be used to achieve a particular analysis objective (e.g., for analysing fluid-structure interaction, structure responses, or WEC control) remains challenging. This challenge motivated an important contribution from Folley (2016), who reviewed state-of-the-art techniques for numerical modelling and analyses of single WEC devices and those in arrays. The numerical modelling of mooring lines and power cables was beyond the scope of the book by Folley. Shortly after, a review dedicated to the numerical modelling of mooring systems for WECs was presented by Davidson & Ringwood (2017). Despite thorough and extensive reviews and comparisons of all available modelling techniques, both reviews concluded that there exists no best-suited numerical analysis or modelling method; rather, determining the most suitable one depends on an ideal balance between the characteristics of the WEC concept, the analysis objectives, computational cost, and accuracy requirements. Davidson & Ringwood (2017) also concluded that fatigue and extreme load analysis require the highest fidelity numerical models of moorings to capture the dynamic tensions throughout the mooring lines.

The main objective of the work presented in this thesis was to develop a complete numerical analysis procedure for the mooring lines and power cables used in WEC systems. Such an

analysis should address the fatigue life assessments of the moorings and cables while providing high-level assessments of the overall performance of the WEC system, such as its power performance. From the motions, hydrodynamics, and structural responses of a simulated WEC system or an array of WECs, the research presented herein contributes to a systems perspective from which the fatigue performance of moorings and cables is predicted, the power performance is estimated, and the levelised cost of energy (LCoE) is calculated with consideration of the interaction effects between WECs in an array.

The main objective was divided into seven sub-goals and main activities that together ensured that the main objective was fulfilled, including both academic and industrial contributions to the research field. The tasks were as follows:

G1. Compare different simulation procedures, leading to a recommendation for the study of the behaviour of WEC systems with regard to the initial fatigue design assessment of WEC mooring lines and power cables.
G2. Through a parametric study, investigate the sensitivity of the predicted service life of the mooring lines and power cables with regard to the environmental and design parameters. Moreover, identify the values or ranges of the environmental and design parameters that are beneficial for long (fatigue) service lives of the mooring lines and power cables and for optimal power performance.
G3. Investigate the potential impact of biofouling on a WEC system, primarily with regard to the power performance of the WEC and the fatigue life of the moorings and cables.
G4. Validate the proposed simulation procedure and model against ocean basin laboratory tests.
G5. Adapt the validated simulation procedure and model to a full-scale WEC installation and demonstrate its prediction capability against full-scale measurement results of WEC motion and mooring force responses.
G6. Quantify how large an influence the hydrodynamic interaction between WECs in an array system has on the fatigue life of their moorings and the power performance of each WEC unit.
G7. Demonstrate, through LCoE calculations, whether hydrodynamic interaction must be considered in a systems analysis and cost estimation of a full WEC system and wave farm.

## 1.3 Outline of the thesis

This thesis comprises a summary of research conducted in five appended papers. Chapter 2 describes the methodology proposed, assumptions and delimitations. The motivation and theoretical background pertaining to the different methods used in the numerical analysis procedure are elaborated in Chapter 3. A description of two experimental studies is then provided in Chapter 4. Selected important results and findings are presented in Chapter 5. The main conclusions, contributions, and novel aspects of the thesis are presented in Chapter 6. Recommendations for future work are presented in Chapter 7, and references are listed in Chapter 8.

# 2 Methodology

This chapter presents the methodology proposed in this thesis. Section 2.1 introduces the methods and analyses used in the thesis. The methods and analyses together constitute the methodology, whose overall framework is discussed in Section 2.2. Finally, the delimitations of the thesis are clarified in Section 2.3.

## 2.1 Methods and analyses

Two types of methods were used throughout the thesis to achieve the main objective:

- Numerical methods
- Experimental methods

Numerical methods were used to analyse various aspects of WEC systems. In this thesis, numerical methods are further divided into sub-categories depending on the goals of analysis:

1. Hydrodynamic analysis
2. Structural response analysis
3. Stress and fatigue analysis
4. Power absorption analysis
5. LCoE analysis
6. Parameter sensitivity analysis

Hydrodynamic and structural response analyses (analyses 1 and 2) were performed for the entire WEC system, including all sub-components and with either one WEC or multiple WECs. Together, hydrodynamic and structural response analyses were used to assess fluid-structure interactions and structure-structure couplings and predict the motions of all system components and the force responses in the moorings and cables under various environmental conditions. The force responses of moorings and cables served as an input to the stress and fatigue analyses, through which the fatigue damage and the corresponding fatigue life of the structures could be estimated (analysis 3). The motion responses of the WEC were further used to assess the power performance of the system. In this thesis, the WEC power performance was evaluated as the power absorption of the PTO system in the power absorption analysis (analysis 4).

The assessment of the overall feasibility of a WEC system can be performed by estimating the LCoE; see examples of such assessments in IEA-OES (2015). In this thesis, LCoE analysis (analysis 5) was not used to assess the exact economic performance of the WEC system but rather to demonstrate the extent to which the fatigue damage of the moorings and cables (obtained from analysis 3) and the power performance of the WEC system (obtained from analysis 4) influence the cost estimation of the entire system.

Numerical analyses 1 – 5 include uncertainties in data and models due to, e.g., uncertainties in the material and mechanical properties of moorings and cables, the random nature of the environmental loads and factors, and the inherent limitations of the numerical model and simulation software. These uncertainties were investigated by parameter sensitivity analyses (analysis 6), in which key parameters were identified, and parametric analyses were performed to quantify the sensitivity of the WEC's dynamics and structural fatigue performance to these parameters.

The experimental method was used primarily to study the hydrodynamic and structural response of the WEC system, i.e., analyses 1 and 2, which were also developed numerically. Experiments were performed at two scales for different purposes: validation of the numerical model and demonstration of the predictive capability of the numerical analysis. An ocean basin laboratory experiment of a model-scale WEC system was carried out to assess the accuracy and suitability of the hydrodynamic and structural responses analyses for validation. In addition, by comparing measurement data gathered from a full-scale WEC installation, the predictive capability of the hydrodynamic and structural response analyses was demonstrated.

An overview of the relationships between the different methods and analyses presented above is shown in Figure 2.

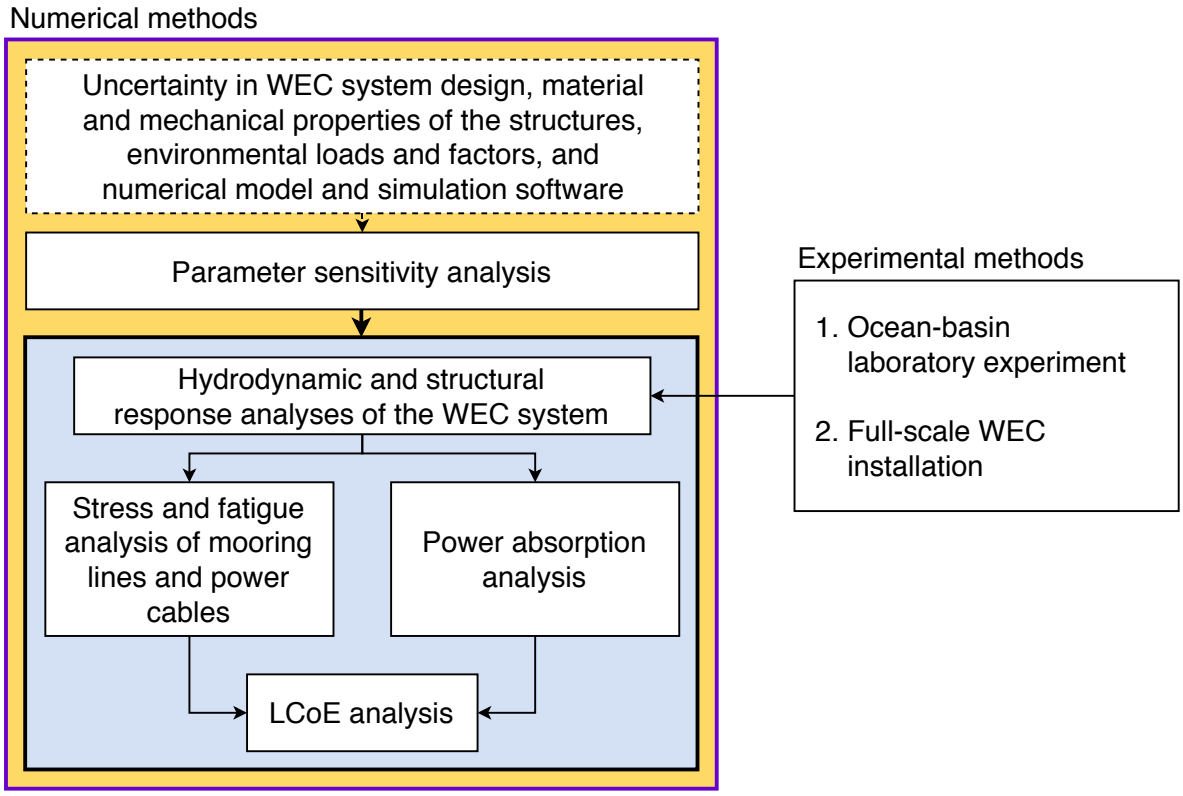


**Figure 2.** Relationships of different methods used to achieve the main objective of the thesis.

## 2.2 Framework

The combination of the methods and analyses presented in the previous section into a unified scheme constitutes the methodology proposed in this thesis for assessing the fatigue characteristics of moorings and cables and, by extension, the LCoE of WEC systems. Figure 3 presents the quantities and data flow directions that motivate the use of these various methods and analyses. The system performance, including the mechanical life, is controlled by the mutual interplay between environmental loading and several factors within a WEC system. The two rounded boxes in Figure 3 show the key aspects pertaining to the strength and loading configuration that affect the mechanical service lives of the moorings and cables. In this thesis, a systems perspective of the WEC was emphasised. Hence, the mechanical lives of the

components (in terms of fatigue) were always evaluated within a larger context in which the WEC, PTO system, and array configuration were also included. The overall WEC system response was evaluated by performing analyses 1 and 2, as presented in Section 2.1.

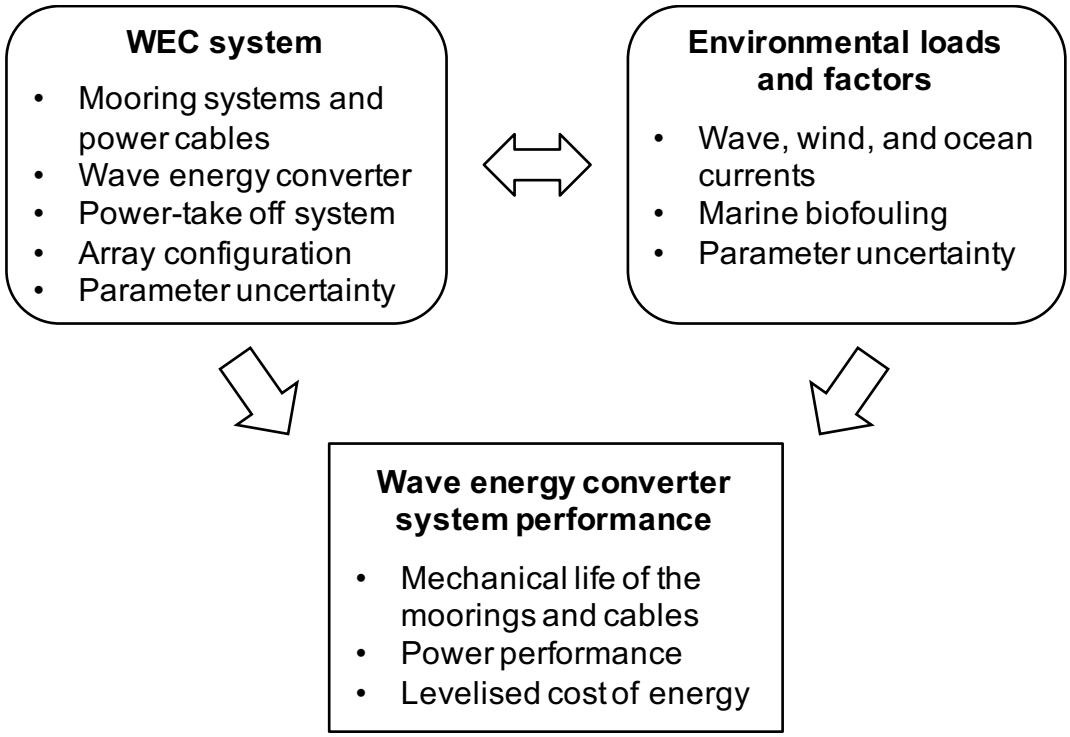


**Figure 3.** Framework of the various topics that motivated the methodology proposed in the thesis.

Items in the square box in Figure 3 entail various measures of WEC system performance. System performance is affected by all key parameters in the rounded boxes. In addition to the mechanical service life of the moorings and cables, power performance and LCoE were identified to be critical in determining overall system performance; hence, those factors were considered in the thesis. The three performance measures of the WEC system were evaluated by analyses 3, 4, and 5 (Section 2.1), respectively. Finally, analysis 6 was used to investigate the implications of uncertainties in the data, parameters, and models on system performance.

The various analyses were sequentially developed in the five papers appended to this thesis; see a schematic summary of the development in Figure 4. The six green cells correspond to analyses 1 – 6, as presented in Section 2.1. If a particular analysis was developed numerically (i.e., the numerical method), the corresponding cells are yellow, while they are blue for experimental development. Each yellow or blue cell represents a new topic or issue added relative to those developed in the previous papers. The chronological development of the numerical analysis should be read from left to right, whereas the chronological development of the experimental investigations should be read from top to bottom. Because the experimental investigation for the full-scale WEC installation has not been presented in any of the five appended papers, these results are presented exclusively in the text of this thesis.

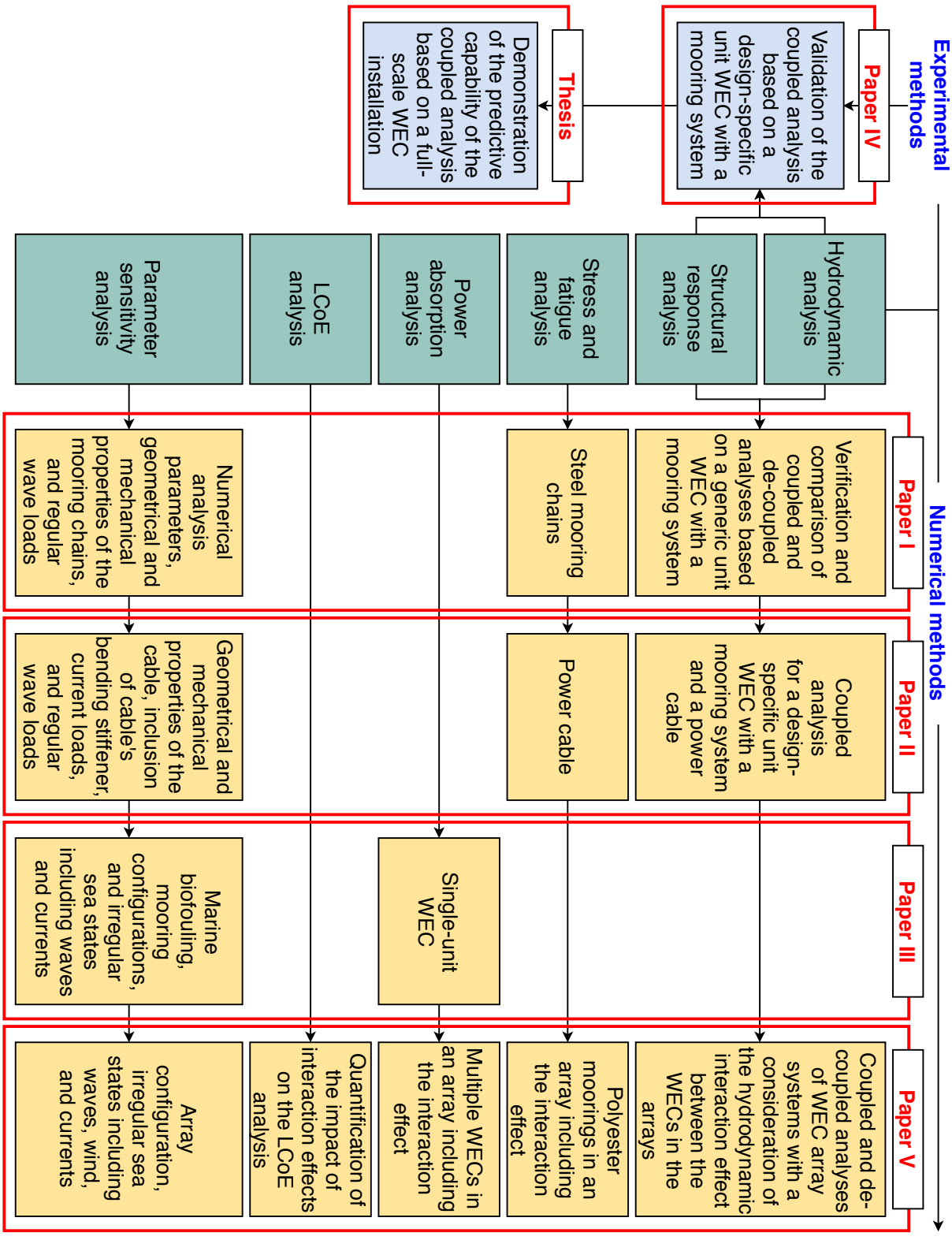


**Figure 4.** Schematic summary of the development of the methodology in the five appended papers. The interpretation of the cells and arrows can be found in the text in Section 2.2.

## 2.3 Delimitations

One specific concept (designed and developed by the Swedish company Waves4Power (2018a), hereafter referred to as the reference concept) was chosen for the case study throughout the thesis. Figure 5 shows a schematic view of the reference concept. One concept was treated as a case study so that the developed numerical model could then also be used to demonstrate the predictive capability of this model for the WEC's motion and mooring forces against a full-scale installation (Goal G5; see Section 1.2). For the same reason, the design of the experiment for validation (G4) and the choices of environmental loads and factors in the parameter sensitivity analyses (G2 and G3) were made such that the overall conclusions drawn from this thesis would be comparable to those for the full-scale WEC installation. Additional delimitations of this thesis are summarised as follows.

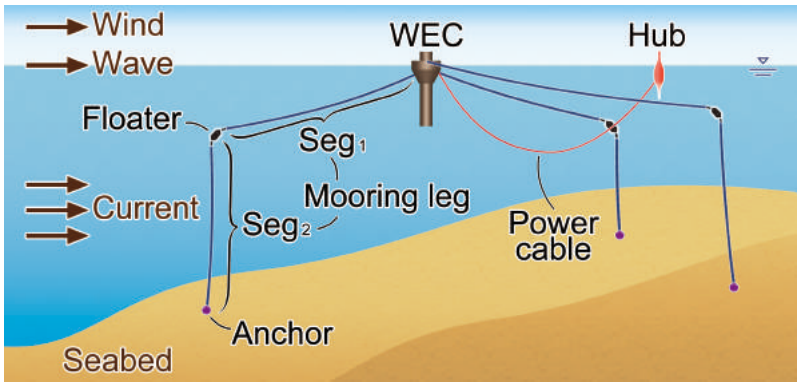


**Figure 5.** Schematic layout of the reference concept and environmental loading conditions. The naming conventions for the components of a WEC system used in the figure are also used throughout the thesis.

*Geometrical and hydrodynamic properties of the WEC*

The WEC was idealised as a rigid body. This thesis does not address the structural response of the WEC; only the properties deemed to be relevant to the WEC's hydrodynamics were considered. The physical properties used to represent a WEC included the WEC's draft, hull geometry, mass, inertial properties, and PTO system.

*PTO system*

The WEC absorbs wave energy through the activation of the PTO system. In this thesis, simplified PTO systems without a control mechanism were considered, unlike the system installed in the reference concept. This simplification was made to restrict our focus to the fatigue characteristics of the moorings and cables while maintaining the possibility of evaluating the power performance of the WEC. In this thesis, the PTO system was assumed to consistently behave as an ideal linear damper that can be represented solely by a constant, linear damping coefficient in the numerical model. However, because the exact configurations of the PTO system used in the reference concept and the one used in the model-scale experiment were both determined to have non-negligible drag damping effects, additional Morison models were

used to capture the potential drag damping effect; see discussions in Sections 3.1 and 4.1. The numerical model of the PTO system used in this thesis was considered to be representative only when the WEC functioned under the operational-mode conditions; these conditions correspond to those involving a wave height of less than eight metres for the reference concept. The uncertainty in the numerical modelling of the PTO system was beyond the scope of the thesis. However, due to the observations made in the experimental investigation, the development of a more advanced PTO system is planned for future work; see Chapter 7.

*Type of mooring system and power cable*

The mooring systems of the WEC can be designed for the sole purpose of maintaining the WEC on station and/or to provide reaction forces for the WEC to extract power from the waves. The mooring systems studied in this work belong to the former category. The marine power cables designed for most offshore structure applications have typical lengths of hundreds of kilometres and are placed on the seabed. During the development of the reference concept, however, a different type of cable was developed: one that is categorised as a dynamic cable in this thesis. In our definition, dynamic cables are designed to not contact the seabed during operation, and the cables are much shorter than the commonly used cables. Dynamic cables operate in a free-hanging state; hence, their dynamic motions are of greater importance. In this thesis, only this special dynamic cable type was investigated.

*Material and mechanical properties of the moorings and cables*

Two mooring materials were investigated in this thesis: steel and polyester. The material response of steel was assumed to remain consistently in the linear elastic region, and its mechanical properties can be represented by constant stiffness values. Polyester moorings exhibit nonlinear material behaviour that can be modelled under the framework of viscoelasticity and viscoplasticity. In this thesis, however, only the nonlinearity between the loads and elongations of the polyester moorings was considered in the numerical model. In the numerical model for the polyester moorings, the moorings' mechanical properties were defined by several points in a load-elongation diagram extracted from a monotonic tensile test; these points composed a pointwise linear curve representing the structural characteristics of the moorings.

The power cables consist of cylindrical and helical members composed of different materials with different mechanical properties. The thesis followed a first-principles design approach for the power cables. To that end, modelling and simulation were performed on a global "model" level in which each cable was represented as an axisymmetric line structure whose mechanical properties were defined for the entire cross-section of the line. The cable was assumed to consistently operate in the linear elastic region; hence, the mechanical properties were defined by constant stiffness values in the numerical model.

*Failure modes and failure points in the moorings and cables*

The goal of the stress and fatigue analyses performed in this thesis was to identify the fatigue-critical locations along the mooring lines and power cables according to the first-principles

design; the intrinsic failure mechanisms of these two structures were not considered in the model. The accumulated fatigue damage and fatigue lives of the moorings and cables were calculated from the stress cycles, adopting the S-N or R-N approach. It was assumed that normal stresses govern the fatigue damage; other phenomena such as wear, fretting, or bird-caging (in the cable) were not considered. To date, the calculated fatigue lives have not been validated against laboratory test results.

The possible failure points were assumed to lie on the main line-structures of moorings and cables themselves. Hence, the connector components (such as the linkage between the WEC and the moorings or between the WEC and cables, for example) were not modelled; consequently, the contributions of these connector components to the fatigue failure of the WEC system was disregarded.

*Stationary hub*

According to the initial design of the hub from the reference concept, the hub was designed to remain in a static position in the sea. Therefore, the hub was modelled as a spatially fixed point, meaning that the motions and force interactions between WECs through the hub were not taken into account.

*Software implementation and numerical modelling of the environmental loads*

Except for Paper I, which focused on comparing different software, the simulation of the hydrodynamic and structural responses of the WEC systems was performed using the software included in the DNV GL SESAM package (DNV GL, 2018b). Consequently, all limitations of the software were naturally inherited. The SESAM package adopts potential flow theory to model environmental loads; hence, restrictions were introduced to study only operational loading conditions.

Environmental loads from ocean currents, winds, and waves were considered in the thesis. The ocean current loads were restricted to be time-invariant. The wind loads were described by the wind spectrum and restricted to operational wind conditions (with extreme wind conditions such as those encountered in a typhoon or hurricane being disregarded, for example). Under the assumption of small wave amplitudes and Airy wave theory, all studied wave conditions were examined with respect to the wave steepness parameter and the shallow water parameter to avoid obtaining invalid results from the numerical simulations; see Paper II for details.

Due to a limitation of SESAM in simulating the complete interaction effect (see Section 3.1 for a description), the numerical analysis of hydrodynamic and structural responses used in this thesis cannot simulate a WEC concept that has bodies with different geometries or hydrodynamical properties or an array system consisting of WECs with different PTO systems. However, this limitation did not prevent the study of the reference concept, despite its two-body design, because in the reference concept, one body could be represented as an additional effect on the other body; hence, a one-body WEC model was sufficient to represent the entire system.

# 3 Numerical analyses

This chapter presents the analyses developed using numerical methods. These analyses include hydrodynamic and structural response analyses (Section 3.1), a stress and fatigue analysis (Section 3.2), a power absorption analysis (Section 3.3), an LCoE analysis (Section 3.4), and a parameter sensitivity analysis (Section 3.5).

## 3.1 Hydrodynamic and structural response analyses

The purpose of the hydrodynamic and structural response analyses was to calculate the motion of the WEC system and the force response of the mooring lines and power cables. When the thesis project was started, no report existed in the literature that compared the advantages and disadvantages of different models and analysis approaches, particularly with regard to the fatigue damage of mooring lines used for wave energy applications. To examine the numerical methods used in this thesis, an initial literature survey of existing numerical methods and simulation software was undertaken and is presented in the next sub-section. Then, the exact analysis workflow and analysis approaches used in the thesis are elaborated.

*Choice of numerical model and simulation software*

Different numerical models and simulation packages exist to simulate WECs and the connected moorings and cables and their interaction with waves, winds, and currents in the surrounding water. Li & Yu (2012) reviewed numerical methods that are suitable for modelling point-absorbing WECs, while Folly (2016) conducted a more general review not limited to any particular type of WEC. For mooring lines used in WECs, a review was provided by Davidson & Ringwood (2017). An assessment of power cables using numerical methods was presented by Thies et al. (2011, 2012). However, to the author's knowledge, there is no specific review addressing the modelling of power cables for WECs. Nonetheless, the methods reviewed by Davidson & Ringwood (2017) can, to some extent, also be applied to power cables.

Wave-structure interactions can be simulated using a frequency-domain, time-domain, or spectral-domain model. Spectral-domain models, including the phase-resolving model and phase-averaging model, were developed to model wave propagation over large domains (a few to hundreds of kilometres). The spectral-domain model uses a statistical representation of waves, which when passed through an appropriate transformation function produces a probabilistic estimate of the WEC response. Examples of using a spectral-domain model for wave energy applications can be found in the work by Beels et al. (2010), Millar et al. (2007), and Iglesias & Carballo (2014). However, the spectral-domain model cannot be used to calculate the temporal responses of the WEC system; consequently, the model cannot be used for a detailed structural response analysis of mooring lines and power cables. The spectral-domain model was therefore not considered in the thesis.

Both the frequency-domain and time-domain models involve defining a specific load that excites the WEC system, whose dynamic motion and structural responses are solved using the equations of motion. These two models are then able to predict the specific response of the WEC system under a specific loading condition, enabling a deeper investigation of the WECs and their attached moorings and cables. Self-evidently, an analysis is performed in the frequency domain using the frequency-domain model, whereas an analysis is performed in the time domain using the time-domain model.

Frequency-domain analysis is the more common method for simulating the hydrodynamic and structural response of floating offshore structures. This type of analysis assumes that the hydrodynamic behaviour of a system can be characterised by a linear approach. Thus, frequency-domain analysis is computationally simpler and requires less computational power than does time-domain analysis. For most floating offshore structures, the responses must be assessed over a wide range of sea states, and the use of frequency-domain analysis can substantially reduce the computational cost.

Frequency-domain analysis does have limitations, however. First, the method is restricted to linear problems. In the study of mooring lines and power cables for WEC systems, however, the coupling between the WEC and these two components introduces nonlinearities, e.g., geometric nonlinearity and seabed friction (Vicente et al., 2013; Vickers, 2012; Thies et al., 2011). The restriction of the linear problem was addressed by Fitzgerald & Bergdahl (2008), who developed a method for linearizing the impedance of mooring lines; this method was later used by Vicente et al. (2009) and extended further by Cerveira et al. (2013). The second limitation of the frequency-domain analysis is that transient responses of systems cannot be captured. The potential failure of mooring lines and power cables may require an understanding of the instantaneous responses of the structures to identify critical scenarios, such as collisions or snap loads (Palm et al., 2017). For these reasons, despite requiring higher computational power, analysis of the dynamic response of moorings and cables in the time domain was deemed necessary for the current thesis.

Time-domain analysis can be performed using linear potential flow theory or other nonlinear theories that require computational fluid dynamics (CFD) to solve the Navier-Stokes equation. Potential flow theory, which is based on the assumption of inviscid and irrotational flow, also holds only for waves and oscillatory device motions with small amplitude. WECs ideally operate in resonance, a mode in which the small-amplitude assumption is not always fulfilled (Falnes, 2002). Different nonlinear theories using the CFD method to analyse WEC systems were reviewed by Wolgamot & Fitzgerald (2015). These nonlinear theories can capture nonlinear interactions between the fluid and structures and are therefore advantageous in evaluating extreme loading conditions and the survivability of WEC systems and their sub-components; see implementation examples by Palm et al. (2013, 2016), Ransley (2015), and Yu & Li (2011). However, the CFD method currently requires considerable computational power that is not yet feasible for structural fatigue problems. The structural fatigue problem typically requires tens to hundreds of simulations of various environmental states and a duration of three to six hours for each environmental state to obtain extreme response estimates with sufficient statistical confidence for fatigue damage estimation (DNV GL, 2017b). Thus, time-domain analysis using linear potential flow theory was adopted to carry out the hydrodynamic and structural response analysis of the WEC system. However, a restriction was made whereby only the operational-mode condition of the WECs was investigated in the current thesis; see the discussion in Section 2.3.

Several numerical software applications enable time-domain analysis using linear potential flow theory for wave energy applications. The commercial software package DNV GL SESAM, which was used in this thesis, integrates several software applications and core solvers to model different parts of an offshore floating structure and perform various types of numerical simulations. Different core solvers in the SESAM package have been compared with other solvers designed for similar purposes; see the comparison of simulated WEC motion and hydrodynamic forces of a three-body oscillating WEC reported by Combourieu et al. (2015), the study of the applicability and mathematical implementation of the method for dynamic mooring analysis reported by Thomsen et al. (2017), and the study of the ability to simulate the

material and geometric nonlinearity of mooring lines reported by Bhinder et al. (2015). Among the solvers compared in these three references, except for a few solvers that exhibit certain limitations, no "best" solver is recommended. Furthermore, it was concluded in all of these studies, following verification and validation studies, that the numerical implementation used by the SESAM package yields sufficiently suitable simulation results. Because the integration of several software applications and core solvers into the SESAM package facilitates the modelling and assessment of the WEC, mooring lines, and power cables (all exposed to a variety of environmental conditions) in a manner suitable to the objectives of this thesis, the SESAM package was chosen.

*Analysis workflow and numerical model*

Figure 6 presents the analysis workflow alternatives provided in the SESAM package to perform the hydrodynamic and structural response analyses of WEC systems in the time domain. A WEC system can consist of either a single WEC or several WECs connected in an array system. The rectangular boxes in the figure represent the actual analysis steps, whereas the rounded boxes represent input/output information for the analysis steps. The rounded boxes can be further divided into two categories: the dashed boxes include the basic information needed prior to performing the analysis, whereas the solid boxes include information extracted from the preceding step in the workflow.

The basic information (dashed rounded boxes in Figure 6) includes physical properties that describe the WEC system and its ocean environment. The physical properties to be used depend on the simulation purpose. In this thesis, the physical information includes the following: (1) site and resource conditions; (2) geometric configuration and hydrodynamic properties of the WECs, including their own PTO systems; and (3) geometric configuration and hydrodynamic and mechanical properties of the mooring lines and power cables.

One piece of information also included in the dashed rounded boxes in Figure 6 but omitted from the abovementioned list is marine biofouling. Marine biofouling (i.e., marine growth) is a collective term for the settlement and growth of sedentary and semi-sedentary organisms on artificial structures situated in marine and estuarine environments (Kingsbury, 1981). The influence of marine biofouling was considered in this thesis and is regarded as an environmental factor (see Figure 3) that affects the performance of a WEC system. In this thesis, the biofouling effect was defined as an increase in the mass and drag of mooring lines and power cables, following the recommendation defined by the Position Mooring Standard (DNV GL, 2015). Although the standard cited is intended for mooring systems, we adopted the same principle for cables because of the similar slender geometric characteristics of the two components of floating WECs. Additionally, it was assumed that an anti-fouling coating had been applied to the main floating WEC. Therefore, only the biofouling effects on the moorings and cables were considered. However, to consider fouling on the WEC, additional mass could be added to the WEC while retaining the WEC's geometry, following the procedure described by Langhamer et al. (2009) and Tiron et al. (2012). Therefore, the dashed rounded boxes pertaining to the properties of the WECs, moorings, and cables are preceded by a box for marine biofouling in Figure 6, and all were categorised as the basic information that describes WEC systems and their ocean environment.

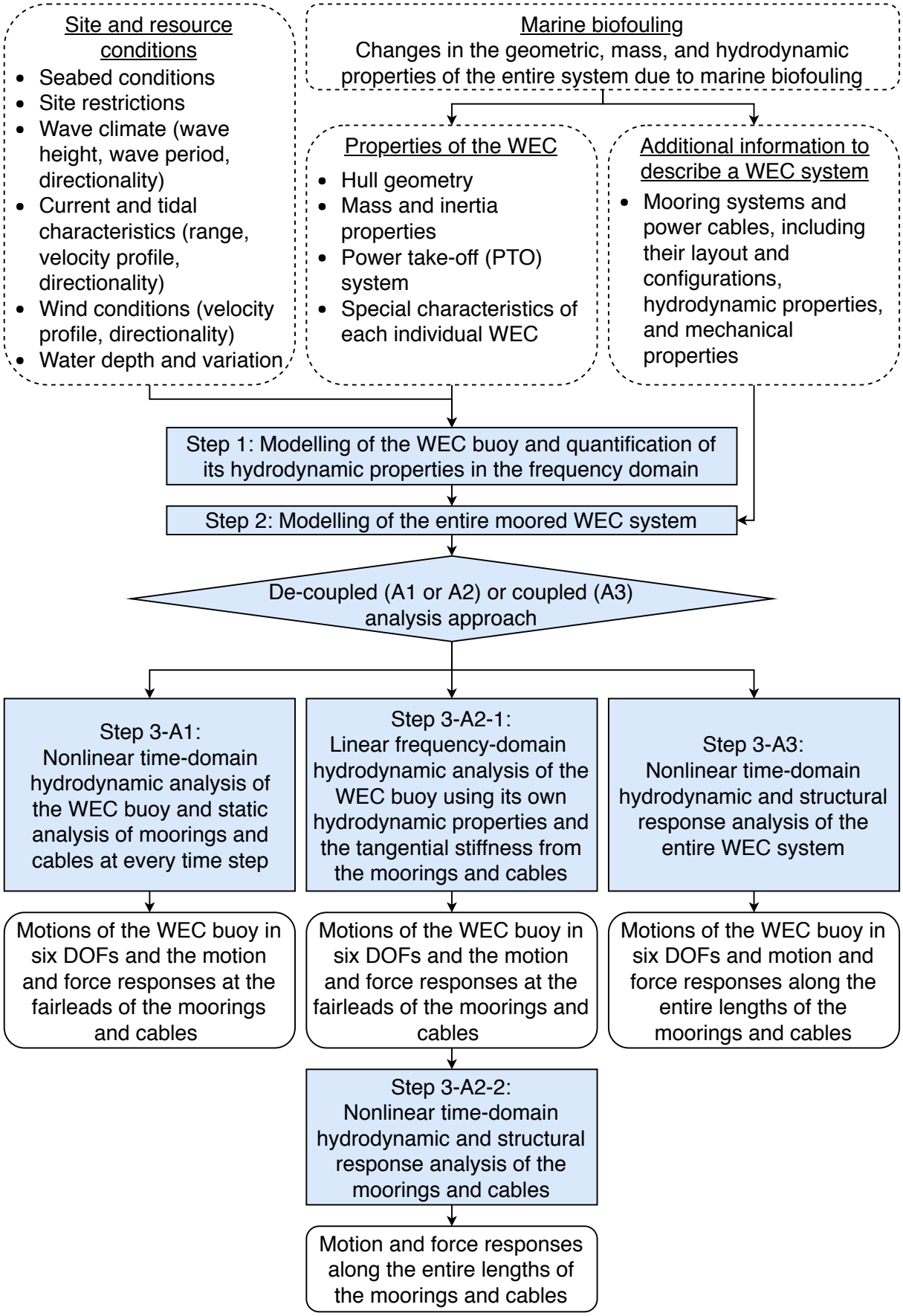


**Figure 6.** Analysis workflow for simulating the hydrodynamic and structural response analyses of WEC systems in the time domain.

The numerical model of WEC systems is composed of six sub-level numerical models that use the information contained in the dashed rounded boxes (see Figure 6). The sub-models include an environment load model, a panel model of the WEC, a point model of the WEC, a Morison model of the PTO system, a Morison model of the WEC, and a finite element (FE) model of the mooring systems and power cables (i.e., all slender structures). Figure 7 presents the information flow from the basic information of the WEC system to the six sub-level numerical models. These six sub-models, except for the two Morison models, are the minimum number required for the hydrodynamic and structural response analysis and were gradually developed from Papers I to V throughout the thesis project.

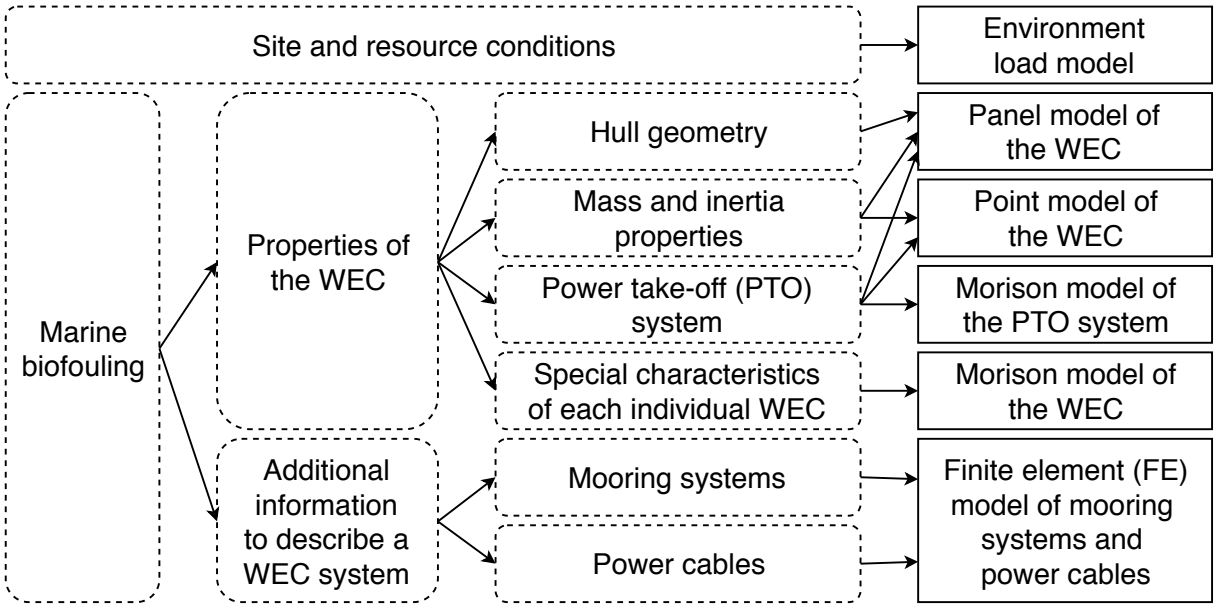


**Figure 7.** Relation between the six sub-level numerical models and the basic information (information in dashed rounded boxes in Figure 6) needed to represent the WEC system for analysis of its hydrodynamic and structural response.

The two Morison models (for the WEC and PTO system) are used with the sole purpose of capturing the drag damping effect and hence can be excluded if a WEC system is deemed to be insensitive to such an effect. The importance of the drag effect was evaluated according to the evaluation criteria reported by Chakrabarti (1987a). Two characteristic hydrodynamic properties were examined: the Keulegan-Carpenter parameters and the Reynolds number. In Paper I, because the studied WEC buoy (a cylindrical buoy with a height-to-diameter ratio of 2) was deemed to be insensitive to the viscous drag damping effect, no Morison model for the WEC was used. In the reference concept, the WEC has a long cylindrical tube, and its PTO mechanism is realised by water movement inside the central hollow tube of the WEC. The Morison model was therefore used to capture the corresponding viscous drag and transverse drag damping from the tube and the moving water. The WEC buoy and PTO system used in the model-scale experiment (Paper IV) were both deemed to have a non-negligible viscous drag effect due to the presence of a long cylindrical tube; a long, thin steel bar; and a thin heave plate. Hence, Morison models were also used in Paper IV to represent the corresponding experimental configuration. Detailed descriptions of the usage of the Morison models of the WEC and the PTO system can be found in Papers II and IV, respectively.

The six sub-level models together represent a complete numerical model for the WEC system. These models are used in different steps and by different software applications and solvers in the SESAM package to capture a particular effect or to simulate the response from a certain component in the WEC system. Table 1 presents a brief summary of the six sub-level numerical models and their relations to different parts of the SESAM package; a comprehensive comparison can be found in Paper IV.

**Table 1.** Overview of the six sub-level models in relation to different software and solvers used for the hydrodynamic and structural response analysis of the WEC system.

| **Sub-model** | **Information of the WEC system to be extracted** | **Software (core solver)*** | **Steps to be used in the workflow (cf., Figure 6)** |
|---|---|---|---|
| Environment load model | • External environmental loads acting on the WEC system | HydroD (WADAM); DeepC or SIMA (SIMO and RIFLEX) | All steps |
| Panel model of the WEC | • Hydrostatic data and inertia properties of WEC buoy<br>• Global responses of WEC buoy in frequency domain, including hydrodynamic added mass and damping, first-order wave-exciting forces and moments, and second-order drift forces and moments | HydroD (WADAM) | Step 1 |
| Point model of the WEC | • First-order motion and force response of the WEC buoy in the time domain<br>• Second-order motion and force response of the WEC buoy in the time domain if using analysis approaches A1 and A3 | DeepC or SIMA (SIMO) | Steps 2 and 3 |
| Morison model of the PTO system | • Drag damping effect of the PTO system | HydroD (WADAM); DeepC or SIMA (SIMO) | Step 1 by WADAM or steps 2 and 3 by SIMO |
| Morison model of the WEC | • Drag damping effect of the WEC buoy | HydroD (WADAM); DeepC or SIMA (SIMO) | Step 1 by WADAM or steps 2 and 3 by SIMO |
| FE model of moorings and cables | • Time-domain motion and force response of the mooring systems and power cables | DeepC or SIMA (RIFLEX) | Steps 2 and 3 |

*References for the listed software and solvers: DeepC (DNV GL, 2018a), HydroD (DNV GL, 2018c), RIFLEX (SINTEF Ocean, 2018a), SIMA (SINTEF Ocean, 2018b), SIMO (SINTEF Ocean, 2018c), WADAM (DNV GL, 2018d).

*Analysis approaches*

Various analysis approaches are provided in the SESAM package to simulate the hydrodynamic and structural response of the WEC system; see the three parallel tracks of the workflow presented in Figure 6. The complete theoretical background and mathematical implementation of each analysis approach can be found in SINTEF Ocean (2017a, 2017b); the major differences between the three approaches relevant to the thesis are highlighted in this sub-section.

Depending on the level of inclusion of the mutual mechanical coupling between the WEC and the slender structures, such as the moorings and cables, the three approaches were categorised as de-coupled (A1 and A2) or coupled (A3). The definition reported by Gao & Moan (2009) was followed for the categorisation: if the equations of motion of the WEC and mooring lines (and power cables in this thesis) are solved simultaneously using time-domain analysis (and thus if the motion and force of the mooring structures implicitly influence the instantaneous dynamics of the WEC and vice versa), then the corresponding analysis is referred to as a coupled analysis approach; otherwise, the analysis is referred to as a de-coupled analysis approach.

The three analysis approaches also capture various degrees of interactions; see the comparison in Table 2. According to the definition in Oxford's *A Dictionary of Physics*, "interaction" is defined as "an effect involving a number of bodies, particles, or systems as a result of which some physical or chemical change takes place to one or more of them" (Law & Rennie, 2015). Based on this definition, the mechanical coupling between the WEC and the slender structures is one type of interaction, while other types of interactions can also occur in a WEC system operating in an ocean environment, such as fluid-WEC interactions, fluid-slender structure interactions, WEC-WEC interactions through the fluid, and interactions through the fluid between the slender structures. To separate the interaction between the WEC and slender structures from all other possible interactions, the former is referred to as the coupling effect in this thesis; this terminology is also used throughout the appended Papers I – V. WEC-WEC interaction through the fluid was studied in the appended Paper V in particular and is referred to as hydrodynamic interaction in that paper.

As shown in Table 2, every approach has its own limitations. A3 is the only available approach that fully considers the coupling effect between the WEC and the moorings and cables. The A2 and A3 approaches could both potentially be used to study the structural response of the moorings and cables because these two approaches can accommodate the interaction between the fluid and the moorings and cables and to analyse the instantaneous dynamic responses along the entire length of these two structures. Another factor to consider is the second-order wave loads on the WEC system, which are included only if the WEC's dynamic response is solved in the time domain in the SESAM package. Thus, the A1 and A3 approaches could both be used to include second-order wave loads; this incorporation is achieved by including the steady-state component of the second-order loads expressed as the mean wave drift force and the second-order wave loads that act together with oscillatory wind loads to induce the low-frequency motion of WECs. Finally, a limitation common to the A2 and A3 approaches is the manner in which they model the interaction between WECs through the fluid. For an array system with more than one WEC, the hydrodynamic responses of the WECs are influenced by each WEC in the system through the radiation and diffraction of waves. Among the three approaches, the A1 approach is the only one that can include both radiation- and diffraction-induced effects. The other two only consider diffraction-induced effects.

**Table 2.** Comparison of the three analysis approaches (A1, A2, and A3) provided in the SESAM package. The paper IDs shown in the last row of the table indicate the paper in which the specific analysis approach was developed and used. For the complete theoretical background and mathematical implementation of each analysis approach, the reader is referred to SINTEF Ocean (2017a, 2017b).

| | **A1** | **A2** | **A3** |
|---|---|---|---|
| Categorisation of the analysis approach* | De-coupled | De-coupled | Coupled |
| Analysis of the WEC | Time-domain analysis | Frequency-domain analysis | Time-domain analysis |
| Analysis of the mooring lines and power cables (i.e., the slender structures)** | Static analysis in every time step | Quasi-static analysis in the time domain | Dynamic analysis in the time domain |
| Inclusion of coupling between the WEC and slender structures | Simplified | Simplified | Included |
| Inclusion of fluid-WEC interactions | Included | Includes only the contribution from the first-order wave loads | Included |
| Inclusion of fluid-slender structure interactions | Simplified | Included | Included |
| Inclusion of WEC-WEC interaction through the fluid | Included | Included only in the diffraction-induced interaction | Included only in the diffraction-induced interaction |
| Inclusion of interactions between slender structures through the fluid | Not included | Not included | Not included |
| In which paper the approach was developed/used | Paper V | Paper I | Papers I-V |

*The distinction between the coupled and de-coupled analysis approaches follows the definitions by Gao & Moan (2009).

**The distinctions among the static, quasi-static, and dynamic analyses for the moorings and cables follow the definitions of the model types by Davidson & Ringwood (2017).

The focus of Papers I to IV was the structural response of moorings and cables in a single-unit WEC system. Without the need to consider the interaction between WECs, either the A2 or the A3 approach could potentially be used because each enables a more detailed investigation of moorings and cables. Examples of the use of the A2 approach for WEC applications are scarce, but examples of using the A3 approach in WEC applications can be found in the literature. Muliawan et al. (2013) used a coupled A3 approach to assess the effect of the PTO system and mooring configuration on the energy capture of a two-body floating WEC. Michailides et al. (2016) and Wan et al. (2015) also adopted the coupled approach and validated a simulation model for survivability conditions against experimental model tests of combined wave and wind energy converters. By using the same analysis approach, Gao & Moan (2009) found that

an individual mooring is more feasible than an integrated mooring configuration in a WEC array farm due to the significantly larger force responses observed in the latter under survival conditions. Because the A2 and A3 approaches had not yet been compared in detail with regard to the mooring fatigue analysis used in WEC applications, one goal of Paper I was to perform such a comparison and provide a recommendation on how to perform a WEC mooring analysis. This recommended approach was further extended to include power cables attached to the WECs in the study described in Paper II.

Furthermore, Paper V addressed the fatigue characteristics of moorings and cables in an array farm configuration. Because of the limitations of the A2 and A3 approaches with regard to their ability to capture the interaction between WECs through the fluid, the suitability of the de-coupled approach A1 was also investigated and compared with that of the other two approaches. Three analysis approaches were therefore adopted and investigated in this thesis, and the A3 approach was selected for studying the fatigue characteristics of mooring lines and power cables for wave energy applications.

## 3.2 Stress and fatigue analysis

The goal of the stress and fatigue analysis was to identify the fatigue-critical locations along the mooring lines and power cables and their overall relative fatigue lives. The stress and fatigue analysis was performed using in-house code developed using MATLAB (The MathWorks Inc., 2016), for which the force histories of the mooring lines and power cables were extracted from the structural responses analysis described in Section 3.1.

It was found by Hall et al. (2014) and suggested by DNV GL (2015) that bending and torsional stiffnesses are of negligible importance to mooring lines' tension response for structures such as barges, spars, tension-leg platforms, and marine renewable devices, regardless of the load case. Thus, the moorings were constrained to exhibit stiffness in the axial direction only, i.e., zero bending and torsional stiffness was assumed. The structural response of each mooring line was characterised in terms of the axial force; then, the corresponding axial stress was calculated using the nominal cross-sectional area of the mooring lines.

A power cable is a structure that is flexible in both bending and torsion, due to low bending and torsional stiffness properties, but maintains a high tensile strength due to a relatively large axial stiffness. Therefore, the mechanical properties of power cables account for stiffness in three directions. Prompted by the suggestion by Karlsen (2010) and Karlsen et al. (2009), we defined the cable stress capacity as the combination of the axial tension and bending curvature. Accordingly, the stress components of a cable include both axial and bending stresses. For each cross-section of a cable, we considered the outermost edge to be the most important area for the stress response, and several points on the periphery were calculated to determine the most fatigue-critical location along the cross-section.

The accumulated fatigue damage and fatigue lives of mooring lines and power cables can be calculated following calculation of their stresses. Preliminary calculations of the stress responses of moorings and cables were carried out in the beginning of this thesis project, and the results of these calculations showed that the stress levels of these two structures are both considerably lower than their design yield stress. Hence, a stress-based approach was adopted in the fatigue analysis. In conjunction with stress history, the rain-flow counting method was employed to extract the stress cycle for fatigue analysis (Endo & Morrow, 1969) using the WAFO toolbox (WAFO Group, 2011). Finally, depending on the material composing the

mooring lines and power cables considered, the accumulated fatigue damage, $FD$, was calculated using the Palmgren-Miner cumulative rule and the S-N (stress - number of cycles to failure) or R-N (relative tension - number of cycles to failure) curve. No fatigue material tests were conducted. Instead, the fatigue material properties of the mooring lines and power cables were extracted from DNV GL (2015) and Nasution et al. (2013), respectively. In addition, the fatigue material properties of moorings and cables were assumed to remain unchanged under the fouled condition with respect to the original fatigue material properties extracted from the two cited studies, i.e., no influence of bio-corrosion on the S-N or R-N curves was considered. For a detailed stepwise description of the procedure used to calculate the fatigue damage of mooring lines and power cables, the reader is referred to Paper I for catenary mooring chains, Paper V for polyester mooring lines, and Paper II for power cables.

## 3.3 Power absorption analysis

The purpose of the power performance analysis was to estimate the theoretically absorbed power of the WEC from waves. In this thesis, a linear PTO system, represented by a linear damper acting in the heave direction of the WEC, was assumed for all studied WECs. The mathematical model of the PTO system is a simplification of that installed in the reference concept. A similar approach was used by Cho & Kim (2017), Fitzgerald & Bergdahl (2008), and Vicente et al. (2009). The model of the PTO system as a linear damper estimates the theoretical energy output and results in minimal modelling complexity; thus, the model was deemed sufficient for this thesis.

No control of the PTO system was considered, and the PTO system was assumed to act exclusively in the heave direction. Thus, the PTO system was defined as a constant damping coefficient relative to the heave DoF of the WEC. The damping coefficient varies for each studied WEC and was determined based on each WEC's unique hydrodynamic properties as the value yielding the optimal PTO, i.e., at the resonance of the WEC in the heave DoF, following the suggestion by Falnes (2002). Note, however, that because no control of the PTO system was considered, an underestimation of the power performance can be expected. The time-averaged power absorption, which corresponds to the mean power consumed by the mechanical damper of the PTO over a certain period, was used in this thesis to represent the power performance of the WEC under a specific operational condition. The reader is referred to Paper III for a detailed description of the procedure for calculating a WEC's power performance.

## 3.4 LCoE analysis

LCoE analyses were performed to demonstrate how the numerically evaluated fatigue damage of the moorings and cables and power performance of a WEC (i.e., the results from Sections 3.2 and 3.3) together affect the economic assessment of the WEC system. The economics of a WEC system can be assessed in various ways, such as by using annual energy production (AEP) per unit displacement, AEP per unit capital expenditure (CapEx), life cycle cost (LCC), or LCoE (Costello & Pecher, 2017; Carbon Trust & DNV 2005). Among these quantities, the LCoE, which considers both the AEP and present value of cost, is the one most often recommended by the governing bodies (IEA & NEA, 2015; IEA-OES, 2015) and hence was used in this thesis.

Several approaches exist for defining the LCoE; see examples in Gross et al. (2007), IEA & NEA (2015), LaBonte et al. (2013), and SI Ocean (2013). The definitions presented in these references have been used by researchers to develop detailed calculation models tailored to a particular purpose or a particular WEC design. Selected examples are listed here. Astariz et al. (2015) presented a calculation model that was used to compare different co-located layouts of wave and wind farms. Frost et al. (2018) developed a calculation model that allows for the spatial dependence of the LCoE for wave energy projects to be considered. An LCoE calculation model was developed by Piscopo et al. (2017) to determine the optimum configuration of heaving point absorbers at different deployment sites, whereas the LCoE calculation reported by de Andres et al. (2017) was developed to provide an overview of the limits for the technical parameters of WECs.

In this thesis, the LCoE calculation model suggested by Castro-Santos et al. (2016a, 2016b) was followed because their calculation was developed for floating wave energy applications and because it provides a detailed description of how to assess various cost aspects in a practical manner. An LCoE analysis was performed in Paper V to assess whether hydrodynamic interaction needs to be considered in a systems analysis and cost estimation of the full WEC system and wave farm. Further development is needed for a complete LCoE assessment in the current methodology; see the discussion in Chapter 7.

## 3.5 Parameter sensitivity analysis

The analysis procedures described in Sections 3.1 – 3.4 involve several numerical and physical parameters that affect the simulation results. Herein, the physical parameters are those that have a direct physical meaning. In contrast, the numerical parameters are used only to assist the numerical simulation and typically depend on the chosen numerical simulation technique and/or software (in our case, the DNV GL SESAM package). Due to, for example, uncertainties in the material and mechanical properties of moorings and cables, the random nature of environmental loads and factors, and inherent limitations of numerical models and simulation software, uncertainties arise in these numerical and physical parameters. A parameter sensitivity study was therefore conducted in this thesis as part of the overall methodology to assess the sensitivity of these parameters on the WEC's dynamics and structural fatigue performance.

The parameter sensitivity study consisted of three procedures. First, relevant parameters were identified; those parameters were normally the ones that showed large uncertainty in the system's properties and environmental conditions or the ones that affect the stability and accuracy of the numerical simulations. Second, several hydrodynamic and structural response analyses were performed with a systematic variation of selected parameters. Third, the sensitivity of the varied parameters with respect to the WEC system characteristics was quantified. In this thesis, the sensitivity of these parameters was evaluated with regard to the fatigue damage of moorings and cables and the WEC power performance. Table 3 summarises all parameters investigated in the thesis and in appended Papers I – V.

**Table 3.** Summary of the numerical and physical parameters investigated in the thesis; the corresponding results can be found in the papers indicated in the second column of the table.

| | Source (Papers I – V or other references) | | | | | |
|---|---|---|---|---|---|---|
| **Numerical parameters** | | | | | | |
| Mesh size of the mooring lines and power cables | I | | | | | Yang et al. (2014) |
| Artificial stiffness of the WEC buoy | | | | | | Yang et al. (2014) |
| Structural Rayleigh damping of the moorings and cables | I | | | | | Yang et al. (2014) |
| Random seed for wave realisation | | | | | | Thesis |
| **Physical parameters** | | | | | | |
| Wave drift force of the WEC buoy | | | | | | Yang et al. (2014) |
| Pretension force of the mooring lines | | | III | | | Yang et al. (2014) |
| Length of the mooring lines | | | III | | | |
| Bending and torsional stiffness of the mooring lines | I | | | | | |
| Configuration of the mooring systems | | | III | | V | |
| Bending stiffness of the power cables | | II | | | | |
| Length of the power cables | | II | | | | |
| Mass of the power cables | | II | | | | |
| Influence from the presence of the bend stiffener | | II | | | | |
| Wave height, wave period, and direction | I | II | III | IV | V | |
| Current speed and direction | | II | III | IV | V | |
| Wind speed and direction | | | | | V | |
| Thickness of marine biofouling | | | III | | | |
| Density of marine biofouling | | | III | | | |
| Duration of development for marine biofouling | | | III | | | |
| Configuration of the WEC array systems | | | | | V | |

# 4 Experimental analyses

This chapter presents two experimental analyses performed in this thesis: an ocean basin laboratory experiment and measurements on a full-scale WEC installation. The former was designed and carried out to validate the numerical simulation model developed and presented in Papers I – III, whereas results from measurements in the latter experiment were used to assess the predictive capability of the simulation models for a real case.

## 4.1 Ocean basin experiment

One research focus in the first half of this thesis project (i.e., Papers I – III) was developing numerical simulation models for the simulation and assessment of hydrodynamic and structural responses for floating point-absorbing WEC systems. These simulation models and the numerical approaches that were used needed to be validated. Therefore, an experiment was designed and carried out in an ocean basin laboratory at the State Key Laboratory of Ocean Engineering in the Shanghai Jiao Tong University in Shanghai (China) (SJTU, 2018) with the objective of providing information to assess the validity of the numerical analyses and the simulation models. All details of the ocean basin experiments are presented in Paper IV; this section presents a brief summary of the motivation, description and planning of the experiments. Note that the contribution of the validation experiment is not limited to the scope of the current thesis; the experiment also provides knowledge pertaining to other similar types of floating WECs. Evaluating the structural reliability of wave energy devices, with an emphasis on the long-term use and survivability of the associated components (such as the mooring lines and power cables), requires validated numerical models; such models can, for example, be used to provide confidence in the cost-efficient development of WEC systems, which is needed to reach large-scale commercialisation.

Guidelines for the experimental tests of WEC systems have been considered by researchers such as Holmes (2009), ITTC (2014), McCombes et al. (2010), Payne et al. (2009), Pecher (2017), and Sarmento & Thomas (2008). Although similarities can be found between these references, the ITTC guideline (2014) was followed because it provides clear guidance on the design, planning, and implementation of the numerical model validation experiment at both the system and component levels. One important advantage of ocean basin tests relative to measurements conducted in field trials is that the ocean basin tests enable detailed investigation of the response of a WEC system under controlled environmental conditions (sea states and ocean current), which can be varied systematically. The experimental data from a laboratory experiment can be used to validate or calibrate a numerical simulation model. This thesis focused on validation, i.e., no calibration of the simulation model was performed. The results presented in Section 5.6.1 and in Paper IV are derived from a validation study of the WEC motions under operational conditions. A validation of the mooring line forces, force responses of the PTO system and survival conditions was planned within the thesis, but this work has not yet been completed and is described in the context of planned future work in Chapter 7.

*Design of the experimental WEC system*

In this sub-section, the design of the experimental WEC system is elaborated, whereas the exact target design values for each component can be found in Paper IV.

As addressed in ITTC (2014), the responses and performances of WECs are normally scaled using Froude similitude, but exceptions occur for some parameters, such as the power output of the device, viscous damping, and mechanical friction; large-scale test models are recommended to minimise scaling effects. Therefore, a 1:20 scale model following Froude's law was chosen for experiments with sea states corresponding to operational conditions. Considering the configuration of the prototype WEC and the sea state conditions to be tested, the ratio of 1:20 was the largest possible scale for the ocean basin. The sea states corresponding to survival conditions were created using a 1:36 scale model due to limitations in wave generation at the test facility.

The development of the numerical models in Papers I – III closely followed the WEC concept developed by the company Waves4Power, which was, at the time, to be installed in Runde, Norway. The design of the experimental model was therefore chosen to be as similar as possible to the already developed numerical model while not substantially different from the prototype system shown in Figure 5. The emphasis of the experimental model design was on the investigation of the WEC's motions, the forces in the mooring lines, and the coupling effect between the WEC and the moorings. The power cable was excluded from the study to maintain an acceptable level of complexity in the experimental system.

The experimental WEC system consisted of a WEC buoy, a three-leg two-segment taut mooring system with submerged floaters, and a PTO system designed for this experiment as a heave plate. The configuration of the experimental WEC system is illustrated in Figure 8, which shows the complete WEC system built for operational loading conditions. The experimental configuration for the survival loading conditions was similar, except that a smaller scale model (1:36) was used and that the PTO system was removed because it was assumed to be inactive under survival operational conditions at full scale.

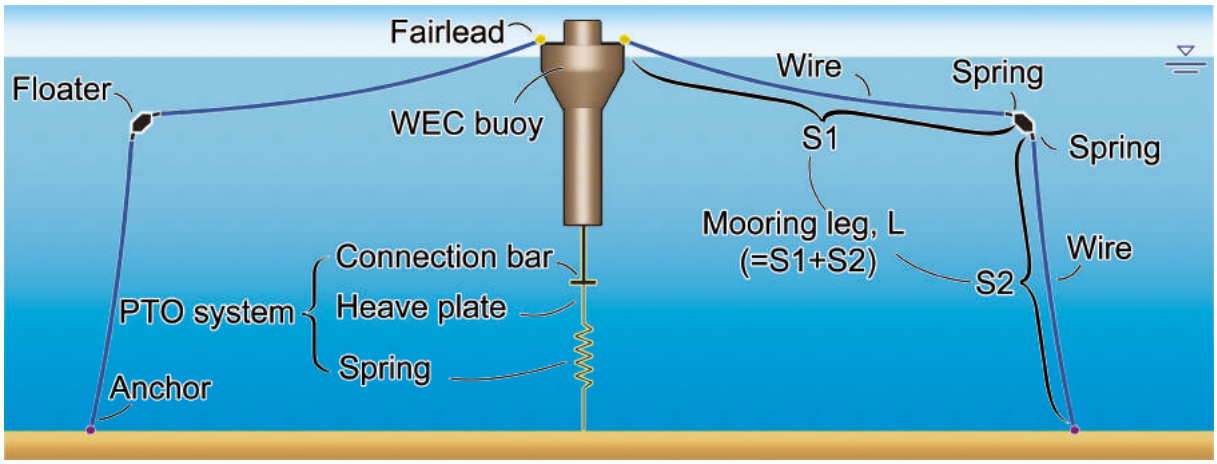


**Figure 8.** Illustration of the configuration of the WEC system for the ocean basin experiment.

The PTO mechanism of the full-scale prototype WEC is realised by water movement inside the central hollow tube of the WEC. Although the behaviour of the full-scale PTO system should ideally be reproduced in the scale model, it is not generally appropriate to geometrically scale down the PTO system because of the challenge of achieving the expected power performance in a scaled system; see discussions by Forestier et al. (2007) and Sheng et al. (2014). Therefore,

the experimental WEC was idealised as a closed buoy, and the PTO system was simulated by a heave plate following the suggestions of Cheng et al. (2014). Note, however, that future work to find a better solution for the experimental PTO system is needed so that the PTO responses from the experimental system can be more similar to the one installed in the full-scale prototype; see the discussion in Chapter 7.

The hull geometry of the WEC buoy was designed to be the same as that of the scaled-down prototype WEC. To determine the mass, centre of gravity (CoG), and inertial properties of the experimental WEC buoy, a numerical mass model was built at the prototype scale. The mass model modelled the mass contribution at the corresponding location in the WEC, including the contribution from the hull structure, principal machinery such as generators and hydraulic systems, water in the cooling tank and ballast tank, and the amount of water that is presumed to oscillate in the hollow tube for power generation. The first three categories together correspond to the displacement of the prototype WEC, whereas the last mass category was used to compensate for the mass due to the simplification of the prototype PTO system. The mass, CoG, and inertial properties calculated from the mass model were used as the target values for the experimental model.

The entire PTO system consists of a heave plate, a connection bar, and a helical spring. The heave plate acts as a damper in the entire WEC system, and its target damping effect at full scale was chosen in the same manner described in Section 3.3. The damping effect of the experimental heave plate was estimated by a decay test through a 1-DoF spring-mass-damping system. The dimensions of the heave plate were determined as those obtained when the equivalent linear damping estimated from the 1-DoF decay system satisfied the target linear damping. The heave plate was rigidly connected to the WEC buoy by a steel rod and to the floor of the ocean basin by a spring. This configuration ensured that the movement of the heave plate consistently followed the motion of the WEC buoy. The heave plate was placed at as great a depth as practically achievable to reduce the influence of the wave motion due to the surface waves. No optimisation was performed with regard to PTO tuning under various frequencies or to the position of the heave plate. While the design choice of the PTO system adopts a linear assumption (i.e., an assumption that an ideal linear PTO system is to be used), its inherent quadratic nature due to the viscous force effect was also numerically modelled through the Morison model to ensure a correct validation process (see the discussion of the Morison model in Section 3.1). Additionally, the spring of the PTO system was numerically modelled in the same manner as the mooring system, whereas the inertial and restoring effects of the heave plate and connection bar were considered by including the corresponding mass contribution to the numerical model of the WEC buoy. Thus, the damping effect induced by the experimental PTO system was faithfully simulated in the numerical model, whereas the dynamic response of the WEC with the influence from the PTO system was captured experimentally with minimum experimental model complexity.

The prototype WEC system uses mooring lines made of polyester. These polyester moorings exhibit nonlinear material behaviour that can be analysed under the frameworks of viscoelasticity and viscoplasticity. Because a properly scaled material was not available, thin steel wires were used instead in the experiments, with additional helical springs that mimicked the mooring segment stiffness at the model scale (relative to the full scale). The target stiffness of the spring was determined by a linear regression analysis of the axial load-elongation diagram of the prototype polyester mooring. Every set of one wire and one spring represented one mooring segment in the prototype WEC, and the total length of each set at full scale was identical to that of the corresponding mooring segment. The prototype mooring lines were designed to be buoyant, an assumption that would be violated if the model-scale moorings were

composed of only steel wires and springs. Thus, the steel wires were covered by plastic tubes (with a significantly lower density than steel) to achieve the target submerged weight at the model scale. Due to the use of three components (steel wires, helical springs, and plastic tubes) to represent the prototype mooring, the geometric similitude of cross-sectional diameters cannot be attained. This effect was therefore accounted for when building the numerical model of the experimental mooring system. The wire (with contribution from the plastic tube) and spring components were defined separately, and the effect of the various cross-sectional diameters was captured by adopting different added mass and drag coefficients for each component. Finally, the submerged floater of each mooring leg was designed to have the same mass, CoG, and geometrical dimension as in the full-scale prototype.

*Measured parameters and instrumentation*

In total, six parameters of the system were measured during the experiments:

1. Motion of the WEC buoy in six DoFs.
2. Forces on the upper and lower side of the heave plate.
3. Six-DoF motion of the floater on one mooring leg.
4. Forces at the upper ends of both segments for all three mooring legs.
5. Acceleration at the three fairleads in the three translational DoFs.
6. Water surface elevation.

Among the six quantities, parameters 1 and 2 are of concern for WEC motion and thus power absorption analysis. Parameters 3 and 4 correspond to the motion and structural responses of the mooring lines, which are critical for fatigue damage evaluation. Parameter 5 served as a redundant measurement that can be used to derive the 6-DoF acceleration of the WEC buoy and the motion at the three fairleads. Finally, parameter 6 was used to ensure that the generation of waves satisfied the target value according to the test programme. All measurements were sampled at a frequency of 25 Hz, which ensured reliable and sufficient data collection from the entire measurement system used in the experiments.

Figure 9 shows an overview of the instrumentation on the WEC system for the abovementioned measurements. The product information of each instrument and the installation details for the system can be found in Paper IV. To ensure that the installation of the instruments did not affect the motion response of the WEC system, the contribution of the weight from all instruments was included during the mass calibration of the WEC buoy. Special attention was paid to the instrumentation to measure the floater's motion. Only the motion of one floater was measured. In addition, because the floater was submerged below the water surface and because the motion measurement can only be taken above the water surface, a long, light rod was attached to the floater, and measurements were taken from the upper end of the rod; see Figure 9(c). For that specific floater attached to a long rod, its mass and CoG were calibrated together with the contribution from the rod. In addition, a sensitivity study was performed prior to the main test scheme, which indicated that the dynamics of the WEC system were not affected by the instrumentation. The results of this sensitivity study can be found in Paper IV.

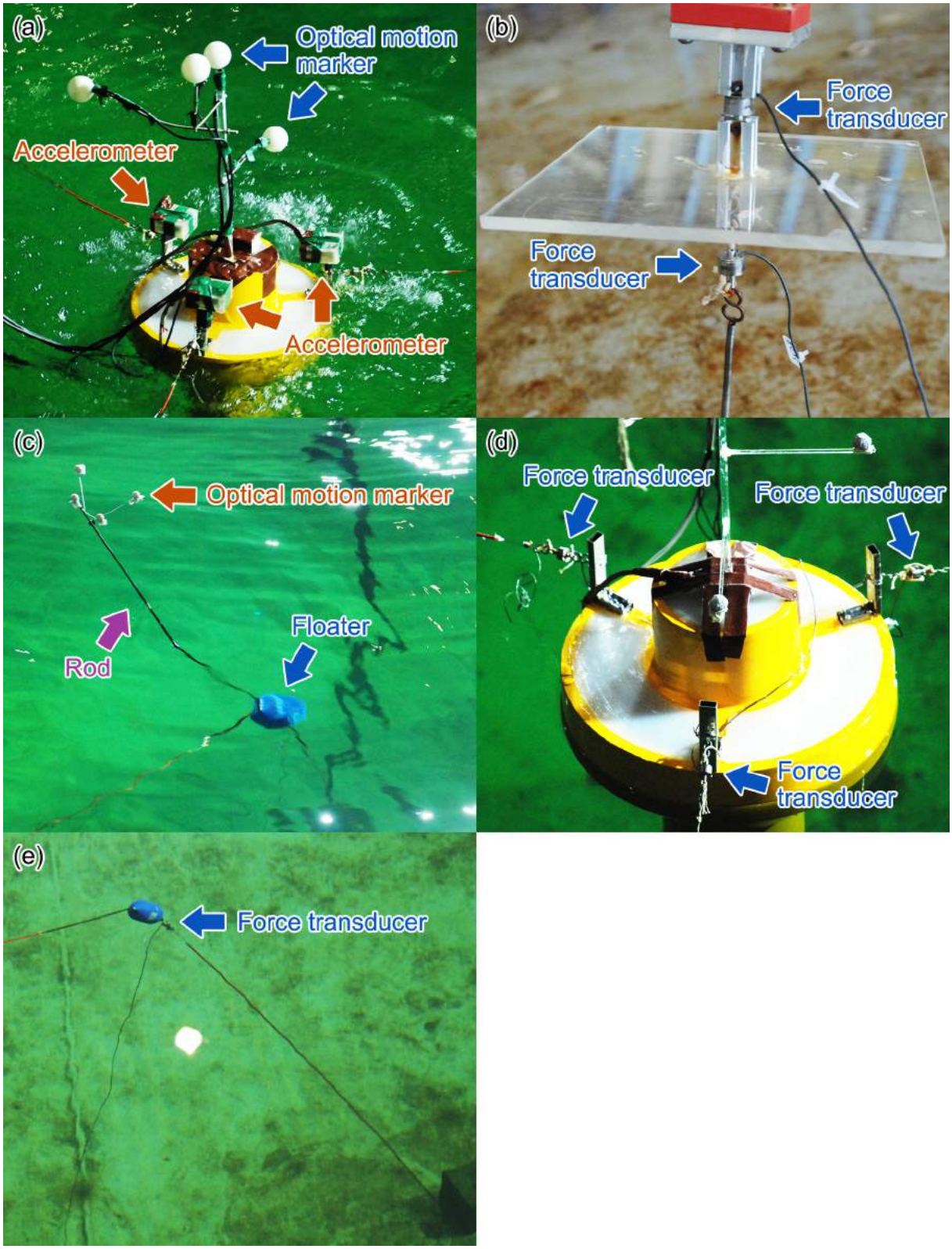


**Figure 9.** Instrument installation in the WEC system: (a) optical motion markers at the upper deck of the WEC buoy and accelerometers at the fairlead of the three moorings; (b) force transducers on the upper and lower sides of the heave plate used in the PTO system; (c) optical motion markers on the upper end of the rod, which attaches to the floater; (d) force transducers at the fairlead of each mooring leg; and (e) force transducer on the upper end of the lower mooring segment.

*Test programme*

The test programme encompassed tests of the mooring stiffness, decay, and various operational and survival loading conditions. The first two parameters were tested under calm water conditions to examine how well the system's basic properties were represented by the numerical model. In contrast, the predictive capability of the numerical model for the dynamic responses of the WEC system was investigated by testing the system under various loading conditions.

Table 4 presents all loading conditions tested during the experiment. Each loading condition represents a specific wave and ocean current scenario; no wind load was considered. All loading conditions were divided into two categories: operational and survival conditions. The survival conditions, cases $\text{Curr}_{36}$, SURV, and $\text{SURV}_\text{c}$, were tested at a model scale of 1:36. All other cases were regarded as operational conditions and tested at a model scale of 1:20.

Both regular and irregular wave cases were included in the test programme. For a regular wave case, the WEC system was excited by a regular wave with a constant wave height and wave period throughout the entire test. The wave periods of regular waves were chosen to be identical to (Re3 – Re5), near (Re2 and Re6), and far from (Re1 and Re7) the resonant period of the unmoored WEC buoy. Then, the wave heights of regular wave cases were determined such that they covered the ranges between linear (Re1-Re3 and Re6-Re7), intermediate (Re4), and nonlinear (Re5) waves. The distinction between linear and nonlinear waves was evaluated by the ratio of the wave height and wave length following the definition of Chakrabarti (1987b). The seven regular wave cases were used to investigate the limitation on the domain of validity of the numerical model with regard to the WEC responses under resonance and to examine the validity of using Airy wave theory for nonlinear wave loading conditions.

For the irregular wave case, the WEC system was excited by irregular waves with varying wave height and wave period throughout the time period. Each irregular wave was defined by the peak wave period ($T_\text{p}$) and significant wave height ($H_\text{s}$) to represent a specific sea state. All irregular waves followed the JONSWAP spectrum, with the peak enhancement factor ($\gamma$) set to 2.4. The sea states were chosen from the wave scatter diagram near Runde, where the full-scale prototype was installed. The OP1 case was defined as the optimum operation condition for the installed WEC system because this case approximates the WEC resonance period and because its probability of occurrence is high in Runde. In contrast to OP1, case OP2 was chosen to be off the resonance period of the unmoored WEC buoy. The WEC system was tested in greater detail under condition OP1, which included an investigation of the effect of the loading direction ($\text{OP1}_\text{d}$), the effect of the wave-current combined loads ($\text{OP1}_\text{c}$), and the effect of the PTO system ($\text{OP1}_\text{n}$).

The combination of wave-current environmental loads can significantly affect the motion response of the entire WEC system and the force response of a sub-component in such systems; see discussions by Barltrop et al. (2006), Johanning et al. (2007), Mazarakos & Mavrakos (2013), and Saruwatari et al. (2013). A similar observation was made in Paper III, which shows that the loads from the ocean currents are of great importance for the fatigue characteristics of mooring lines. Therefore, a current with constant velocity and slab profile over the water depth was tested, where the chosen velocity was established as the design value for the installed full-scale prototype WEC system.

**Table 4.** Summary of tested wave and current scenarios, presented as full- and model-scale values. All cases are operational conditions tested at a model scale of 1:20, except for cases $Curr_{36}$, SURV, and $SURV_c$, which are survival conditions tested at a model scale of 1:36.

| Case name | Regular or irregular waves* | Regular wave period ($T_w$) or peak wave period ($T_p$) | | Regular wave height ($H_w$) or significant wave height ($H_s$) | | Current velocity ($V_{curr}$) | | Wave and current direction ($Dir_{wave}$ and $Dir_{curr}$)** |
|---|---|---|---|---|---|---|---|---|
| | | Full scale | Model scale | Full scale | Model scale | Full scale | Model scale | Full and model scale |
| | | [s] | [s] | [m] | [m] | [m/s] | [m/s] | [deg] |
| Re1 | Regular | 3.185 | 0.712 | 0.238 | 0.012 | – | – | 0 |
| Re2 | Regular | 5.370 | 1.201 | 0.675 | 0.034 | – | – | 0 |
| Re3 | Regular | 6.370 | 1.424 | 0.950 | 0.048 | – | – | 0 |
| Re4 | Regular | 6.370 | 1.424 | 1.900 | 0.095 | – | – | 0 |
| Re5 | Regular | 6.370 | 1.424 | 3.801 | 0.190 | – | – | 0 |
| Re6 | Regular | 7.370 | 1.648 | 1.272 | 0.064 | – | – | 0 |
| Re7 | Regular | 12.740 | 2.849 | 3.679 | 0.184 | – | – | 0 |
| OP1 | Irregular | 6.5 | 1.453 | 2.5 | 0.125 | – | – | 0 |
| $OP1_d$ | Irregular | 6.5 | 1.453 | 2.5 | 0.125 | – | – | 180 |
| $OP1_c$ | Irregular | 6.5 | 1.453 | 2.5 | 0.125 | 0.514 | 0.115 | 0 |
| $OP1_n$*** | Irregular | 6.5 | 1.453 | 2.5 | 0.125 | – | – | 0 |
| OP2 | Irregular | 9.6 | 2.147 | 4.5 | 0.225 | – | – | 0 |
| Curr | – | – | – | – | – | 0.514 | 0.115 | 0 |
| $Curr_{36}$ | – | – | – | – | – | 0.514 | 0.086 | 0 |
| SURV | Irregular | 13.8 | 2.3 | 9 | 0.25 | – | – | 0 |
| $SURV_c$ | Irregular | 13.8 | 2.3 | 9 | 0.25 | 0.514 | 0.086 | 0 |

*A regular wave is defined by the wave period ($T_w$) and wave height ($H_w$), while an irregular wave is defined by the peak wave period ($T_p$) and significant wave height ($H_s$). All irregular waves follow the JONSWAP spectrum, with the peak enhancement factor ($\gamma$) set to 2.4.

**The definition of the loading direction in relation to the orientation of the WEC system is shown in Figure 10.

***The test condition of $OP1_n$ is the same as that for OP1 except that the PTO system is removed in $OP1_n$.

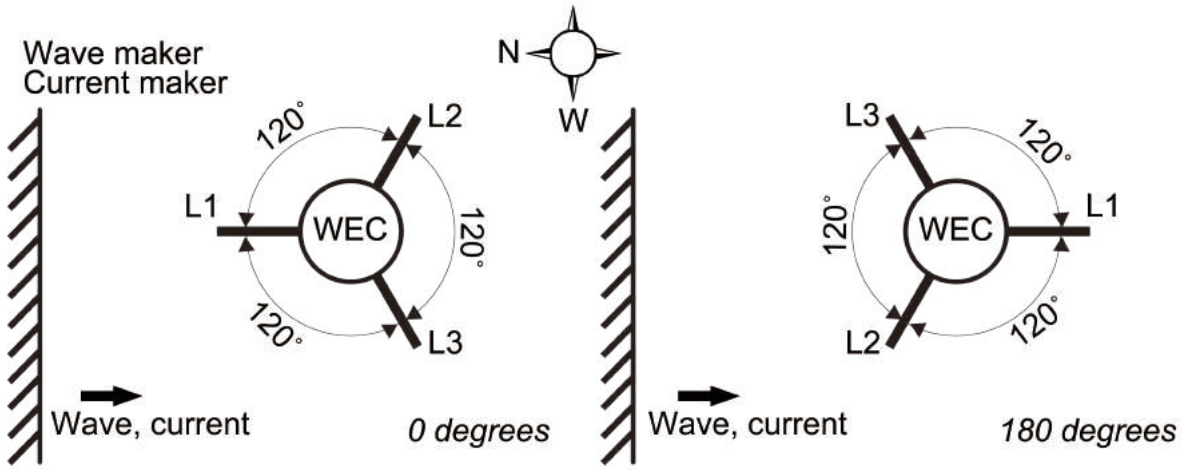


**Figure 10.** Orientation of the WEC system for loads coming from the direction of 0 degrees (left) and 180 degrees (right).

The survival loading condition was determined by considering several factors: (1) the wave scatter diagram near Runde where the full-scale prototype was installed and the generation capacity of the wave and current makers at the ocean basin and (2) the measurement range of the instruments for the WEC's motions and mooring forces. Finally, a 1:36 scale model was built to test a survival condition consisting of a peak wave period of 13.8 seconds and a significant wave height of 9 metres at the full scale.

## 4.2 Full-scale installation

One of the objectives of this thesis was to develop a simulation model for floating point-absorbing WECs, which can be used to assess the fatigue characteristics of mooring lines and power cables and to analyse the WEC's motions for power performance calculation. Section 4.1 presents ocean basin experiments used in a validation study of the simulation model. In this section, another important asset to the thesis project is presented. An industrial collaboration with the WEC development company Waves4Power offered an opportunity to compare results using the developed simulation model with results from full-scale measurements on their WEC system prototype WaveEL 3.0.

In early 2016, the company Waves4Power installed their concept WaveEL 3.0 at full scale in Runde for proof of concept with regard to functionality, survivability, and reliability (Waves4Power, 2018b). The installed WEC operated under a measurement campaign from June to November 2017. The following sub-sections describe the WaveEL 3.0 installation in Runde, the parameters that were measured and monitored, and how the numerical simulation model was adapted to be similar to the full-scale installation.

*WaveEL 3.0 installation*

The system was installed at approximately 5 degrees east longitude and 62 degrees north latitude. The location is just outside the island of Runde, and the distance between the installed

system and the nearest coastline of the island is approximately 0.8 kilometres. Figure 11 presents a photograph of the installation site.

**Figure 11.** WaveEL 3.0 installation in Runde, Norway. The WEC and two of its mooring legs are shown to the left, and the hub is shown to the right. The power cable between the two is submerged.

The system consists of a floating point-absorbing WEC that extracts energy from waves, primarily from heave motions. The installed capacity of the WEC system is 125 kW. The WEC has a three-leg taut mooring system. Each mooring leg has two segments joined by one floater, which is designed to be submerged at all times. The power generated by the WEC is transmitted to a power-gathering hub through a dynamic low-voltage (<1 kV) power cable. The dynamic cable is submerged and is designed to operate in a free-hanging state between the WEC buoy and the hub. At the hub, the power is transformed to a high voltage of 22 kV and then transmitted to the shore-based power grid via a subsea power cable. The hub itself has a single-leg taut mooring system; the mooring system is designed to maintain the hub in a stationary position. All of the mooring legs (three mooring legs for the WEC and one mooring leg for the hub) are anchored to the seabed by gravity anchors, where the depths of anchors vary between 50 and 80 metres due to the non-uniform seabed. Illustrations and the orientation of the WEC system installation are presented in Figure 12.

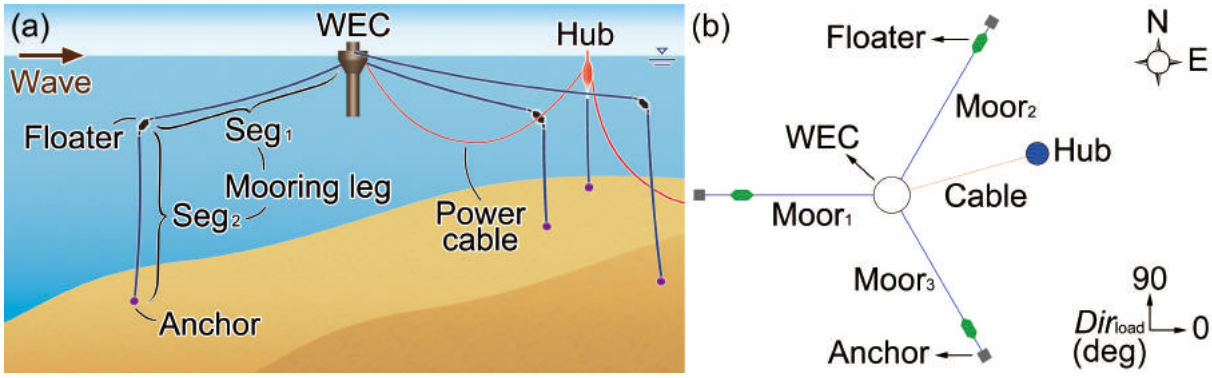


**Figure 12.** Illustration of the WaveEL 3.0 installation in Runde: (a) profile and (b) top views of the system without the subsea cable. The compass with symbols N (north) and E (east) in Figure 12(b) indicates the geographic orientation of the installation.

*Instrumentation of the WEC*

Waves4Power instrumented the WEC system with a large number of sensors that measure and monitor the performance of the system, its characteristics and its responses. Table 5 presents a summary of the measurement data provided to the Chalmers University of Technology within this thesis project to compare with results obtained from the numerical simulation model.

**Table 5.** Summary of WaveEL 3.0 measurement and instrumentation data provided by Waves4Power for this thesis project.

| **Measured quantity** | **Instrument** | **Measurement accuracy** | **Data sampling frequency*** | **Measurement duration** | **Installed position on the system** |
|---|---|---|---|---|---|
| Position of the WEC represented by north, east, and down with respect to the original installed position | GNSS sensor using a JAVAD receiver and a Leica antenna | < 3 cm | 2 Hz | 13 – 19 June 2017 | Upper deck of the WEC buoy |
| Pitch and roll motions of the WEC | MEMSIC vertical gyro sensor VG350 | < 0.75 deg | 2 Hz | 13 – 19 June 2017 | Upper deck of the WEC buoy |
| Position of the hub represented by north, east, and down with respect to the original installed position | u-blox GPS sensor | 2.5 – 5.0 m | 1 Hz | 2 – 19 June 2017 | Near the top of the hub |
| Pitch and roll motions of the hub | MEMSIC vertical gyro sensor VG350 | < 0.75 deg | 10 Hz | 1 – 19 June 2017 | Near the top of the hub but slightly below the u-blox GPS sensor |
| Force in the mooring lines | Dacell compression load cell | < 10 N | 10 or 60 Hz** | 1 June – 3 July 2017 | Near the fairleads of the mooring lines |

*The frequency refers to the sampling frequency of the provided data rather than to the original measurement frequency of the sensors.

**The data provided consist of two sampling frequencies, with part of the data provided at a frequency of 10 Hz and the other part provided at a frequency of 60 Hz.

Transformation of the measurement data from the sensors to time histories, which enabled comparison with the results from the numerical simulations, was carried out in another project conducted in parallel to the thesis project; see Lang et al. (2018) for more details. The time series data for the WEC's motions in three translational DoFs and the axial force of the moorings $Moor_1$ and $Moor_2$ were then used in this thesis project. Due to a lack of a clear coordinate definition for the vertical gyro sensor, a comparison of the rotational DoFs of the WEC is left to future work. Unreliable measurement data (a malfunction of the load cell) were found in the load cell for $Moor_3$; therefore, no data were used for that specific mooring leg. The measurement data from the hub were not used at all due to poor resolution and accuracy of the results from its sensors.

The environmental conditions in Runde were not recorded during the measurement period. A methodology that estimated the environmental loads to which the WEC system was subjected was therefore developed based on the responses measured by the sensors; see Lang et al. (2018) for details. The identification of the sea states required both a statistical analysis of the measurement data from the WEC motions and results from numerical simulations using the simulation model of the WaveEL 3.0 installation developed in this thesis project. After the evaluation of the measurement data and the results from the numerical simulations, three stationary sea states were identified; see Table 6. Note that no current or wind loads were included, as the sea states identified during the measurement period were considered calm sea conditions. The three stationary sea states presented in Table 6 served as the basic input to the environmental load modelling in the numerical simulations, and the corresponding measurement data were used for comparison in this thesis. Due to the lack of direct measurement of the environmental conditions, a sensitivity study relevant to the uncertain loading conditions was also performed in this thesis; see Section 5.6.2. A detailed investigation of the sources of the uncertainties was presented by Lang et al. (2018).

**Table 6.** Dates, durations, and wave conditions of the stationary sea states identified from the measurement data.

| **Date** | **Time span** | $\boldsymbol{H_s}$ **[m]** | $\boldsymbol{T_p}$ **[s]** | $\boldsymbol{Dir_{wave}}$ **[deg]**[*] |
|---|---|---|---|---|
| 16 June 2017 | 10:00 – 13:00 | 0.95 | 10.00 | 30 |
| 18 June 2017 | 08:00 – 11:00 | 1.40 | 6.75 | 30 |
| 19 June 2017 | 15:00 – 18:00 | 1.75 | 7.50 | 30 |

[*]Direction of the wave, whose definition can be found in Figure 12(b).

*Simulation model of WaveEL 3.0*

A numerical model of the WaveEL 3.0 installation was built following the modelling principles presented in Papers I – III. The model consisted of a WEC buoy, a three-leg taut mooring system, a power cable, and a hub located at a spatially fixed point. Although minor motions of the hub could be observed from the measurement data, it was assumed that the hub could be considered and modelled as a stationary object. Table 7 presents the main properties that define the numerical model of the WaveEL 3.0 system. These properties, except for $B_{\mathrm{PTO}}$, were retrieved from Waves4Power from their installation of WaveEL 3.0. The PTO system was modelled according to the simplified model presented in Sections 3.1 and 3.3, i.e., the PTO system was modelled as a linear damper and as a Morison model to account for the drag

damping effect. Note that Table 7 does not present the full set of parameters required to define the numerical simulation models. The reader is referred to Papers I, III, and V for additional properties, such as the drag and added mass coefficients for the moorings and cables and the kinematic viscosities of air and water.

**Table 7.** Main properties of the installed WEC system WaveEL 3.0 considered in the numerical model.

| **WEC** | |
|---|---|
| Mass, $M_{\mathrm{WEC}}$ [metric tonnes] | 268.42 |
| Draft, $D_{\mathrm{WEC}}$ [m] | 15.265 |
| CoG ($x$, $y$, $z$) [m] | (0, 0, -5.248) |
| CoB ($x$, $y$, $z$) [m] | (0, 0, -4.974) |
| PTO damping in the heave DoF, $B_{\mathrm{PTO}}$ [kNs/m] | 40.180 |
| **Mooring system*** | |
| Lengths of two segments of mooring leg $\mathrm{Moor}_1$, ($L_{\mathrm{Moor}_1,\mathrm{Seg}_1}$, $L_{\mathrm{Moor}_1,\mathrm{Seg}_2}$) [m] | 96.0, 76.6 |
| Lengths of two segments of mooring leg $\mathrm{Moor}_2$, ($L_{\mathrm{Moor}_2,\mathrm{Seg}_1}$, $L_{\mathrm{Moor}_2,\mathrm{Seg}_2}$) [m] | 98.0, 56.5 |
| Lengths of two segments of mooring leg $\mathrm{Moor}_3$, ($L_{\mathrm{Moor}_3,\mathrm{Seg}_1}$, $L_{\mathrm{Moor}_3,\mathrm{Seg}_2}$) [m] | 113.0, 44.0 |
| Anchor radii of the three mooring legs, ($r_{\mathrm{Anchor}_1}$, $r_{\mathrm{Anchor}_2}$, and $r_{\mathrm{Anchor}_3}$) [m]** | 127.3, 122.49, 132.1 |
| Anchor depths of the three mooring legs, ($h_{\mathrm{Anchor}_1}$, $h_{\mathrm{Anchor}_2}$, and $h_{\mathrm{Anchor}_3}$) [m]*** | 86.6, 66.6, 54.1 |
| Cross-sectional outer diameter, $d_{\mathrm{Moor}}$ [m] | 0.08 |
| Mass of each mooring segment, $M_{\mathrm{Moor}}$ [kg/m] | 4.9 |
| Mass of each anchor, $M_{\mathrm{Anchor}}$ [kg] | 40000 |
| Axial stiffness, $EA_{\mathrm{M}}$ [MN] | Represented by the load-elongation diagram in Figure 13 |

*The names of the various components in the mooring systems can be found in Figure 12.

**The anchor radius ($r_{\mathrm{Anchor}}$) is defined as the horizontal distance between the geometric centre of the WEC at its still-water plan and the anchor point of each mooring leg.

***The anchor depth is defined as the vertical distance between the still water surface and the anchor point of each mooring leg.

**Table 7.** (Continued)

| | |
|---|---|
| **Power cable** | |
| Horizontal distance between the WEC and the hub, $d_{\mathrm{WEC-Hub}}$ [m] | 100 |
| Length of the power cable, $L_{\mathrm{Cable}}$ [m] | 135 |
| Cross-sectional outer diameter, $d_{\mathrm{Cable}}$ [m] | 0.038 |
| Mass, $M_{\mathrm{Cable}}$ [kg/m] | 2.3 |
| Axial stiffness, $EA_{\mathrm{C}}$ [MN] | 4.7 |
| Bending stiffness, $EI_{\mathrm{C}}$ [Nm$^2$] | 5 |
| Torsional stiffness, $GK_C$ [Nm$^2$/rad] | 3 |
| | |
| **Bending stiffener** | |
| Density, $\rho_{\mathrm{B}}$ [kg/m$^3$] | 1200 |
| Cross-sectional inner diameter, $d_{\mathrm{B_{in}}}$ [m] | 0.038 |
| Cross-sectional inner diameter, $d_{\mathrm{B_{out}}}$ [m] | Varying along the entire bending stiffener; see the illustration in Figure 14 |
| Young's modulus, $E_{\mathrm{B}}$ [MPa] | 14.0 |
| Shear modulus, $G_{\mathrm{B}}$ [MPa] | 4.67 |
| | |
| **Environment** | |
| Still water mean level, $Z$ [m] | 0 |
| Water depth, $h_{\mathrm{Seabed}}$ [m] | 86.6 |

The seabed was modelled as a horizontal plane due to a limitation of the SESAM package, which does not allow for inclined planes. The depth of the seabed, and thus the water depth ($h_{\mathrm{Seabed}}$), was taken to be the maximum gravity anchor depth of the three mooring legs. The different mooring lengths (i.e., anchor positions at different water depths) were considered by assigning each gravity anchor a specific depth. Because the taut mooring system in the full-scale installation was designed to never come in contact with the seabed, the modelling approach for the seabed and the mooring configuration was considered acceptable. Furthermore, the gravity anchors for the mooring system were designed to be spatially fixed. Therefore, the three anchor points were represented as six-DoF fixed points in the numerical model.

One issue arose regarding the definition of the axial stiffness of the mooring lines. The moorings used in the WEC system WaveEL 3.0 were made of polyester, which exhibits nonlinear material behaviour. In this thesis, only the nonlinear relation between the axial load and elongation was considered; this relation was used to determine the axial stiffness properties of the moorings. In the numerical model, the axial stiffness was defined by several points on a load-elongation diagram as shown in Figure 13; a pointwise linear relation was assumed between every two neighbouring points in the diagram.

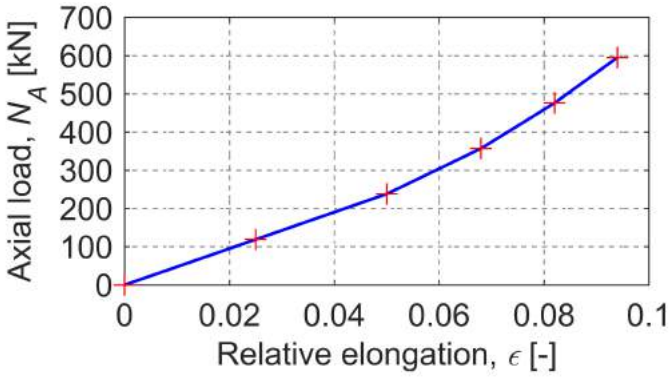


**Figure 13.** Axial stiffness of the moorings ($EA_{\mathrm{M}}$) described in terms of a load-elongation diagram. The red crosses shown in the diagram represent the exact data points (determined by a monotonic loading test) used to define the mechanical properties of the mooring lines, whereas the blue solid line is the curve interpolated by the software describing the strain characteristics of the modelled mooring material.

The two ends of the power cable were covered by bending stiffeners to protect the cable from large bending (large curvature) and from contacting the WEC or the hub. The bending stiffeners were included in the simulation model with the geometry and dimensions presented in Figure 14. The larger cross-section of the bending stiffeners was attached to the WEC and the hub. Other material properties for the bending stiffeners are presented in Table 7.

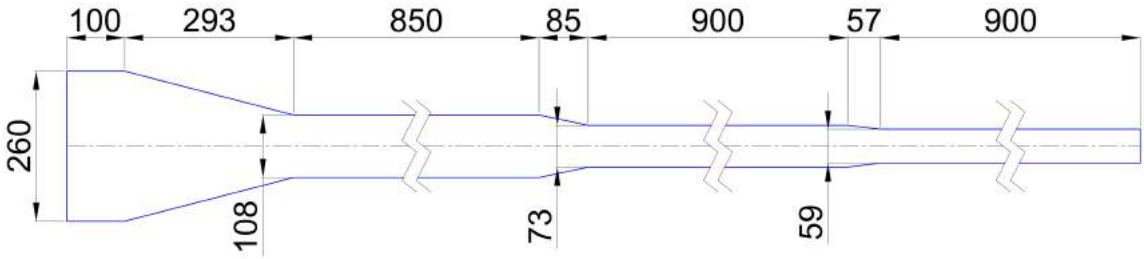


**Figure 14.** Bending stiffener geometry. The bending stiffener has a hollow core with a cross-sectional inner diameter of 38 millimetres (units: millimetres). (Courtesy of Waves4Power.)

The sea states presented in Table 6 were simulated using the JONSWAP spectrum, with the peak enhancement factor set to 2.4, following the practice recommended by DNV GL (2017a). The duration of each stationary sea state was taken as three hours. In addition, to account for the potential uncertainty in the identified sea states, parametric analyses were carried out with regard to $Dir_{\mathrm{wave}}$ and the realisation of the waves; see the results discussion in Section 5.6.2. Finally, because no visible biofouling was observed from the on-site inspection of the WaveEL 3.0 installation, all of the structural properties of the WEC buoy, moorings and cables were modelled as a biofouling-free condition, i.e., the original design properties of each structure were used to define the numerical model to represent the WaveEL 3.0 installation at Runde.

# 5 Example of results and discussion

This chapter presents sample results obtained from the appended Papers I – V and additional simulations that support the goals of the thesis. The chapter is divided into six sections in which sample results from numerical simulations and analyses are presented and discussed: hydrodynamic and structural response of the WEC system (Section 5.1), stress and fatigue evaluation of the moorings and cables (Section 5.2), analysis of power absorption (Section 5.3), parameter sensitivity analysis (Section 5.4), and LCoE analysis (Section 5.5). The results from the experimental and full-scale measurement studies are presented and discussed in Section 5.6.

It should be noted that throughout this thesis, the design of the reference concept configuration was altered, as were some of the properties of the WEC system's components. In each of the appended papers, it is clear which WEC system was modelled and studied. It should, however, be highlighted that these changes did not affect the choice of numerical method or simulation procedure or the conclusions of this thesis. In addition, Figure 15 presents a schematic overview of the studied WEC configurations in appended Papers I – V, and Table 8 provides an overview of the model details, including those of the full-scale installation model of WaveEL 3.0 in Runde. As an introduction to the forthcoming sub-sections, the reader should pay attention to the following issues:

- The Waves4Power WEC concept WaveEL was used in the majority of the appended papers, except in Paper I, in which a simple cylinder was used. Note, however, that the detailed geometry and mass distribution of the WaveEL concept vary among all the appended papers as development of this WEC continued during the thesis work. The numerical model of the WEC buoy for the full-scale installation is the same as that for the one modelled in Paper V.
- An ideal linear PTO system was used throughout the thesis. However, the exact numerical model of the PTO system varied among the papers. In Paper I, the PTO system was represented solely as a linear damper. In Paper IV, the PTO system was represented by a linear damper, a Morison model, and an FE model to mimic the entire experimental setup. Finally, the PTO system in Papers II, III, and V and that of the WaveEL 3.0 installation was represented by a linear damper and a Morison model.
- Catenary spread mooring systems were studied in Papers I – III, whereas a taut mooring system similar to the WaveEL 3.0 installation in Runde was used in Papers IV and V.
- In Paper V and in the simulation model of WaveEL 3.0 (Section 4.2), the mooring lines were made of polyester material, which exhibits nonlinear load elongation, unlike the steel used in the mooring chains.
- Papers I – IV focused on a single WEC system. In Paper V, array configurations were studied using the simulation models and knowledge gained from Papers I – IV.
- The power cable was included in the simulation models in Papers II and III and in the full-scale installation simulation model of WaveEL 3.0. The end of the cable connected to the WEC included a model of a bending stiffener, and this end followed the motions of the WEC. The other end was connected to the hub, which was modelled as a spatially fixed structure. Furthermore, this end featured a bending stiffener model at the cable-hub connection point.
- Different environmental loads and factors were considered in the appended papers. However, all the irregular waves considered in this thesis followed the JONSWAP spectrum. Except for the wave loadings simulated for the ocean basin experiment and for the full-scale Runde installation, all other wave loadings were simulated with a peak enhancement parameter, $\gamma$, of 3.3. This value was suggested by DNV GL (2017a)

as the average value for the JONSWAP spectrum. The peak enhancement factors for the ocean basin experiment and for the full-scale Runde installation were both set to 2.4. The velocity of the ocean current was consistently modelled to be time-invariant but could vary as a function of depth. The wind loads were modelled following the NPD spectrum. A detailed investigation of the influence of biofouling was presented in Paper III, and the influence of wind loads was considered only in Paper V.

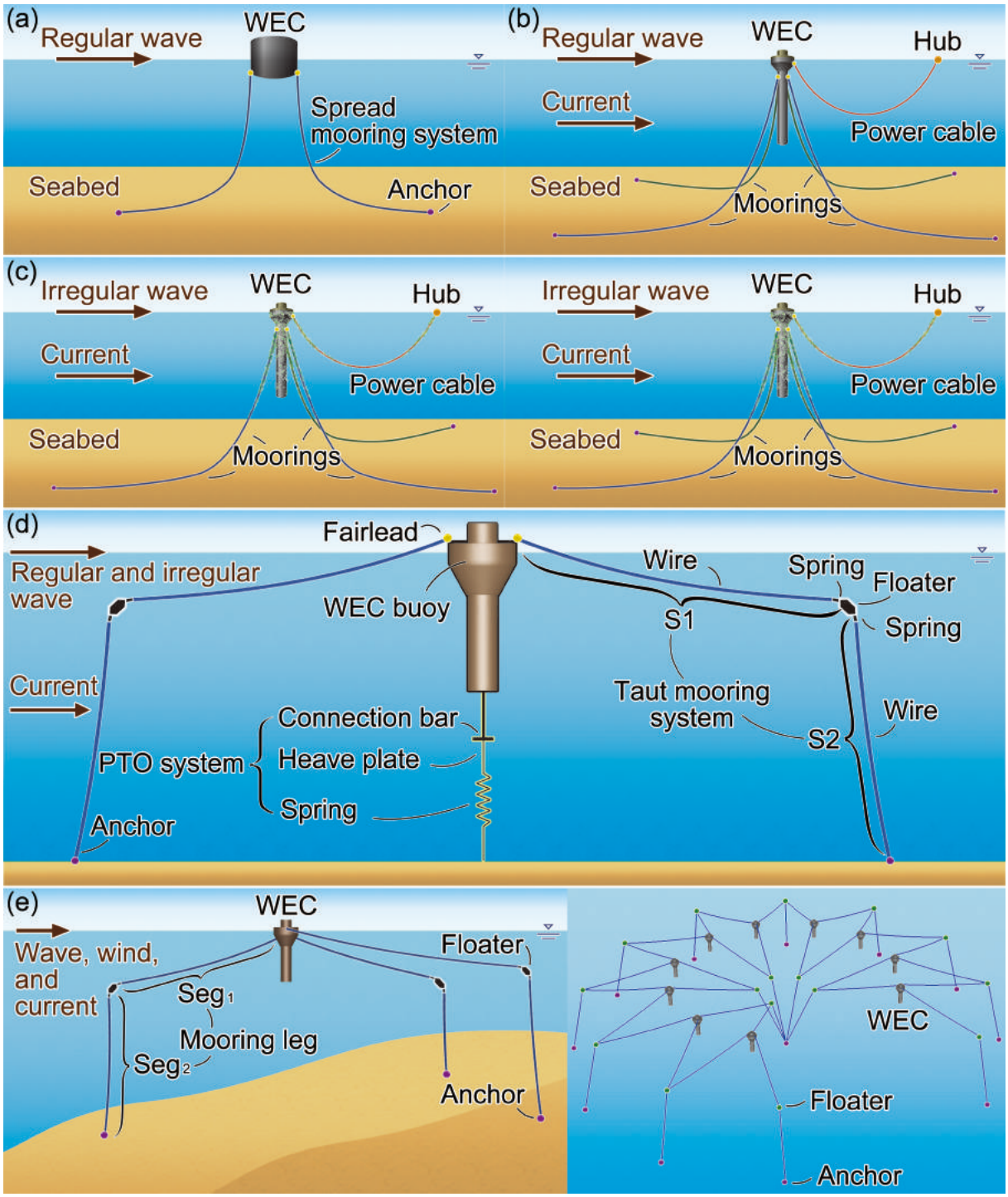


**Figure 15.** Case study systems in the appended papers: (a) Paper I, (b) Paper II, (c) Paper III, (d) Paper IV, and (e) Paper V.

**Table 8.** Overview of the WEC configurations studied in Papers I – V and in the full-scale installation. For the detailed properties of each component, the reader is referred to the appended papers.

| | **WEC** | **PTO system** | **Mooring system** | **Power cable** | **Environmental loads and factors** |
|---|---|---|---|---|---|
| Paper I | Generic cylinder | Linear damper | Four-leg catenary spread mooring chain system | Not considered | Regular waves |
| Paper II | Design concept from Waves4Power | Linear damper | Four-leg catenary spread mooring chain system | Free-hanging submerged power cable with simplified bending stiffeners | Regular waves, and ocean current |
| Paper III | Design concept from Waves4Power | Linear damper | Three- and four-leg catenary spread mooring chain systems | Free-hanging power cable without bending stiffener | Irregular waves, ocean current, and marine biofouling |
| Paper IV | Design concept from Waves4Power | Heave plate damper | Three-leg two-segment taut mooring system with a constant axial stiffness | Not considered | Regular and irregular waves, and ocean current |
| Paper V | Design concept from Waves4Power | Linear damper | A three-leg two-segment taut mooring system was used as the reference system. A shared mooring system was also considered for an array configuration. | Not considered | Irregular waves, ocean current, and wind |
| System for full-scale installation (Section 4.2) | Design concept from Waves4Power | Linear damper | Three-leg two-segment taut mooring system | Free-hanging submerged power cable with bending stiffeners | Irregular waves, ocean current, and wind |

## 5.1 Hydrodynamic and structural response analysis

Section 3.1 presents three simulation approaches that were used and compared in this thesis. The key differences among the three approaches are summarised below, whereas Table 2 provides a detailed comparison.

- **A1 – De-coupled analysis approach**
  Analysis of the WEC: time-domain analysis
  Analysis of the mooring line and power cable: static analysis in every time step
- **A2 – De-coupled analysis approach**
  Analysis of the WEC: frequency-domain analysis
  Analysis of the mooring line and power cable: quasi-static analysis in the time domain
- **A3 – Coupled analysis approach**
  Analysis of the WEC: time-domain analysis
  Analysis of the mooring line and power cable: dynamic analysis in the time domain

Approaches A2 (de-coupled) and A3 (coupled) were compared in Paper I using a cylindrical WEC with a catenary mooring chain system, whereas approaches A1 (de-coupled) and A3 (coupled) were compared in Paper V using the WaveEL buoy with a taut mooring system. The reason for the comparisons in the different papers is provided in Section 3.1.

To gain an overall understanding of the similarities and differences between the three analysis approaches, the three approaches are compared in this section. Section 5.1.1 compares the simulated WEC motion of single-unit WEC configurations, while Section 5.1.2 compares the simulated motion and force responses of moorings. A comparison of the simulated multiple WECs in an array is presented in Section 5.1.3.

### 5.1.1 Comparison of simulated WEC motion of single-unit WEC configurations

Figure 16 shows the motion of a WEC under a regular wave loading condition. The simulations were carried out under a regular wave condition with a regular wave height, $H_{\mathrm{w}}$, of 2 metres and a wave period, $T_{\mathrm{w}}$, of 7 seconds without ocean current or wind loads. Two WEC systems, one from Paper I and the other from Paper V, were simulated for comparison.

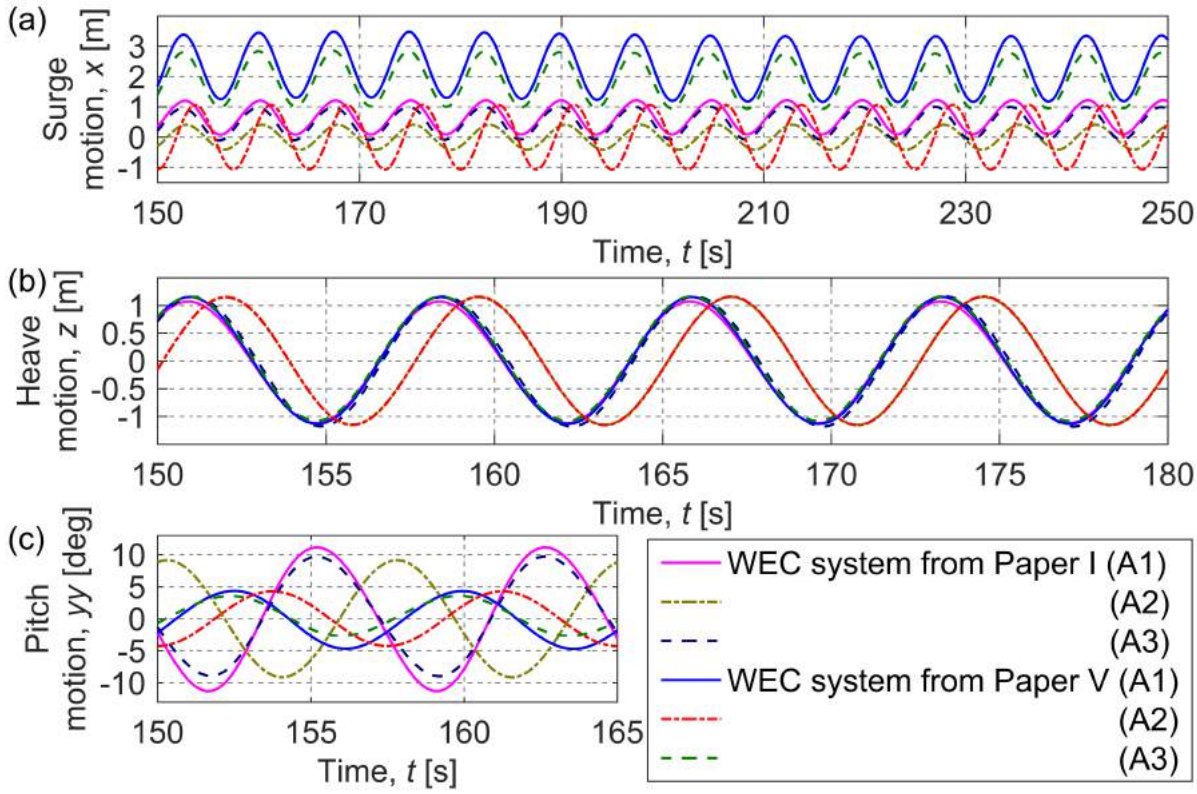


**Figure 16.** (a) Surge, (b) heave, and (c) pitch motions of the WEC under regular wave conditions consisting of $H_{\mathrm{w}} = 2$ m, and $T_{\mathrm{w}} = 7.5$ s.

Because the A2 (de-coupled) approach simulates the motion of the WEC using its first-order response amplitude operator (RAO) from the frequency-domain analysis, it does not account for the phase shift or any effect originating from the second-order force. The discrepancy in the phase shift can already be observed in Figure 16 under a regular wave loading condition. The steady-state component of the second-order force leads to mean wave drift, which can also be observed under a regular wave load condition. As shown in Figure 16(a), the mean values of the surge motion simulated by the A2 approach are close to zero. Conversely, both the A1 and A3 approaches capture the mean wave drift effect, resulting in a non-zero mean in the surge motion. Under the same loading condition, it was found that the WEC buoy discussed in Paper V often exhibits a larger mean wave drift than that discussed in Paper I. This observation was attributed to the fact that the WEC buoy in Paper V has a larger projected area normal to the wave loads.

Sample results obtained under irregular wave conditions align with the trend observed under the regular wave conditions with regard to the mean wave drift; see sample results in Figure 17. In Figure 17, the second-order wave forces in the horizontal direction of the three different WEC buoys were compared. As shown in Figure 17(b), the second-order wave force was generally larger for the WEC buoy from Paper V than that from Paper I. Furthermore, if one keeps the same mooring system as that used in Paper V and replaces the WEC buoy from Paper V (with a shorter tube) with the one from Paper IV (with a longer tube), a larger second-order wave force on the one from Paper IV is generally observed. A larger second-order wave force in the horizontal direction of the WEC buoy leads to a larger motion in the surge direction both in terms of the maximum and mean values; see Figure 17(c).

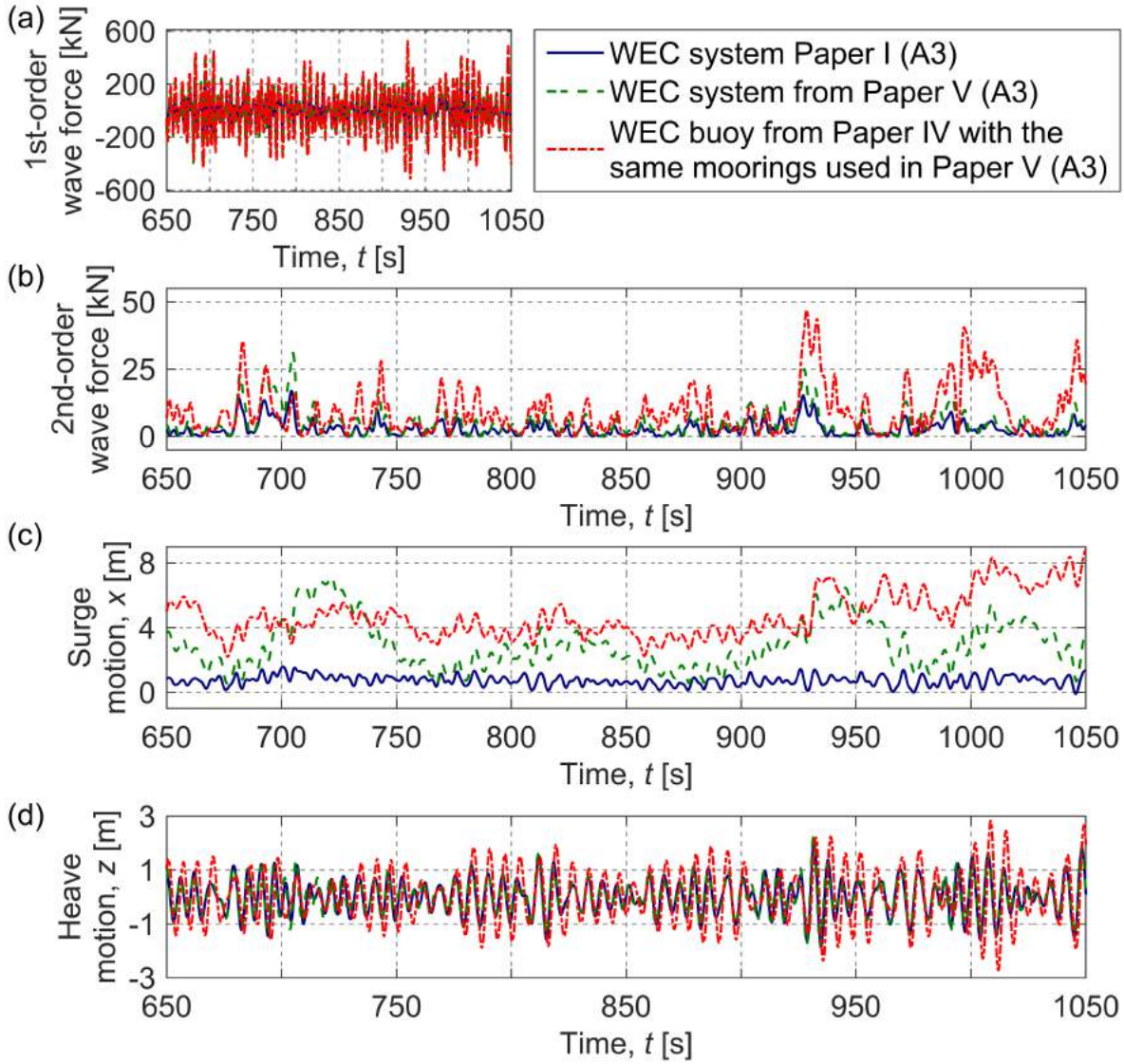


**Figure 17.** (a) First-order and (b) second-order wave forces in the horizontal direction of three WEC buoys under an irregular loading condition consisting of $H_s = 2.5$ m, $T_p = 7.5$ s, and $\gamma = 3.3$. $Dir_{wave}$ were defined as heading into the surge direction of the WEC buoy. The resulting WEC surge motions are presented in sub-figure (c). Sub-figure (d) shows the heave motion of the WEC over the same period.

Additionally, the second-order wave force may excite a large resonant response in the horizontal direction due to the slowly varying wave loads; see sample results in Figure 18. The WEC system simulated in Figure 18 is taken from Paper V, and the simulation was performed using three analysis approaches. As shown in Figure 18(a), in addition to the primary motions responding at the wave frequency, superimposed motions with a lower frequency were observed for the WEC motion simulated by the A1 and A3 approaches. The response spectrum of the surge motions shows that the peak value in the surge response spectrum occurs at the surge resonant frequency of the WEC system. This phenomenon is, however, not captured when using the A2 analysis approach. Hence, when using the A2 approach, an underestimation in the horizontal motion response of the WEC is expected, and this limitation is expected to be more crucial for the WEC buoy with a large projected area, as used in Papers IV and V.

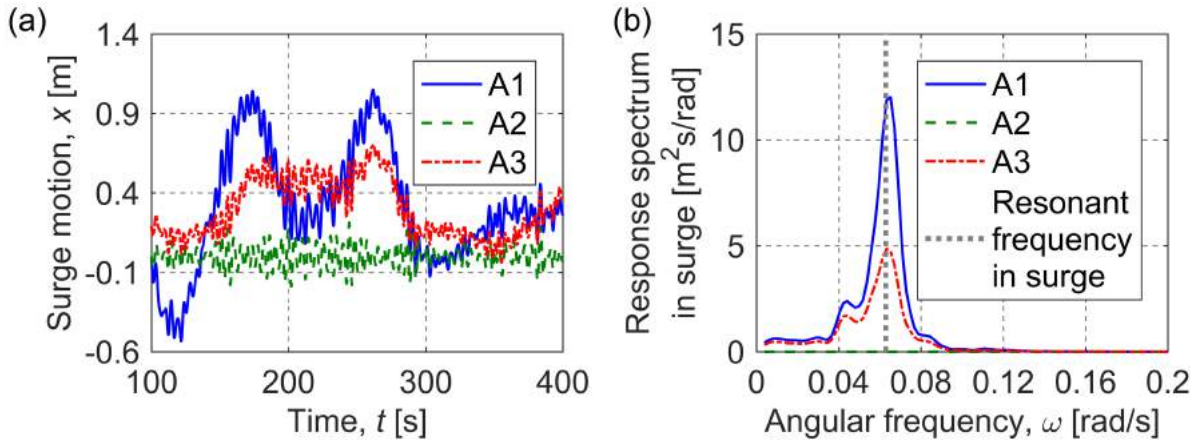


**Figure 18.** Comparison of the simulated surge motion of the WEC buoy from Paper V using three analysis approaches. Sub-figure (a) shows the time histories of the surge motion for a duration of 300 seconds, whereas the response spectrum from the three-hour simulation results is presented in sub-figure (b). An irregular loading condition was simulated, consisting of $H_{\mathrm{s}} = 0.5$ m, $T_{\mathrm{p}} = 4.5$ s, $\gamma = 3.3$, and $Dir_{\mathrm{wave}} = 0$ deg.

The three analysis approaches also varied with respect to the simulated heave motion of the WEC; see Figure 16 (b). Under a regular wave load condition, the WEC motion in the heave direction followed the encountered wave period. However, the heave response amplitude of the WEC calculated by the A3 (coupled) approach was smaller than the amplitudes calculated by the A1 and A2 (de-coupled) approaches. This discrepancy occurred because the A3 approach implicitly includes all the restoring, inertial, and damping effects of the mooring system. A similar observation was made for the heave motion of the WEC under irregular wave loading conditions; see one example in Figure 19. In fact, due to the absence of the dynamic effect from the mooring systems, it was also found during post-processing that for a large wave height, the WECs had unrealistically large vertical motions when the simulations were carried out using the de-coupled analysis approach A1 or A2.

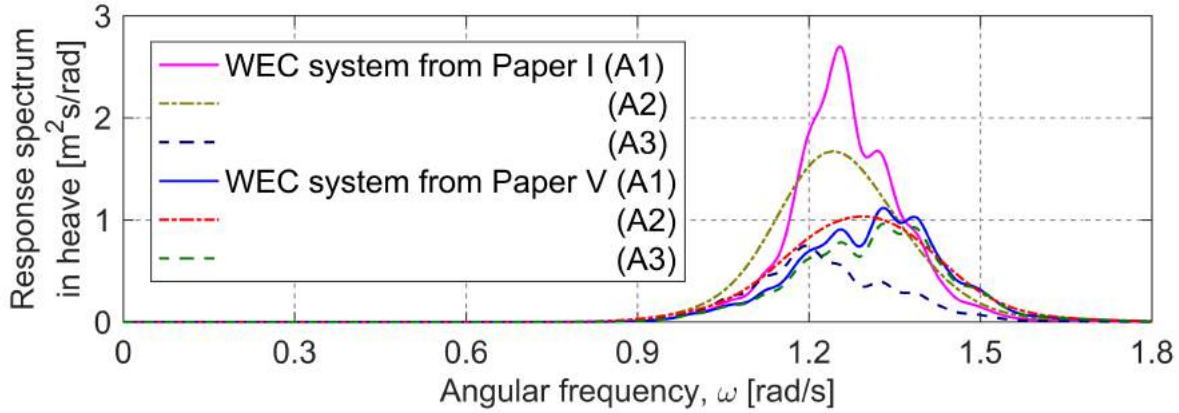


**Figure 19.** Response spectrum of the heave motion of the WEC buoy simulated by three analysis approaches. The duration of one simulation was three hours, with an irregular loading condition defined by $H_{\mathrm{s}} = 2.5$ m, $T_{\mathrm{p}} = 4.5$ s, and $\gamma = 3.3$.

As shown in Figure 16(b) and Figure 19, the discrepancy in the simulated heave motion between the three analysis approaches was found to be more evident in the WEC system from Paper I than in that from Paper V. The finding may be due to the different mooring configurations used in these two systems. As discussed by Harris et al. (2004), the catenary mooring system (such as that used in Paper I) presents a restraining stiffness in the vertical direction and thus affects the heave motion of a WEC, whereas the taut mooring system with floaters (used in Paper V) is purposely designed to minimise such an influence from the mooring system. Therefore, when a de-coupled analysis is used, the extent by which the heave motion of the WEC is overestimated is expected to be more noticeable for the WEC system from Paper I.

To conclude, the A2 approach is not able to account for the influence of second-order wave loads and phase shifts due to the exclusive use of the first-order RAO derived from the frequency-domain analysis for the WEC buoy. The limitation of the A2 approach is remedied by the A1 approach because the latter simulates responses of the WEC in the time domain. However, the A1 approach still exhibits issues with regard to the overestimated WEC motion due to the absence of a dynamic coupling effect from the mooring systems. Hence, from the standpoint of the WEC motion, the coupled analysis approach A3 is recommended in the numerical simulation.

### 5.1.2 Comparison of simulated motion and force responses of mooring lines

This section compares different analysis approaches with regard to the simulated motion and force responses of mooring lines. Note, however, that because of their similar slender geometric characteristics relative to the floating WEC, the conclusions drawn in this section for the moorings are regarded as also applicable to the power cables.

As discussed in Section 3.1, one shortcoming of the A1 (de-coupled) approach is that the response of moorings (as well as power cables) is solved using a static analysis in every time step. Because the WEC buoy was modelled as a rigid body and the fairleads of moorings were modelled as slave nodes to the WEC buoy, how large an effect this static analysis procedure has on the simulated fairleads' motions can be observed directly from the results presented in the previous section. The A1 approach in SESAM is not able to provide the motion response results along the entire length of mooring structures; hence, no further comparison was made with regard to the simulated motion of the moorings using the A1 approach.

Figure 20(a) presents the time histories of the simulated force response in a mooring line using the A1 and A3 approaches. The results show a large difference in the axial force response, where A1 does not capture the dynamic of the mooring lines' response. Furthermore, a mooring line fatigue analysis requires a histogram of the force ranges, which is presented in Figure 20(b). It was found that the force ranges are largely underestimated by the A1 approach because of the absence of the inertial loads due to the mooring system and the absence of the hydrodynamic loads acting on the mooring lines. The A1 approach was therefore deemed unsuitable to simulate the structural responses of the moorings and power cables.

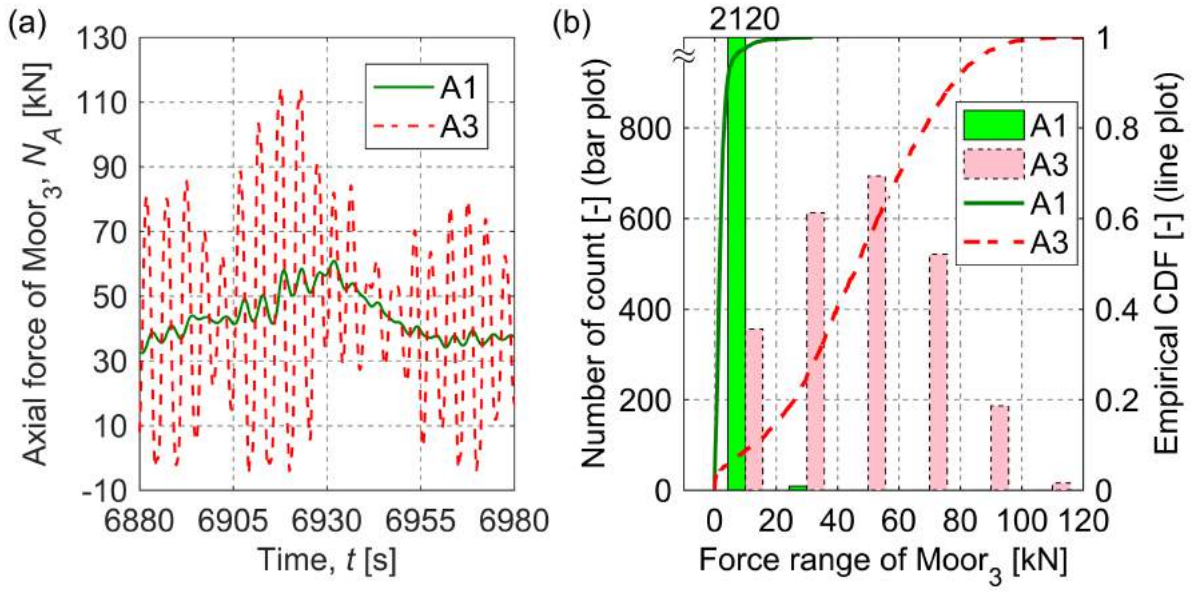


**Figure 20.** Comparison of results from simulations using the A1 (de-coupled) and A3 (coupled) analysis approaches: (a) the force response of a mooring line and (b) the force range histogram of the mooring line in Figure 20(a). A numerical model of the full-scale WaveEL 3.0 WEC installation was used. The duration of one simulation was three hours, with an irregular loading condition defined by $H_s = 1.5$ m, $T_p = 5.5$ s, and $\gamma = 3.3$. The ocean current velocity was set to $V_{curr} = 0.514$ m/s, and the wind load was $V_{wind} = 9$ m/s. All load directions coincided at $Dir_{load} = 90$ deg; see Figure 12.

In contrast, the A2 (de-coupled) and A3 (coupled) approaches are able to consider the hydrodynamic loading effect on mooring structures and to provide simulation results along the entire length of moorings. Thus, the two approaches could both potentially be used to study the structural response of moorings. Figure 21 presents sample results from Paper I for three points on the mooring leg that faces the encountered wave first: the fairlead point ($P_f$), the touchdown point ($P_t$), and the midpoint ($P_m$) between the fairlead and the touchdown points. The simulations were carried out under a regular wave condition with a regular wave height, $H_w$, of 2 metres and a regular wave period, $T_w$, of 7 seconds without ocean current or wind loads.

The motion responses of the three points on the mooring line are regular and follow the encountered wave period. For the motion responses in Figures 21(a) to (c), the maximum position $z$ of point $P_f$ determined by the A3 approach is somewhat lower than that determined by the A2 approach, and the trough to crest motions in the fairlead and midpoint points are smaller than those determined by the A3 approach. These results are attributed to the following: (1) the weight of the mooring lines pulling down the WEC and (2) the seabed friction and restoring force from the mooring line, both of which dynamically change the mean position of the WEC buoy and consequently the motion response of the mooring lines. These two effects can only be accounted for in the A3 approach. Figure 21(d) illustrates how the axial force responses in the same positions are affected.

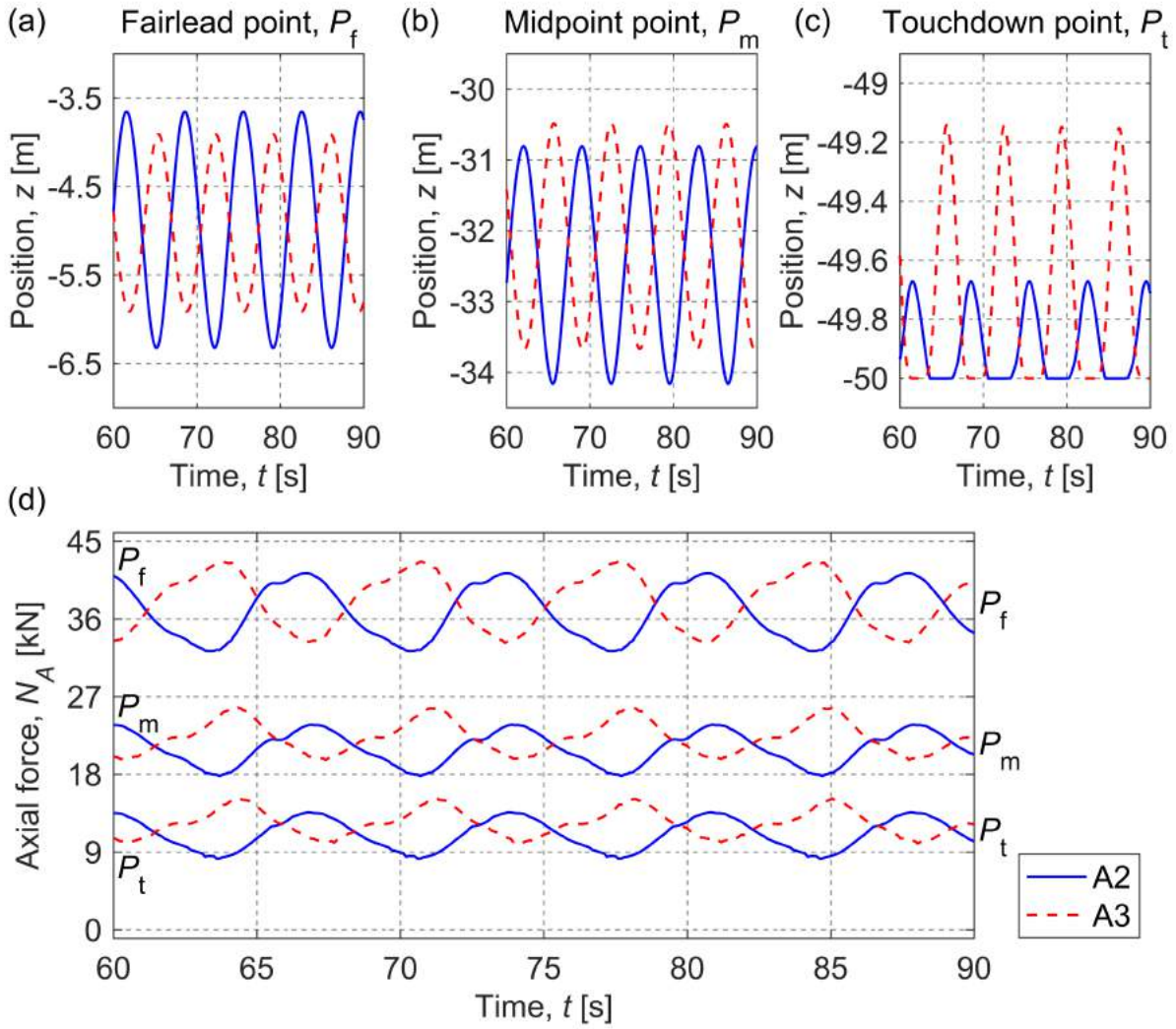


**Figure 21.** Harmonic motion in the vertical direction (sub-figures (a), (b), and (c)) and axial force (sub-figure (d)) responses of a catenary mooring chain simulated by the de-coupled (A2) and coupled (A3) analysis approaches. Three positions along a mooring leg are presented: the fairlead point ($P_f$), the midpoint ($P_m$), and the touchdown point ($P_t$). A regular wave condition was simulated, consisting of $H_w = 2$ m, and $T_w = 7$ s.

As discussed in Section 5.1.1, the A2 approach is not able to account for the second-order load effect or to capture low-frequency motion, and the approach may overestimate the vertical motion of a WEC under a large wave height condition. The combined effect of these limitations on the simulated mooring force under an irregular loading condition is presented in Figure 22. In this comparison, the WEC system from Paper I was simulated using the A2 and A3 approaches. Only the irregular wave load was considered in the simulation, and the duration of the simulation was set to three hours. The results were extracted from the fairlead point of the mooring line facing the encountered wave first.

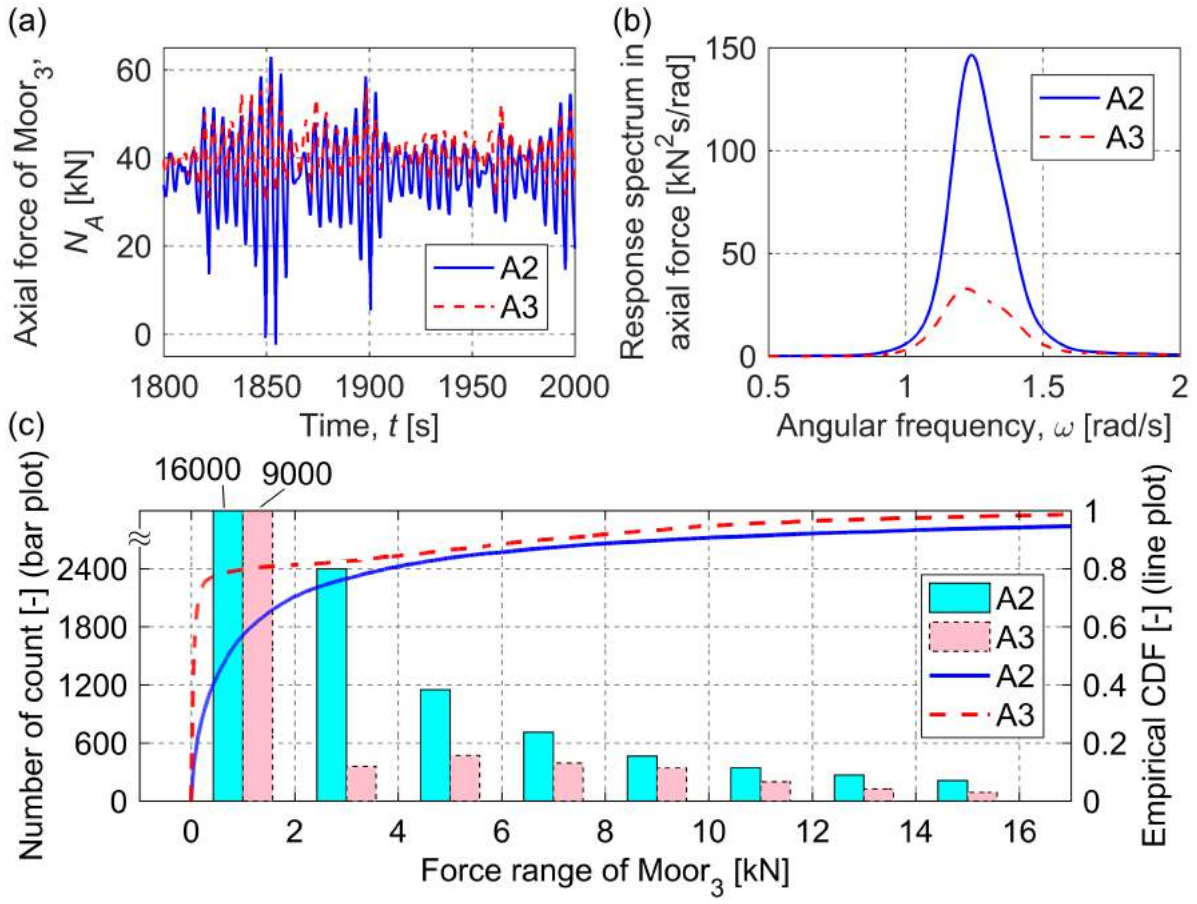


**Figure 22.** Comparison of results from simulations using the A2 (de-coupled) and A3 (coupled) analysis approaches: (a) time histories of the force response of a mooring line, (b) the response spectrum of the force response after subtracting the mean value, and (c) the force range histogram of the mooring line in Figure 22(a). The WEC system from Paper I was used for the simulation. An irregular wave loading condition was simulated, consisting of $H_s = 2.5$ m, $T_p = 5.5$ s, and $\gamma = 3.3$. The wave load propagated in the direction from the anchor to the fairlead point of mooring leg 3, $Moor_3$.

Figure 22(a) shows that the two approaches yield similar estimates for the mean value of the axial force: 37 kN and 40 kN for the A2 and A3 approaches, respectively. However, the A2 approach significantly overestimates the trough to crest force range, which is one of the key parameters for determining structural fatigue damage. The overestimated force range can also be observed in the response spectrum of the force responses; see Figure 22 (b). Note that in Figure 22(b), the response spectrum of the force response was calculated after the mean value of the force response was subtracted. A comparison of the histograms of the force range also shows that more force cycles and larger force ranges were calculated through the A2 approach.

The comparisons of the three analysis approaches with regard to the simulated mooring forces were found to be valid regardless of the mooring configuration. Because the A1 approach largely underestimates the force range, whereas the A2 approach could overestimate the force range specifically under a large wave height, the coupled analysis approach A3 is required and recommended in the numerical simulations and analyses of the hydrodynamic and structural responses of the mooring lines and power cables for floating point-absorbing WEC systems.

### 5.1.3 Comparison of the analysis approaches for WEC array configurations

From a single-unit WEC analysis perspective, the A3 simulation approach is recommended. However, one important feature of the A1 approach is that it can account for all hydrodynamic interaction effects between WECs if an array of WECs defines the simulation model. In contrast, the A3 approach is limited to accounting for the diffraction-induced interaction effect between the WECs. The two approaches were therefore compared in Paper V, which focused on WEC interaction effects, in a sensitivity study using a two-WEC simulation model. The two-WEC model was defined by two identical single-unit WEC systems similar to the reference WEC system (see Paper V for details). There was no mechanical coupling between the two WECs, i.e., they did not share anchors or mooring lines.

Sample results demonstrating the significant heave motion of the two WECs in the two-WEC model simulated by the A1 and A3 approaches are shown in Figure 23. In this example, the separation distance between the two WECs was set to 250 metres. The numbers in parentheses represent the heave motion ratio $WEC_1/WEC_2$. $WEC_1$ is located on the upwind side when the load direction is $Dir_{\text{load}} = 0$ deg. The two analysis approaches yield nearly the same results for the three simulated conditions, and the same trend was observed for all two-WEC cases presented in Paper V. Because there is no mechanical coupling between the two WECs, the only interactions between the two WECs are hydrodynamic interaction, as reflected in the differences between the two WECs with respect to their heave motions. Although the A3 approach considers only part of the hydrodynamic interaction effect, this limitation is found to be negligible based on the sensitivity study. As a final conclusion, the coupled A3 approach is the recommended and preferred option for numerical simulations and investigations based on the current thesis work and its objectives.

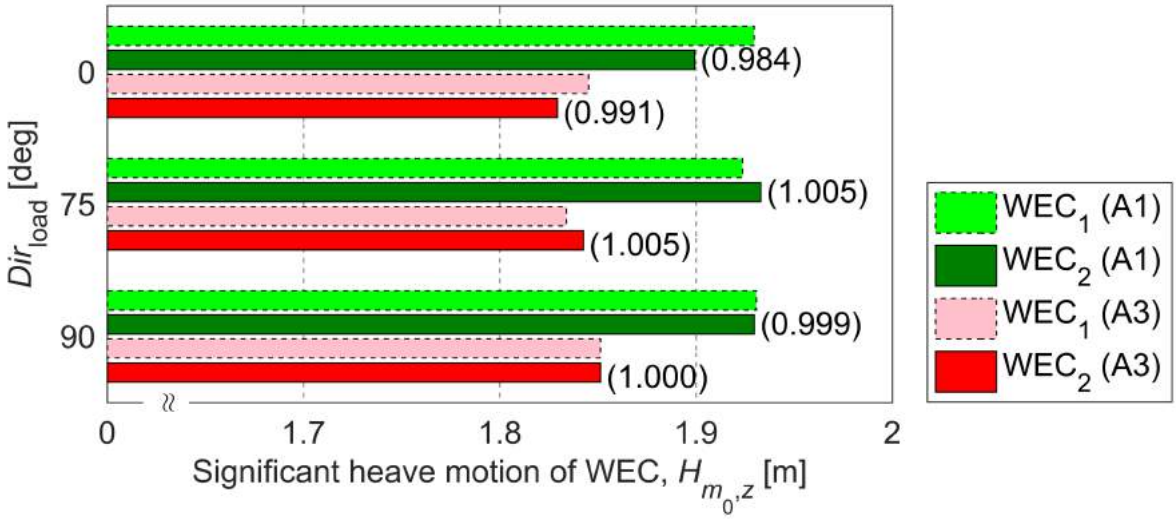


**Figure 23.** Motion responses of the WECs determined using the A1 (de-coupled) and A3 (coupled) analysis approaches. The values are presented in terms of the significant heave motions, namely, $4\sqrt{m_0}$, or the mean of the highest third of the crest to trough motion response in heave. The numbers in parentheses represent the significant heave motion ratio $WEC_1/WEC_2$. The simulations were carried out under an irregular load condition, with $H_s = 1.5$ m, $T_p = 5.5$ s, $\gamma = 3.3$, $V_{\text{curr}} = 0.514$ m/s, $V_{\text{wind}} = 9$ m/s, and $Dir_{\text{load}}$, as stated in the figure.

## 5.2 Stress and fatigue damage evaluation of the moorings and cables

After obtaining the structural responses of moorings and cables from the time-domain simulations (see Section 5.1), the stress histories of these structures could be calculated. Figure 24 presents an example of the stress responses corresponding to different stress terms at various points along a power cable. In this example, the mass of the power cable was varied as an independent variable to examine how different design parameters affect the cable's stress responses. All other design parameters were held fixed at the initial cable design values; detailed model definitions can be found in Paper II.

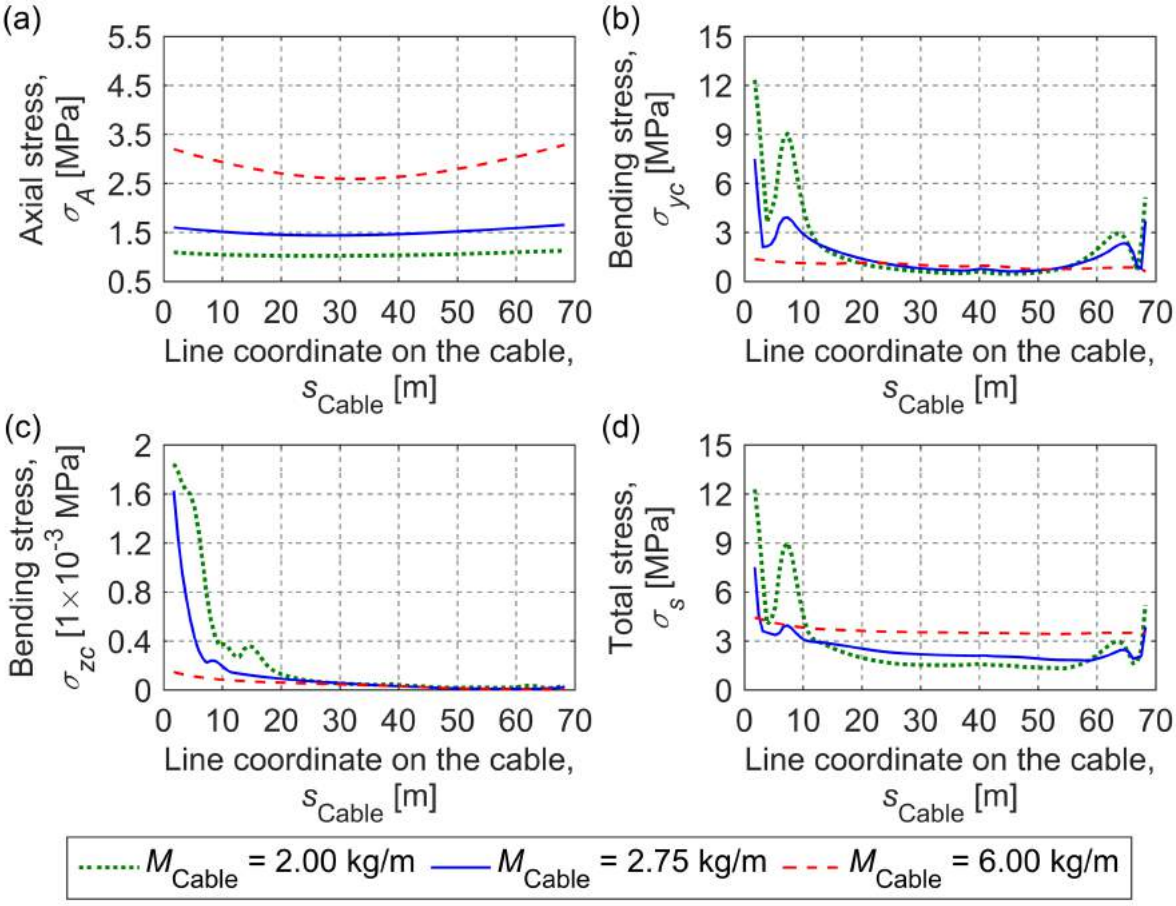


**Figure 24.** Maximum (a) axial stress $\sigma_A$, (b) bending stress $\sigma_{yc}$, (c) bending stress $\sigma_{zc}$, and (d) total stress $\sigma_s$ responses for different cable masses, $M_{\text{Cable}}$. A loading condition consisting of $H_{\text{w}} = 3.5$ m, $T_{\text{w}} = 7.5$ s, and $V_{\text{curr}} = 1.0$ m/s was simulated. The loading direction, $Dir_{\text{load}}$, was defined as propagating from the cable near the WEC side ($s_{\text{cable}} = 0$ m) to the hub side ($s_{\text{cable}} = 70$ m). (Note that the results were extracted from Figure 12 of Paper II.)

For different cable masses, either the contribution of the axial stress to the total stress of each cable was minor ($M_{\text{cable}} = 2.00$ kg/m), meaning that bending stress was the major source of the total stress, or the axial stress showed a pronounced contribution ($M_{\text{cable}} \geq 2.75$ kg/m) when the line coordinate $s_{\text{cable}}$ was (approximately) in the interval $5 < s_{\text{cable}} < 65$. For a given stress history, the fatigue damage of the cable can be estimated using the stress-based

approach presented in Section 3.2. The accumulated fatigue damage values of the cables simulated in Figure 24 are presented in Figure 25. A comparison with Figure 24(d), which indicates the critical area for the total stress response, shows that the most important areas for fatigue damage are expected to be located at the two ends of the cable. However, the exact trend for the fatigue damage along a power cable is found to be slightly different from the trend observed for the maximum total stress response. In other words, to fully understand the fatigue characteristics of a structure, an evaluation solely of the stress response is not sufficient; calculation of the fatigue damage itself is also required.

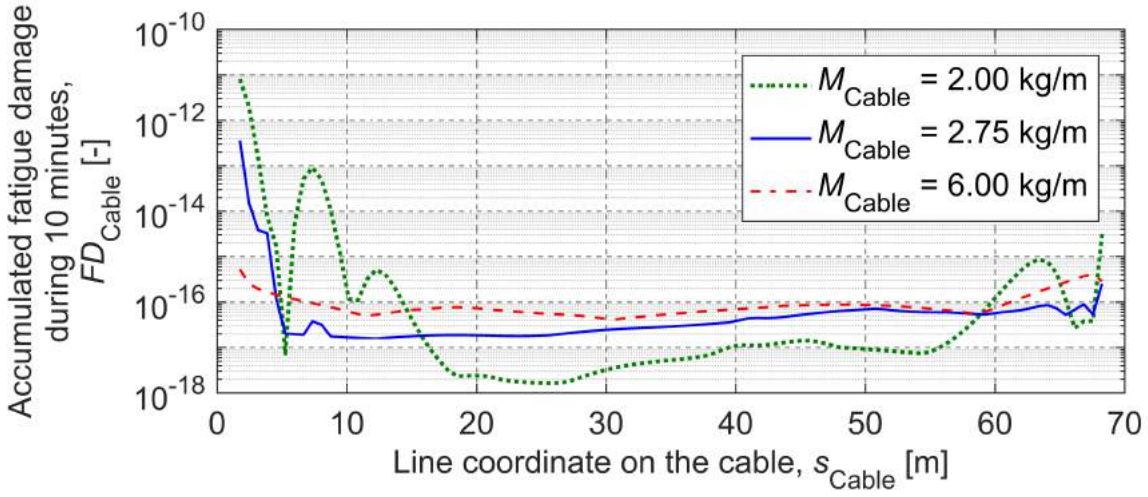


**Figure 25.** Accumulated fatigue damage over 10 minutes of a stable response for different cable masses. The three cables and loading condition simulated for this figure are the same as those simulated for Figure 24. (Note that the results were extracted from Figure 13(a) of Paper II.)

### 5.2.1 Fatigue characteristic evaluation for moorings and cables

Three types of slender structures were investigated in this thesis: spread mooring lines, taut mooring lines, and free-hanging power cables. The reader is referred to the appended Papers I – III and V for details.

Throughout this work, the importance of analysing the stress responses along the lengths of the slender structures was highlighted. The stress histories were used to calculate the accumulated fatigue damage along the lengths of the structures for each specific environmental condition; see Figure 26 for an example and Paper III and Section 4.2 for the definition and setup of the WEC system and its components. This methodology demonstrated that one loading direction may result in a fatigue-critical location in one position of the system, while that location will be in a different position for another loading direction or environmental condition. This finding demonstrates the importance of analysing the actual environmental loads and loading directions the WEC system is subject to prior to simulation; otherwise, the assessment results and conclusions may be inaccurate.

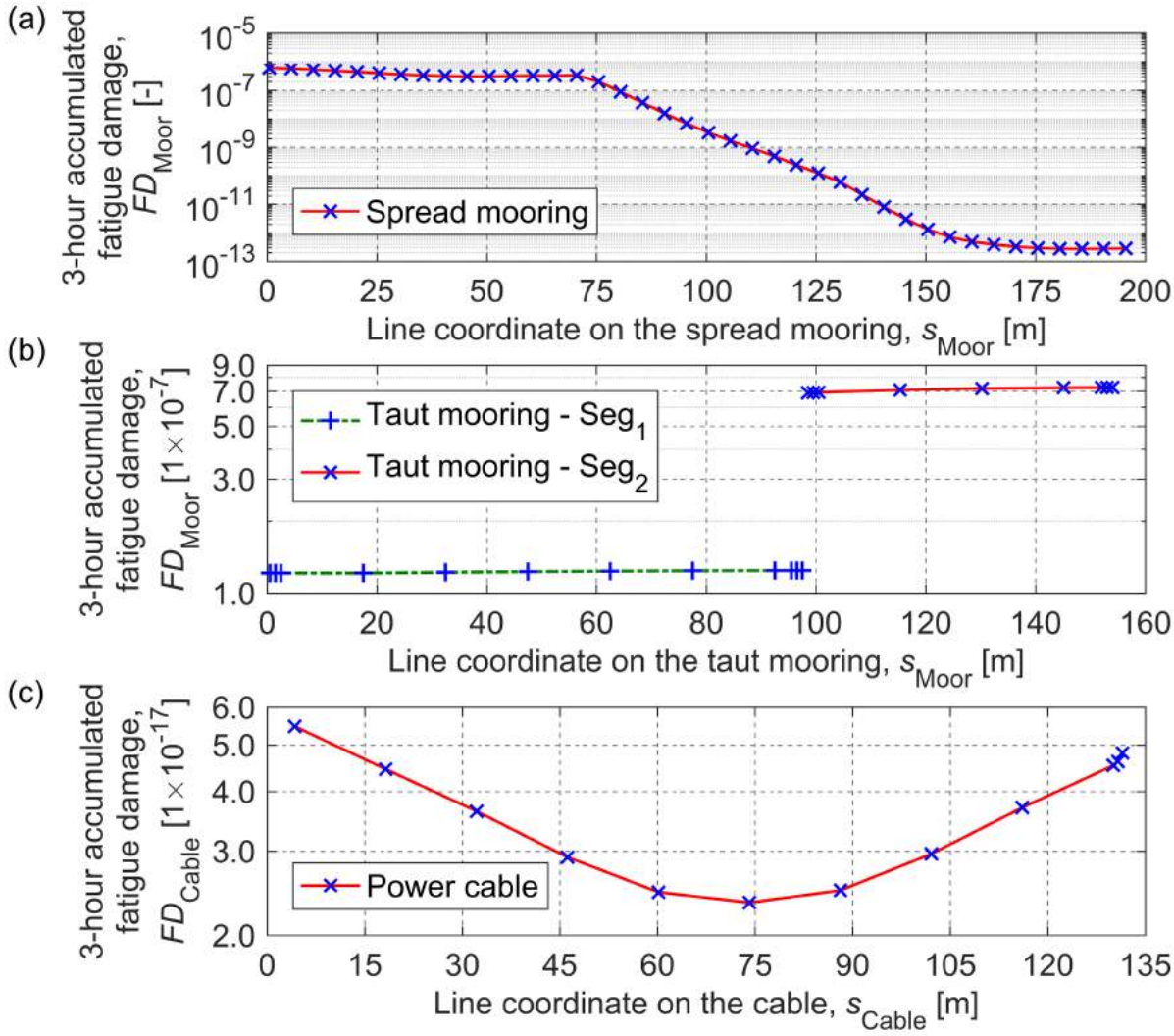


**Figure 26.** Example of the three-hour accumulated fatigue damage, $FD$, of (a) a spread mooring line, (b) a two-segment taut mooring line, and (c) a power cable. An irregular loading condition was simulated, consisting of $H_s = 3.5$ m, $T_p = 7.5$ s, $\gamma = 3.3$, $V_{curr} = 0.514$ m/s, and $V_{wind} = 9$ m/s. $Dir_{load}$ was defined differently for each result and such that the slender structure was in the upwind position. See Paper III and Section 4.2 for the definition and setup of the WEC system and its components.

Different fatigue characteristics were observed for the three structures. For the spread mooring lines in Figure 26(a), the fatigue damage is the largest at the fairlead point of the mooring line, i.e., at $s_{Moor} = 0$, and the accumulated fatigue damage decreases as the distance from the fairleads increases. For the taut mooring lines with two segments separated by a floater (see Figure 26 (b)) the accumulated fatigue damage is different. The two segments exhibit large differences in their accumulated fatigue damage. The sample case shows that the lower segment is more critical than the upper, but this is not the general trend. If a variation in the environmental load directions and conditions is included according to the scatter diagram from Runde, the largest accumulation of fatigue damage will occur in the fairlead point of the most stretched mooring segment; see Paper V.

An example of the fatigue characteristics of the power cable is presented in Figure 26(c). Both ends of the power cable were connected/covered by a bending stiffener. Despite the inclusion of the bending stiffeners, the most fatigue-critical locations were still at the connections between the bending stiffener and the cable. For all the WEC system configurations studied in this thesis, the fatigue-critical location of the cable was near the WEC under most of the moderate loading conditions, and the location gradually shifted closer to the hub as the loading conditions became harsher. Note that the hub was modelled as a spatially fixed structure, an assumption that requires further study to ensure that it is realistic and applicable.

Because the most fatigue-critical locations in and among the mooring legs and power cable depend on the simulated environmental load conditions and incident load directions, an important outcome of the fatigue assessment procedure presented in the appended papers is that a thorough and systematic numerical simulation of WEC systems is recommended. It is recommended that the results be presented as fatigue scatter diagrams (see Figure 27 for an example from Paper II) for the most fatigue-critical location or for several locations for comparison.

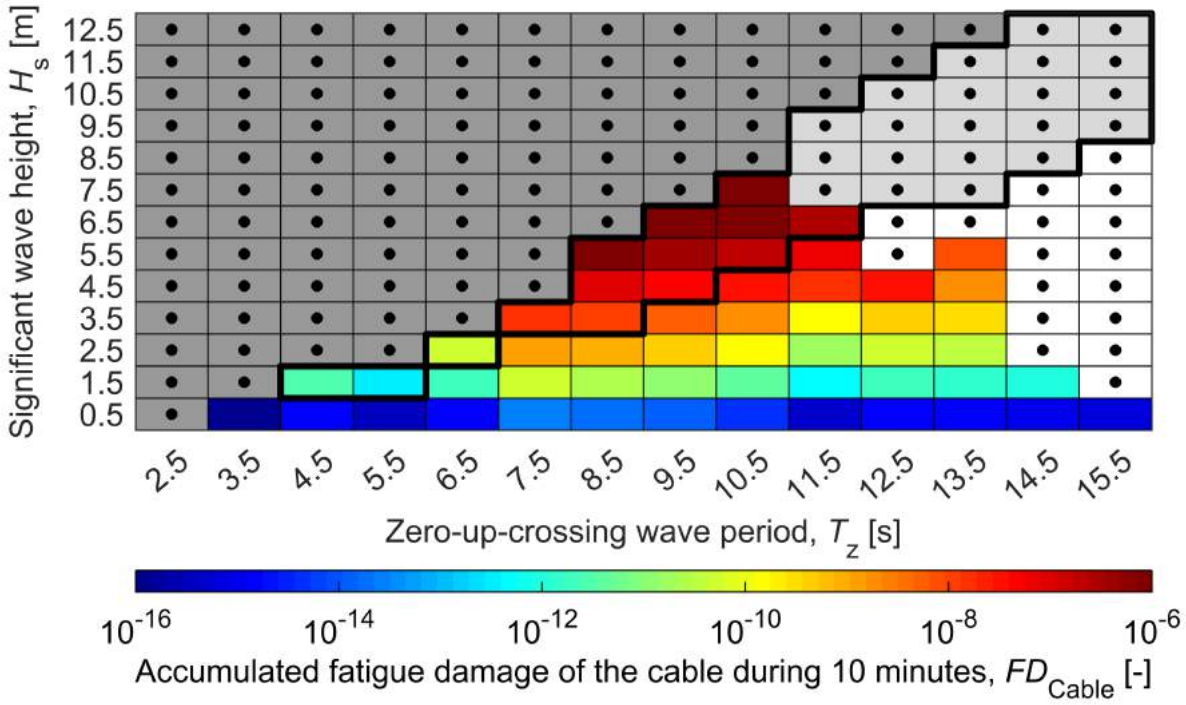


**Figure 27.** Example of a fatigue scatter diagram: maximum accumulated fatigue damage along the cable over 10 minutes for different wave heights, $H_s$, and wave periods, $T_z$. The results were extracted from Figure 14 of Paper II, in which detailed definitions of the numerical model and the colour scheme of the figure can be found. For all the wave conditions that were not simulated, the corresponding cells are marked with black dots.

## 5.3 Power absorption analysis

Figure 28 shows sample results obtained from a numerical simulation reported in Paper III in which the heave motion response of the WEC for a duration of ten minutes is presented together with the applied wave loading conditions and the calculated power absorption. The example is

based on a numerical simulation in which the model of the four-leg spread mooring configuration in Paper III was used, and the wave loading is represented by an irregular sea state with $H_s = 3.5$ m, $T_p = 7.5$ s, and $\gamma = 3.3$ and an ocean current load $V_{curr} = 0.514$ m/s. Both the wave and current loads coincided with $Dir_{load} = 0$ deg. Figure 28(b) shows that the heave motion of the WEC is generally elevated by the waves for large wave loads. A phase shift between the wave load and the heave motion response can also be observed, as well as smaller heave motions relative to the wave elevation for the smaller waves. These two effects occur due to the coupling effect (see Section 5.1.1) between the WEC and the mooring system, which gives rise to an additional load that suppresses the heave motion response of the WEC.

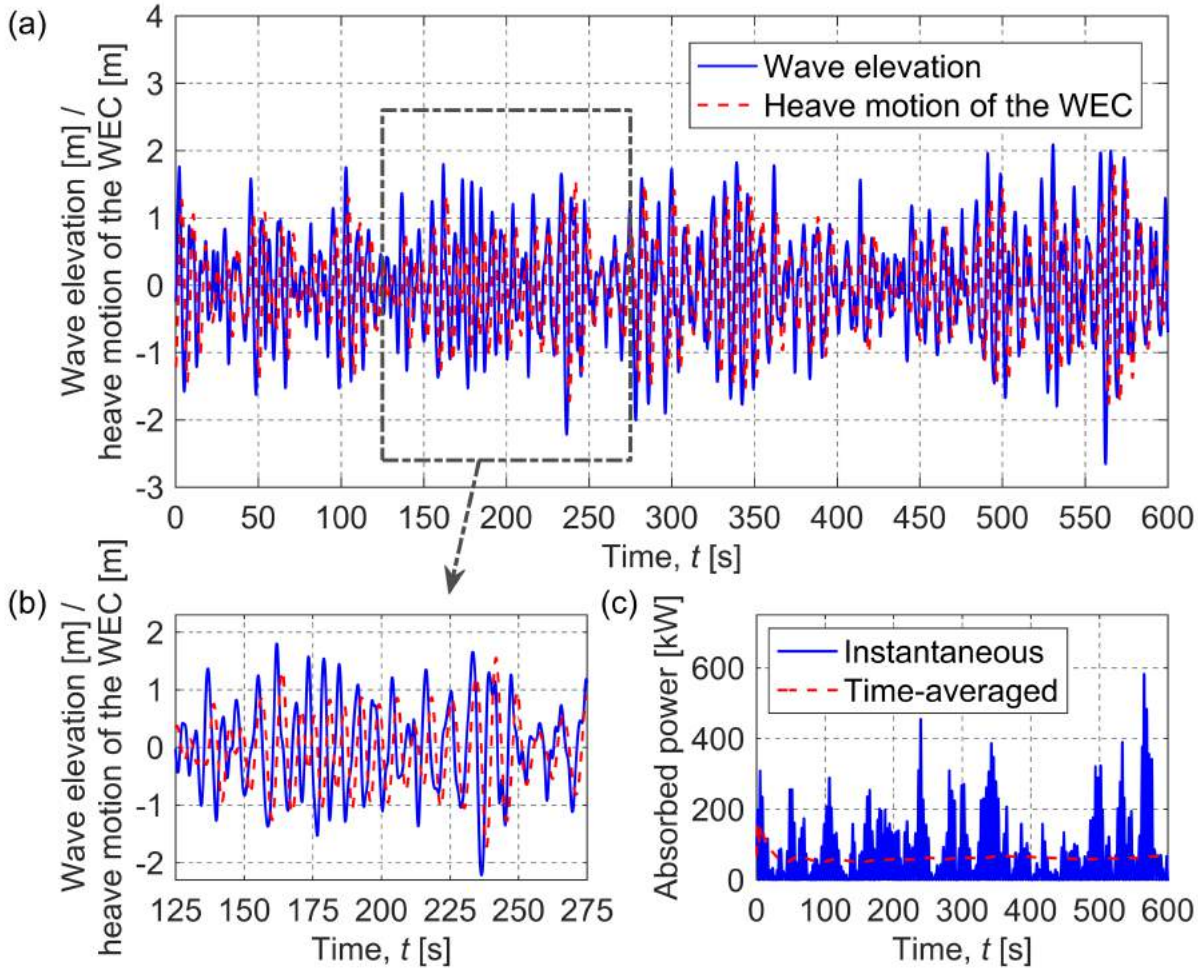


**Figure 28.** Results from Paper III: time history of wave elevation and WEC heave motion: (a) 600 seconds and (b) 150 seconds, a magnification of (a). (c) Absorbed power calculated from the time history presented in (a).

The instantaneous absorbed power and time-averaged absorbed power of the WEC were calculated using the WEC's heave motion as shown in Figure 28(a). The instantaneous absorbed power was calculated based on the heave motion velocity of the WEC, see Equations (1) and (2) in Paper III, which is considered to have a direct correlation with the heave motion of the WEC. The time-averaged absorbed power was calculated as the average power absorption over

a certain period. In the figure, the full time series was used, reaching a steady state after a few minutes. The value of the time-averaged power absorption has an upper bound that depends on the energy content of the waves in a specific sea state and on the power absorption efficiency of the WEC. The latter is determined by the hydrodynamic properties of each WEC. In this thesis, the time-averaged power absorption was used to represent the WEC's power performance in every simulated sea state.

In the WEC numerical simulation model developed in this thesis, a linear damper model of the PTO system was used, and the time-averaged absorbed power reflected the system's power performance; see similar studies by Cho & Kim (2017), Fitzgerald & Bergdahl (2008), and Vicente et al. (2009). This measure was deemed sufficient for the purpose of this thesis, but there are at least two issues that must be improved and investigated in further work. First, the numerical model does not account for any power curtailment of the WEC generator; hence, the time-averaged power is calculated by integrating the entire instantaneous power curve. In reality, curtailment is included to avoid sudden, large fluctuations in the electrical current, which can damage the electrical system of the WEC (Tokat, 2018). If a power curtailment is included in the numerical model, the time-averaged power will be reduced. Second, the control strategy of the PTO system was not modelled. Such a system is important because it aims to optimise the power performance of the WEC's PTO system for every incident wave profile (Hals et al., 2010; Korde et al., 2016; Sidenmark et al., 2015). Thus, the power performance results presented in this thesis are not realistic values and are also lower than those of WaveEL 3.0 in Runde. Nevertheless, the results can be used to assess and compare the power performance in the LCoE analysis with respect to e.g., the fatigue lives of the moorings and the power cables for different operational conditions.

### 5.3.1 Variation in WEC design

The WEC in the reference concept has different geometries and mass properties in the appended papers because of design changes made throughout during the thesis project. The properties of the PTO systems were determined using the procedure presented in Section 3.3. In the following, a comparison of the power performance between the two Waves4Power WECs in Papers IV and V is presented. The difference in geometry between the WECs is in the length of the tube, while the moorings were the same for the WECs.

The resonant heave period is 6.4 seconds for the WEC in Paper IV (the longer tube) versus 5.0 seconds for the WEC in Paper V (the shorter tube). These two wave periods were used to define the $T_{\mathrm{p}}$ of the incoming waves for an irregular wave load, and each $T_{\mathrm{p}}$ was simulated with three values of $H_{\mathrm{s}}$, together with additional ones to examine the performance of the WEC systems offset from the resonant periods. An ocean current load of $V_{\mathrm{curr}} = 0.514$ m/s and a wind load of $V_{\mathrm{wind}} = 9$ m/s were also included; all loads were heading in the same direction $Dir_{\mathrm{load}} = 0$ deg. Both WEC models featured a mooring system design resembling that of the WaveEL 3.0 full-scale installation, and each numerical simulation was run for 3 hours. The results of the simulations are presented in Figure 29.

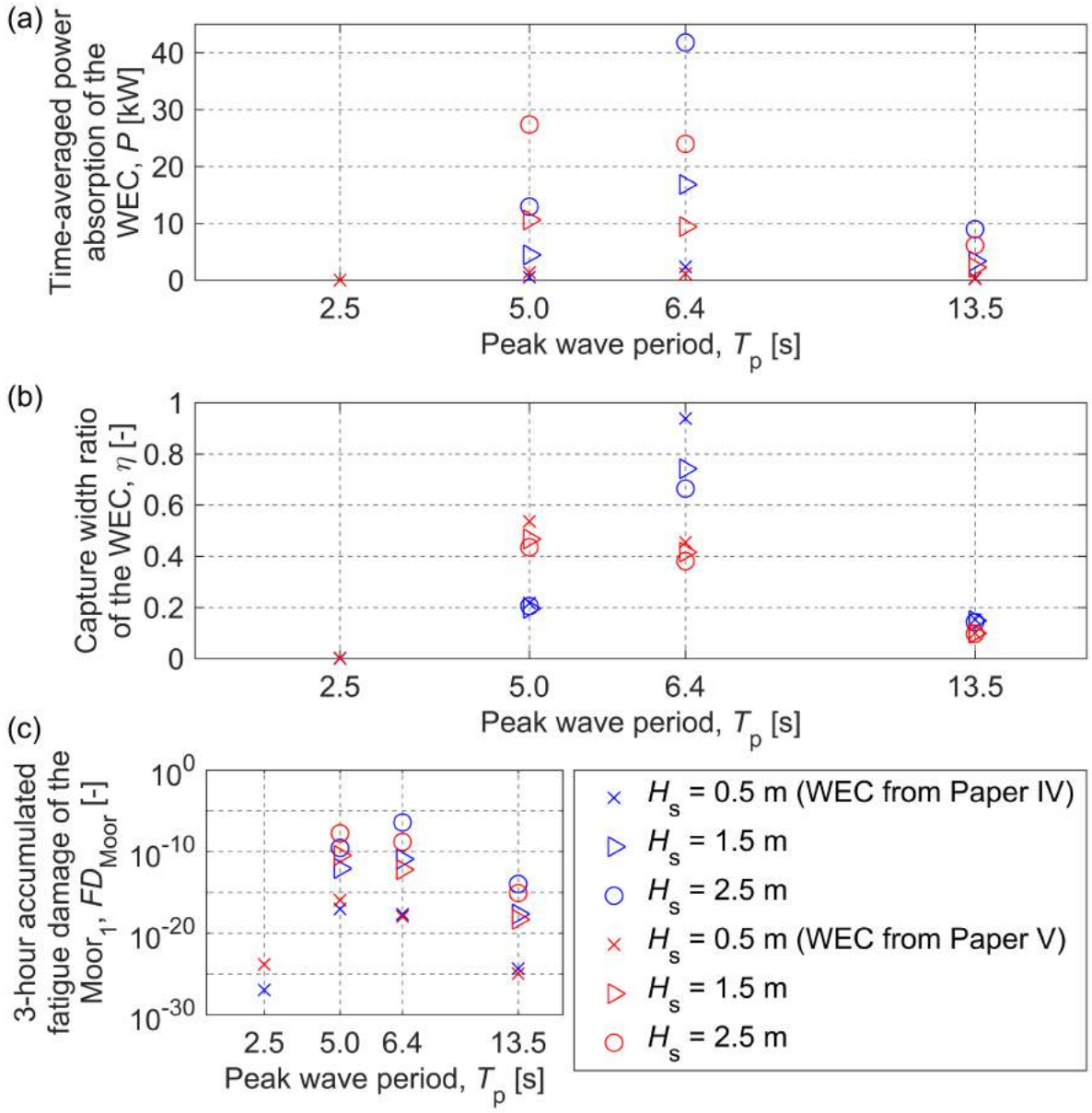


**Figure 29.** Comparison of the WEC designs from Paper IV (long tube design) and Paper V (short tube design): (a) calculated time-averaged power absorption, (b) calculated capture width ratio, and (c) calculated fatigue damage of $Moor_1$. See the text for details on the ocean current and wind loads.

The results in Figure 29(a) show that both WECs exhibit their highest time-averaged power absorptions under their respective resonant conditions. The WEC model in Paper IV appears to show better general performance because its values (blue points) are larger for all of cases except for the resonant condition of the WEC in Paper V. In addition, Ambli et al. (1982) introduced the capture width ratio, a measure for estimating the effectiveness of a WEC system in absorbing the energy in waves. The capture width ratios for the two WECs are presented in Figure 29(b), confirming that the WEC model with the longer tube reported in Paper IV is the better alternative of the two with regard to the power absorption. The results also show that, for each $T_p$, the capture width ratio decreased as the wave height increased. There are likely two

reasons for this behaviour: an effect due to the viscous damping on the WEC, and the coupling effect between the WEC buoy and its attached moorings and power cable.

The accumulated fatigue damage in the mooring lines of the WECs was calculated. Figure 29(c) presents the results for the mooring leg $\text{Moor}_1$, which accumulated the most fatigue damage in both cases; the values were calculated for the fairlead point, which was identified as the fatigue-critical position. Through a comparison of the results in Figure 29(a), a clear and logical relationship between the time-averaged absorbed power and the accumulated fatigue damage was found: the higher the power absorption (i.e., large heave motions) is, the larger the fatigue damage in the mooring lines becomes. The same trend was found in the other mooring legs and in the power cable. These results confirm the importance of designing the WEC and its components together as an integrated system via coupled numerical simulation to avoid compromising the structural reliability of the components.

## 5.4 Parameter sensitivity analysis

Throughout the work presented in the appended Papers I – V, a large number of parameters were investigated with regard to their effect on the fatigue characteristics of the mooring lines and power cables and the power performance of the WEC. In this section, some of the parameters found to have the highest uncertainty or that yielded the largest effect in the determination of the long-term structural service lives are elaborated: the sea state conditions (Section 5.4.1), the incident load direction (Section 5.4.2), and marine biofouling (Section 5.4.3).

### 5.4.1 Sea state conditions

Due to the changing nature of ocean environments, the investigation of the fatigue life of the moorings and cables, as well as the power performance of the WEC, must account for variations in the wave loads at the expected site for the WEC's installation. As presented by Pecher (2017), the overall power performance of WECs can be estimated by power matrices. As a counterpart to the power matrices, fatigue matrices (i.e., fatigue scatter diagram as presented in Figure 27) for the mooring lines and power cables were introduced in this thesis. Figures 30 and 31 present examples of power and fatigue matrices for which the simulation model in Paper V was used. The environmental conditions were set to the prevailing conditions at Runde determined from the scatter diagram. Each environmental condition was simulated for three hours and consisted of wave, wind, and ocean current loads; biofouling was not included. The wave load was defined by $T_\text{p}$ and $H_\text{s}$ and followed the JONSWAP spectrum with $\gamma$ set to 3.3. When $H_\text{s}$ was lower than 1.5 metres, $V_\text{curr}$ was set to 0 m/s. Otherwise, the current velocity was set to 0.514 m/s. $V_\text{wind}$ was set to a constant 9 m/s. The choice of $V_\text{curr}$ and $V_\text{wind}$ was based on the weather observations presented in Eugster (2010) and Yr (2017). The wave, wind, and current loads were directed along an angle of 90 degrees, i.e., $Dir_\text{load} = 90$ deg.

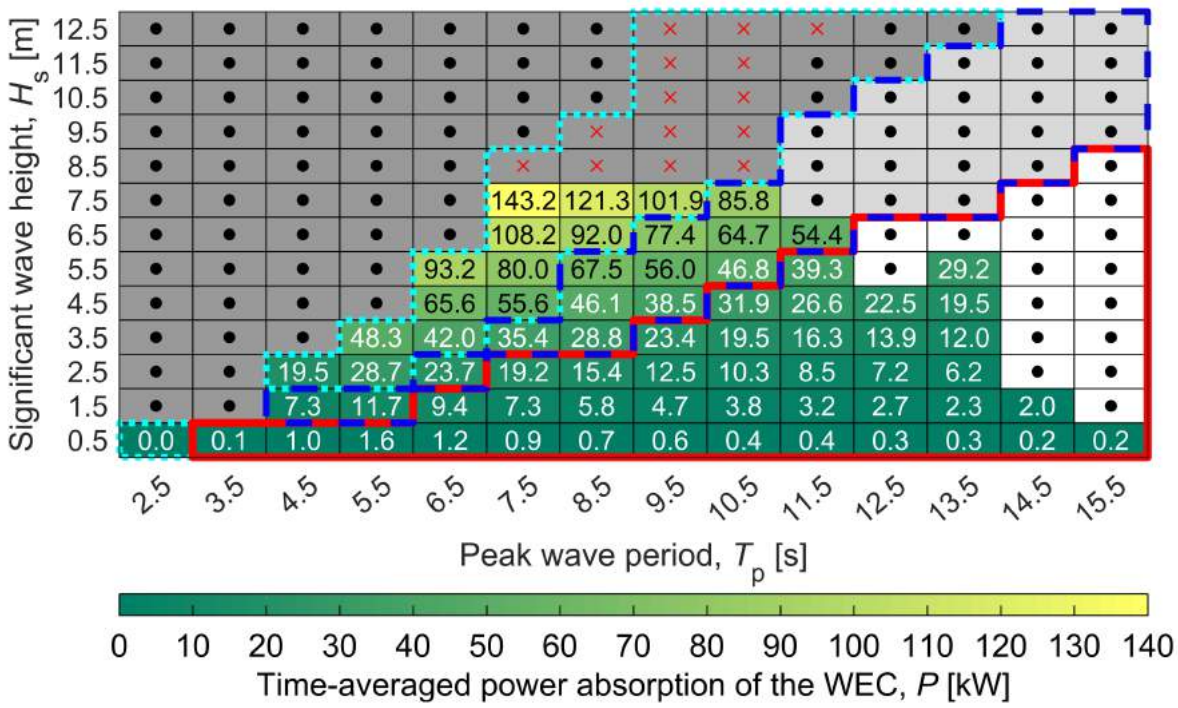


**Figure 30.** Power matrix of the WEC installed at Runde, Norway. Each cell represents the time-averaged absorbed power of the WEC, $P$, estimated from a three-hour simulation. The cells surrounded by a red line are in the valid range for linear wave theory. The wave conditions in the invalid and transitional ranges for the application of linear wave theory are indicated by light-blue dotted and dark-blue dashed lines, respectively. All cells with a black dot were excluded from the simulations because their probabilities of occurrence are zero according to the wave scatter diagram acquired at the Runde test site. The cells marked with a red cross are beyond the operational mode for power absorption for the WaveEL concept and hence were excluded from the numerical simulation. Other details regarding the definition of the loading conditions can be found in the text in Section 5.4.1.

The cells marked by a black dot have no probability of occurrence according to the wave scatter diagram acquired at the Runde test site. Due to the linear wave theory used in the SESAM package, all possible wave conditions were divided into three categories: the cells surrounded by a red line (shown with a value or filled with white colour) are in the valid range for linear wave theory, the cells surrounded by a dark-blue dashed line (shown with a value or filled with light grey colour) lie in the intermediate range between linear wave theory and other nonlinear wave theories, and the cells surrounded by a light-blue dotted line (shown with a value or filled with dark grey colour) require higher-order nonlinear theories in the simulations. A discussion on the categorisation of the wave conditions is provided in Section 4.1.

The WEC WaveEL 3.0 is considered to be in the operational mode when $H_s$ is less than 8 metres and in survival mode for a larger $H_s$. The survival-mode conditions are marked with a red cross in the matrices, and the simulation model was not used to simulate these sea state conditions. Although some sea states required higher-order nonlinear theories in the simulations, all operational-mode conditions, i.e., all contoured cells with values, were simulated because they were of major interest in this thesis. The simulation model for the sea states requiring nonlinear theory was used to indicate the potential levels of the fatigue damage and absorbed power.

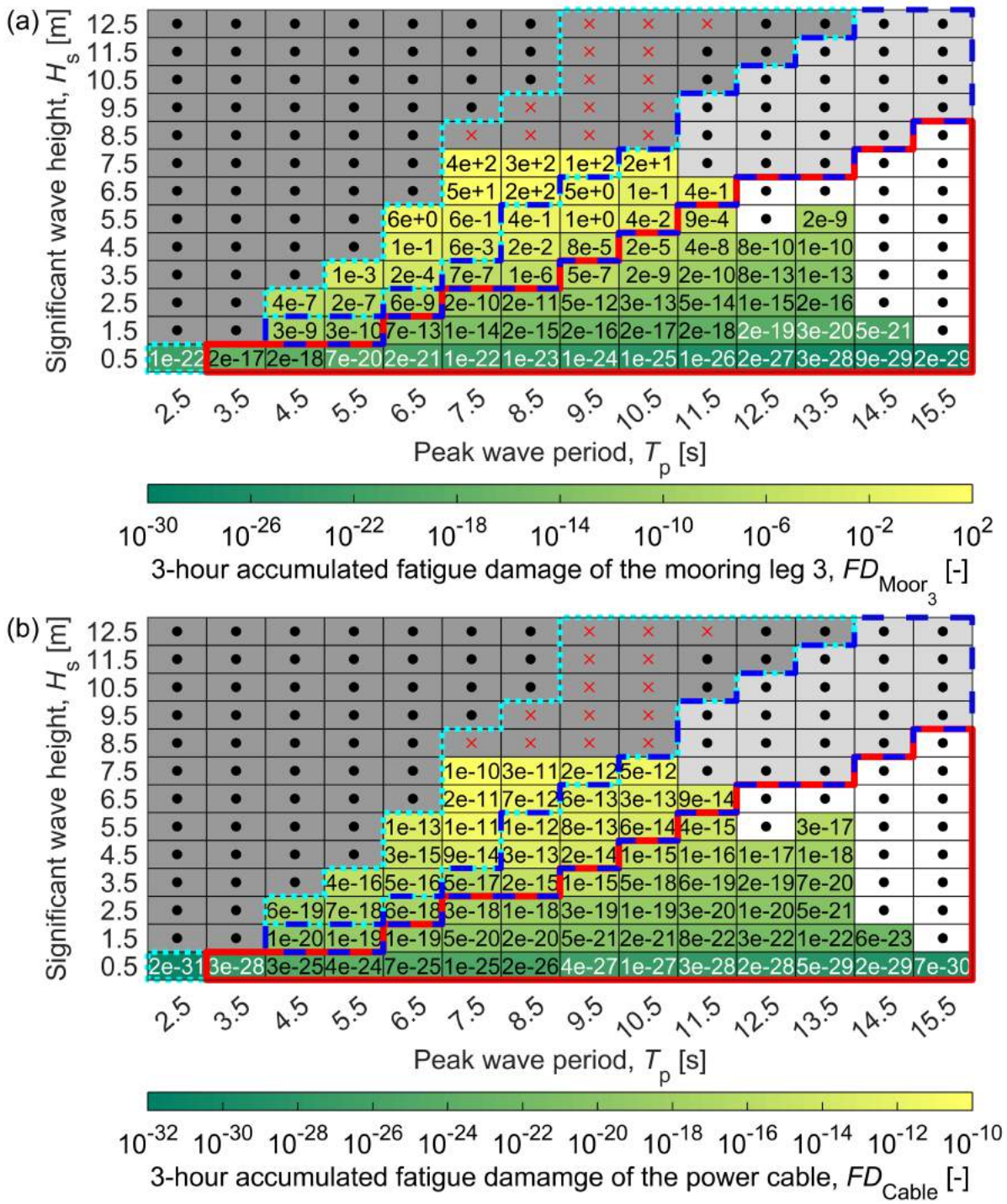


**Figure 31.** Fatigue matrices for (a) mooring leg 3, $Moor_3$, at its fairlead point and (b) the connection point between the bending stiffener and the power cable near the WEC. The value shown in each cell represents the three-hour accumulated fatigue damage, $FD$. Definitions of the different symbols and border lines in the figure can be found in the caption of Figure 30.

The results in Figure 30 show that for the same magnitude of the significant wave height, the largest absorbed power occurs near the resonant wave period of the WEC buoy (in this case, a wave period of 5.0 seconds). For the same value of a wave period, the absorbed power does not increase linearly with the energy contained in a given wave height. The reason is the coupling

effect between the WEC and the moorings and cables. It was also observed that the coupling effect is more profound near the resonant wave period of the WEC; hence, the relation between the energy contained in a wave and the absorbed wave power is not linear. The results demonstrate the importance of using the coupled analysis approach A3 together with the actual environmental conditions for a realistic estimation of the energy performance of a WEC system. The methodology and results can also be used to improve and optimise the power performance of the WEC system, demonstrating the sensitivity of its power performance to different sea state conditions.

The fatigue matrices for mooring leg 3 and the power cable represent the accumulated fatigue damages in the most important locations; see Figure 31. The procedure presented in Section 5.2 was used. For mooring legs 1 to 3 and the power cable, the accumulated fatigue damage along their lengths were calculated for each sea state condition in the matrix. An assessment of the results showed that for the environmental conditions presented earlier in this section, the most fatigue-critical point in the mooring system was consistently the fairlead point of mooring leg 3 ($\text{Moor}_3$ at $s_{\text{Moor}} = 0$ metres), and for the cable, it was at the top end near the bending stiffener on the WEC side ($s_{\text{Cable}} = 3.185$ metres).

The results in Figure 31 show that the power cable has a long fatigue life based on the low values of the accumulated fatigue damage; cf., Paper II where this issue is discussed. The results for the mooring line, however, show that the current simulation model and its mechanical properties of the mooring lines indicate that $H_s$ values greater than 5.5 metres are critical. This issue must be investigated in detail in future work; see the discussion in Chapter 7.

The results in Figures 30 and 31 demonstrate the importance of performing both power performance and fatigue analyses of WEC systems for a large number of environmental conditions. The response of the WEC system is sensitive to the environmental loads to which it is subjected. The region in the power performance matrix where the power performance is the best is also the region in the fatigue matrix where large accumulations of fatigue damage occur both in the moorings and in the power cable. Thus, designers of WEC systems must carry out an economic analysis that balances the benefits – the energy performance of the WEC – and the costs – such as the fatigue damage of the mooring systems and power cables – of the WEC systems. The power matrix (Figure 30), together with the fatigue matrix (Figure 31), contributes to an understanding of the system's overall characteristics in terms of profitability and reliability. These issues are further addressed through an LCoE analysis, which is presented in Section 5.5.

### 5.4.2 Incident load direction

Section 5.4.1 presents simulation results obtained when sea state conditions were varied to assess how the power performance and accumulated fatigue damage of the mooring system and the power cable were affected. In these simulations, the incident load direction was the same for all of the simulated cases. Thus, the matrices are valid only for the incident load direction used to generate their values.

In reality, the incident load direction is not constant but varies. Additionally, the wave, ocean current and wind loads are not unidirectional (i.e., $Dir_{\text{wave}} = Dir_{\text{wind}} = Dir_{\text{curr}} = Dir_{\text{load}}$), which further complicates the analysis of the responses of the WEC system. It is challenging to define real load scenarios, and often, design load cases are used instead, which can be considered (i) the most representative load direction case for WEC installation or (ii) the most

severe load direction case from a fatigue life perspective of the moorings and the power cable. If case (ii) is employed, the accumulated fatigue damage of the moorings and power cable will be large and the fatigue lives short; see Figure 31, which presents such a case. The case will thus represent the worst-case scenario of the moorings and power cable. Consequently, the parameter sensitivity analysis plays an important role in clarifying the WEC system's response characteristics to both (i) and (ii). The appended Papers I – III present comprehensive parameter sensitivity analyses with regard to the influence of the incident load direction and the mutual directionality between primarily wave and ocean current loads and their magnitudes.

The characteristics of the directionality of the loads acting on WaveEL 3.0 in Runde were not available. Hence, a sensitivity study was carried out with respect to the influence of the wave and wind load directions (assumed here to coincide, i.e., $Dir_{\mathrm{wave}} = Dir_{\mathrm{wind}}$) and the ocean current load direction on the power performance and accumulated fatigue damage in the most fatigue-critical points of the mooring system and the power cable. The numerical simulation was performed for the environmental load case $H_{\mathrm{s}} = 1.5$ m, $T_{\mathrm{p}} = 5.5$ s, $\gamma = 3.3$, $V_{\mathrm{curr}} = 0.514$ m/s, and $V_{\mathrm{wind}} = 9$ m/s. $Dir_{\mathrm{wave}}$, $Dir_{\mathrm{wind}}$, and $Dir_{\mathrm{current}}$ were varied according to the values presented in Figure 32. A reference incident load direction case was set to 90 degrees, which is the same case used to generate the results in Figures 30 and 31. This case is indicated by the dark-blue square in Figure 32 and was used to normalise the values in all other cells.

The results presented in Figure 32 show that the power performance of the WEC system is not highly sensitive to the loads' directions. The largest difference between the simulated cases is approximately 7%. However, the loads' directions have a strong effect on the accumulated fatigue damage of the mooring line and the power cable. The 90-degree load direction is the most severe load direction for mooring leg $\mathrm{Moor}_3$; however, the accumulated fatigue damage could be reduced by a factor of $10^{15}$ for a few load directions. The results for the power cable demonstrate the importance of having a good understanding of the directionality of all three types of loads. Depending on the load direction differences among the waves, wind and ocean current, the accumulated fatigue damage can be either higher or lower relative to the reference case. This discrepancy was studied in detail in, among other papers, Paper II.

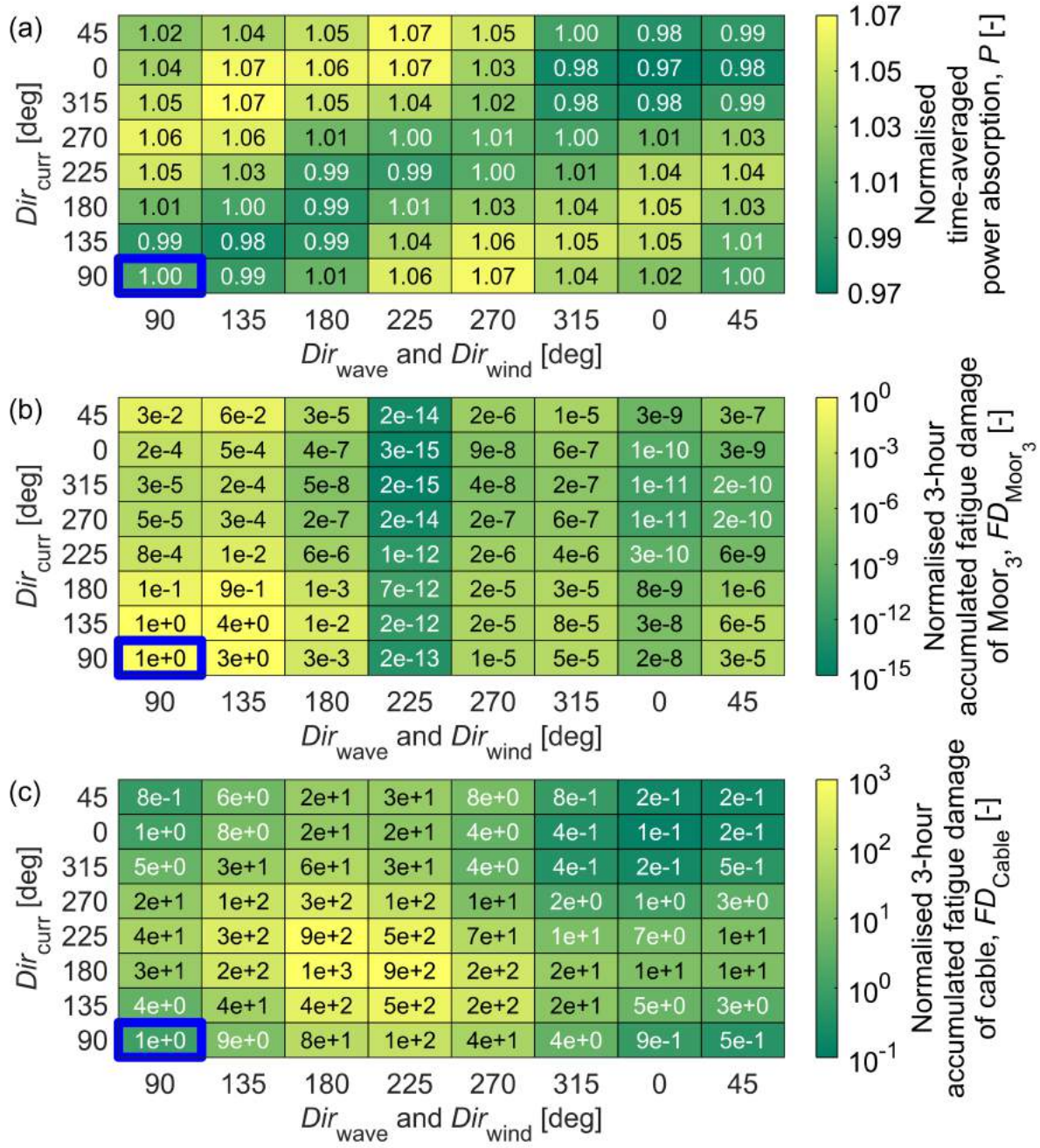


**Figure 32.** Sensitivity study of incident load direction on the (a) power performance and the three-hour accumulated fatigue damage of (b) $\text{Moor}_3$ and (c) the power cable. The numerical simulation was performed for the environmental load case $H_\text{s} = 1.5$ m, $T_\text{p} = 5.5$ s, $\gamma = 3.3$, $V_\text{curr} = 0.514$ m/s, and $V_\text{wind} = 9$ m/s. The loading directions, $Dir_\text{wave}$, $Dir_\text{wind}$, and $Dir_\text{current}$, were varied according to the values presented in the figure. All values are normalised with respect to the reference case, which is indicated by a blue border around the corresponding cell in each sub-figure. The absolute values for the reference case can be found in Figures 30 and 31.

In the design of WEC array systems, it is not as straightforward to analyse the influence of loads' directionality as it is for single-unit WEC systems, especially if their designs are complex with shared mechanical couplings between the mooring lines, because of the interaction effects

that occur between the WECs. An example of a 10-WEC array configuration was presented and studied in Paper V; see a schematic layout in Figure 15(e). The WEC array consists of ten WECs with a shared mooring design in which a floater can be shared between two WECs or an anchor can be shared between two mooring legs; the reader is referred to Paper V for a detailed description. A sensitivity study of the incident wave load direction was carried out for this array configuration. Figure 33 presents the accumulated fatigue damage in the most fatigue-critical mooring line of each sub-unit WEC for the four incident load directions; see Paper V for details.

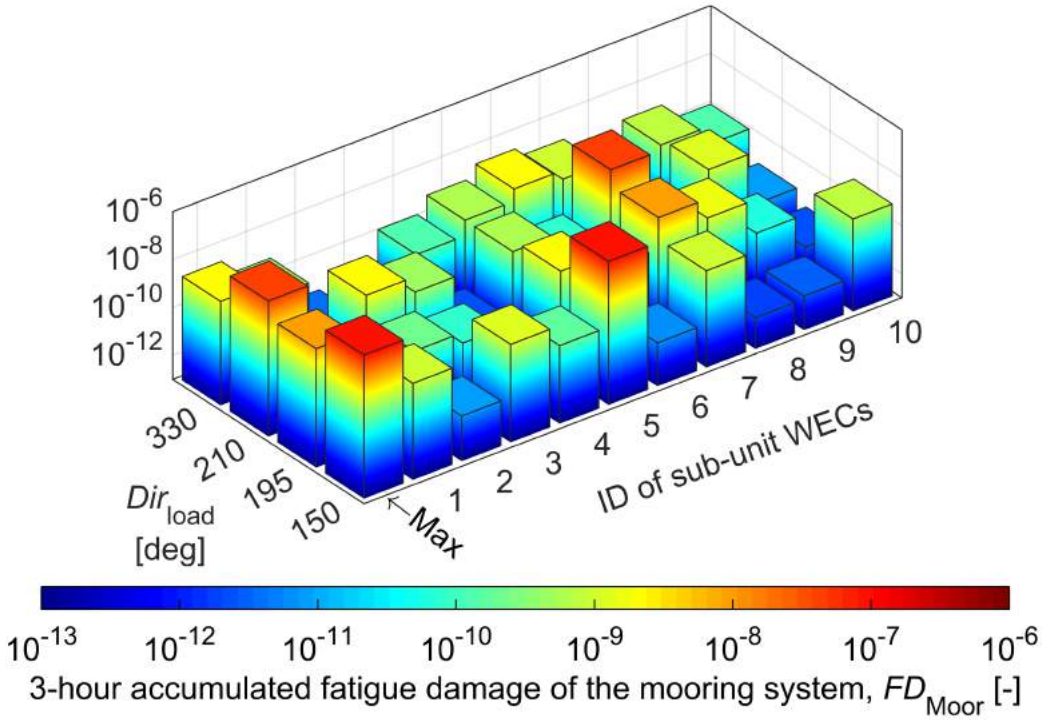


**Figure 33.** Calculated accumulated fatigue damage, $FD_{\mathrm{Moor}}$, for the 10-WEC array system. The simulation was performed at $H_{\mathrm{s}} = 1.5$ m, $T_{\mathrm{p}} = 5.5$ s, $\gamma = 3.3$, $V_{\mathrm{curr}} = 0.514$ m/s, and $V_{\mathrm{wind}} = 9$ m/s. $Dir_{\mathrm{load}}$ was varied according to the definition presented in the figure. The $FD_{\mathrm{Moor}}$ value for each WEC for the different incident load directions ($Dir_{\mathrm{load}}$) and the maximum value of $FD_{\mathrm{Moor}}$ for each $Dir_{\mathrm{load}}$ are shown. The results were generated from simulations in which hydrodynamic interaction effects were included, whereas the simulation results obtained for the same load conditions without considering hydrodynamic interaction effects are presented in Figure 15(b) of Paper V.

The design of this array configuration has a symmetry line with regard to two incident load directions, $Dir_{\mathrm{load}}$ of 150 degrees and 330 degrees. The results for these two loading directions are also found to be symmetric, as expected. The deviation from symmetry in some results is due to the non-symmetric grouping of some sub-unit mooring lines; see Paper V for details.

Because the 10-WEC array system adopts a circular and symmetrical pattern, the orientation of the array system is ideally less sensitive to the uncertainty in the loading direction. However, due to a change in $Dir_{\mathrm{load}}$, the ratio of the maximum to minimum fatigue damage among all the mooring lines is still on the order of two for the four $Dir_{\mathrm{load}}$ presented in Figure 33. Another

interesting observation can be made with respect to the discrepancy in the fatigue damage accumulation between the sub-units. For each $Dir_{\mathrm{load}}$, some moorings are consistently oriented in the direction most vulnerable to the incoming loads, while others are located in a more sheltered area. If one compares the fatigue damage between the most and the least fatigue-critical mooring lines, a difference of up to a factor of $10^5$ can be found.

Several conclusions can be drawn based on the results presented in Figures 32 and 33. First, the large variation in the estimated fatigue damage of the moorings and cables highlights the uncertainty in the system's fatigue life estimation if the loading direction at the expected operational site is unknown. Second, together with the results in Figures 30 and 31, a concern was raised with regard to the design principle of the mooring system. For the case study system examined in this thesis, all the mooring legs were designed to achieve the same strength criteria. If such a system is to be deployed in an area with one dominant loading direction, it is likely that a few components could be extremely critical with respect to the fatigue, whereas the others are designed with unnecessarily large safety margins. In this scenario, establishing an efficient maintenance plan for the mooring components will become challenging. However, if the mooring lines in the system are to be designed differently, a thorough geotechnical study and analysis of the environmental load conditions of the deployment site are essential to a reliable design of the components.

### 5.4.3 Marine biofouling

As discussed by Langhamer (2012) and Tiron et al. (2015), given their expected long service life, WEC systems will inevitably act as artificial reefs, and the resulting population of bio-inhabitants or marine growth could impede their power production or cause an expected decrease in the durability of the systems. Thus, an investigation of biofouling was performed, forming the main focus of Paper III.

A precise quantitative estimate of marine biofouling on a WEC system requires detailed *in situ* measurements of the flow properties and biological activity. However, such information is typically lacking during the initial design phase and will only become available once the device has actually been deployed for a certain period. The uncertainty in fouling development poses a challenge when marine biofouling must be considered to estimate the overall performance of WEC systems.

The numerical population-dynamic model developed by Tiron et al. (2012) predicts biofouling development in terms of the areal density (expressed in kg/m$^2$). Using the methodology presented in the thesis, however, the mass density (expressed in kg/m$^3$) is needed to accurately simulate the dynamic response of the mooring lines or power cables. Therefore, a parameter sensitivity study was presented in Paper III, which exemplifies a possible solution for accounting for the uncertainty due to the mass density of marine biofouling.

According to a literature survey of publicly available sources, mass densities of marine biofouling can range from 900 to 2200 kg/m$^3$ (Carswell, 2015; Fevåg, 2012; Westgate & DeJong, 2005). This wide range is attributed to various factors, such as the difference in the considered operational site, the geometrical characterisations of offshore structures, and the effectiveness of the anti-fouling coating, all of which are uncertain for a system that is yet to be deployed on site. Hence, by collecting available information from the literature, a sensitivity study that investigated the influence of the mass density of marine biofouling on the estimated fatigue damage and power performance was performed. In this thesis, the areal density of

biofouling was defined as the control variable, whereas the mass density was chosen as the independent variable. Therefore, the dependent variables that will also affect the dynamics of the WEC system include the thickness and induced drag of marine biofouling. The results of this sensitivity study are presented in Figure 34.

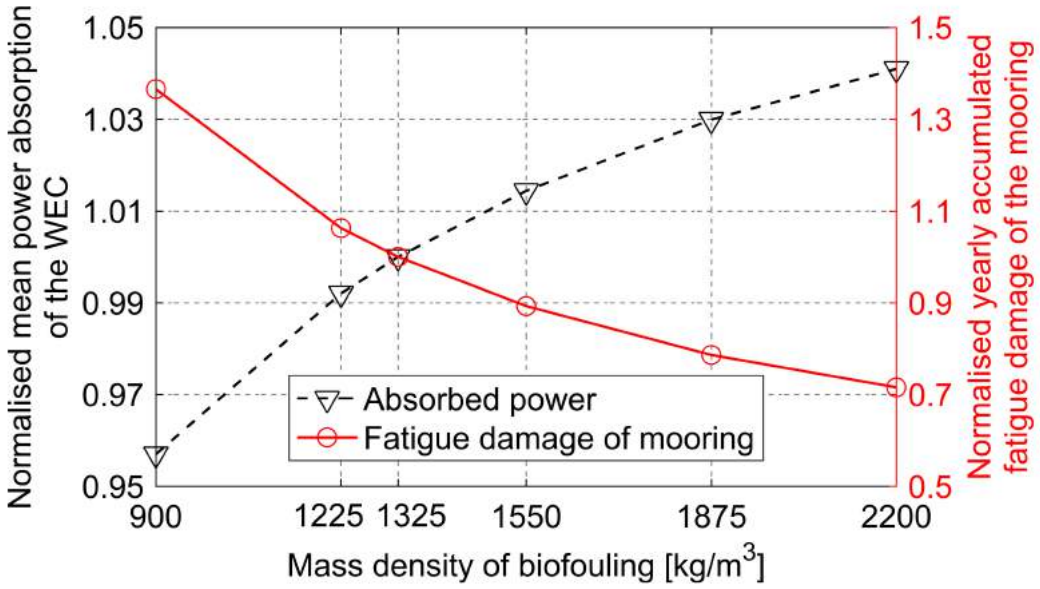


**Figure 34.** Correlation diagram of the power performance and fatigue life of moorings with respect to the mass density of marine biofouling. The areal density of marine biofouling was defined as the control variable for all data points presented in the figure, i.e., the layer thickness of biofouling was adjusted between cases. The simulated sea state condition consisted of $H_s = 2.0$ m, $T_p = 5.5$ s, $\gamma = 3.3$, $V_{curr} = 0.514$ m/s, $V_{wind} = 0$ m/s, and $Dir_{load} = 180$ deg, and the numerical model was defined as presented in Paper III. All values are normalised with respect to the reference case, in which the mass density is assumed to be 1325 kg/m$^3$ (a value suggested in NORSOK (2007)).

Given the same areal density of marine biofouling, a lower mass density corresponds to a larger thickness of the fouling layer and, hence, larger additional drag forces induced by the marine growth. As shown in Figure 34, as the mass density of the biofouling decreased, a decrease in the mean power absorption and an increase in the fatigue damage were observed. The results from this sensitivity study suggest that, from a mooring design perspective, if detailed information about marine biofouling at the installation site is not available, one may assume a low mass density of marine biofouling, which yields a larger safety margin for structural design compared than that afforded by assuming a large mass density.

As discussed by Titah-Benbouzid & Benbouzid (2015), anti-fouling systems are normally designed with one particular area for the prevention of a certain type of fouling. In addition, due to the variation in the fouling composition, different marine species exhibit different layer thicknesses and drag effects. The results in Figure 34 can therefore also be used to indicate a strategy for fouling prevention: the prevention of biofouling should prioritise the biofouling type that leads to a large accumulated thickness and a large drag.

As discussed by Tiron et al. (2012), biofouling is a gradual process, and one should consider its long-term influence on a system. Therefore, the effect of the duration of fouling development was further investigated in Paper III; see Figure 35 for the results. The values are normalised with respect to the biofouling-free condition, i.e., at year zero. The change in the absorbed power and the fatigue damage are most significant during the first year, contributing to 40% of the total changes observed after ten years. Over ten years of fouling development, both the power performance and the fatigue damage to the mooring reach a stable state.

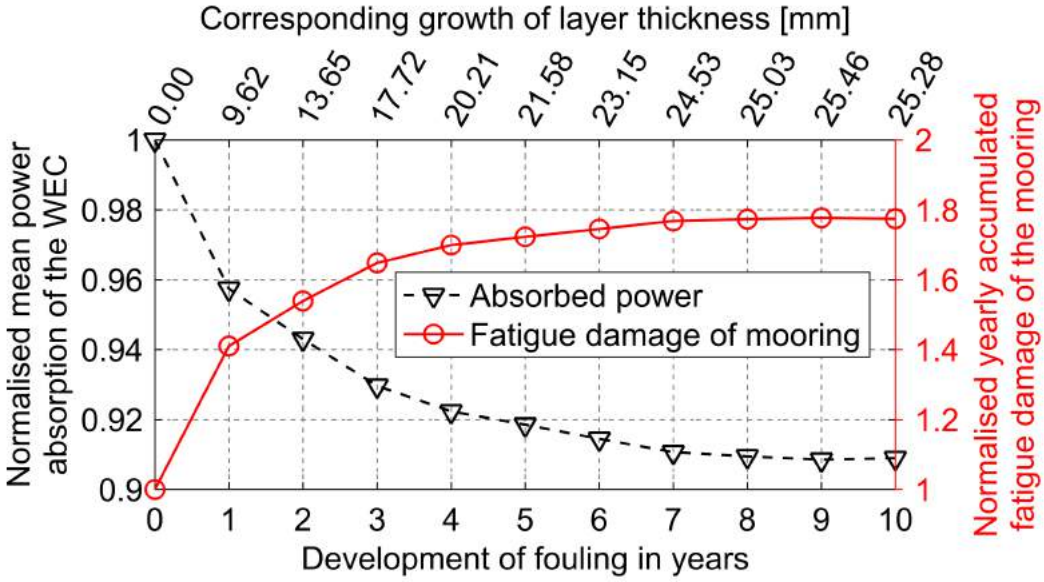


**Figure 35.** The effect of biofouling on the power absorption and fatigue damage of the WEC system after various time durations. The simulated sea state condition consists of $H_s = 2.0$ m, $T_p = 5.5$ s, $\gamma = 3.3$, $V_{curr} = 0.514$ m/s, $V_{wind} = 0$ m/s, and $Dir_{load} = 180$ deg, and the numerical model was defined as presented in Paper III. All values are normalised with respect to the biofouling-free conditions.

Using the results presented in Figure 35, together with the power and fatigue matrices in, for example, Figures 30 and 31, a long-term estimate of the structural fatigue life and power performance can be carried out. The estimation procedure was elaborated and discussed in Paper III, whereas the most important conclusions drawn from the investigation with regard to the biofouling effect are as follows:

- The modelled biofouling on the cables and moorings is found to result in a maximum 17% reduction in the WEC's mean power absorption.
- The presence of biofouling can significantly reduce the fatigue life of the moorings by up to 76% among all the simulated cases in Paper III.
- If various sea state conditions and variation effects from fouling development are taken into consideration, the presence of biofouling can lead to a 10% reduction in the absorbed power and a 20% decrease in the fatigue life of the moorings that accumulate the most fatigue damage.

- The fatigue life of the power cable is also reduced due to biofouling. However, due to the long fatigue life calculated for the power cable, the influence of biofouling on the cable's fatigue is considered to be negligible.

## 5.5 LCoE analysis

LCoE analysis was used to evaluate the profitability and feasibility of the WaveEL 3.0 WEC system. Irrespective of the investigation of the system with regard to its fatigue and power performance, as presented in the thesis, an initial LCoE calculation of the WaveEL 3.0 reference concept could be carried out based on its basic design target. These design targets, among others, were specified as follows: (1) the design target life of the WaveEL 3.0 system should be 25 years, (2) the installed power of a WEC is assumed to be 125 kW, (3) the mooring lines should be designed to be replaced twice over the 25-year design target life, and (4) the power cable should be designed such that it does not require replacement. Based on these design targets, together with other fixed cost terms, e.g., manufacturing, installation, and exploitation, the initial LCoE of the reference concept was calculated as 2.28 EUR/kWh. Details on the cost terms used in the initial calculation are presented in Paper V and by Ringsberg et al. (2018).

The purpose of this section is to present and discuss how the numerically evaluated fatigue damage of the moorings and cable and power performance of the WEC will together affect the LCoE assessment. Two aspects are considered in this section: the inclusion of the numerically calculated power performance and fatigue damage (Section 5.5.1) and the effect of hydrodynamic interactions in an array system (Section 5.5.2).

### 5.5.1 Effect of the inclusion of the fatigue damage and power performance

In Paper V, the LCoE of the single-unit reference concept WaveEL 3.0 was compared with that of two other WEC systems: a 2-WEC system and a 10-WEC array system. Adopting the same design targets described above, assuming that all other costs are calculated according to the configuration and to the number of components used in each respective system, the LCoE values will be as presented in the first row of Table 9. Note that the calculations were performed for either one WEC or an array with an exact number of sub-unit WECs in each configuration; see Paper V for details.

Using the methodology presented in this thesis, the LCoE of the different systems can be recalculated based on the power matrix and fatigue matrices estimated from numerical simulations (as in the examples presented in Figures 30 and 31). To demonstrate this procedure, a simple estimation is presented in the following, which involved the following assumptions:

- Short-term measurement data extracted from the full-scale installation in Runde showed that the loads are generally heading towards directions between 0 and 30 degrees. Hence, an incident load direction (waves, wind, and ocean current) of 15 degrees was used to calculate the power and fatigue matrices of the WaveEL 3.0 system.

**Table 9.** LCoE calculation for four WEC systems based on design targets specified in the text (unit: EUR/kWh).

| | **WaveEL 3.0 system** | **2-WEC system, 250-m separation distance** | **2-WEC system, 600-m separation distance** | **10-WEC array system** |
|---|---|---|---|---|
| Initial calculation | 2.28 | 1.50 | 1.55 | 1.10 |
| Recalculation with (i) a consideration of the mooring fatigue, and (ii) an assumption of an installed power of 125 kW for each WEC | 2.47 | 1.88 | 1.93 | - |
| Recalculation with (i) a consideration of the mooring fatigue, and (ii) power performance of each WEC based on the power matrix calculated from simulations | 12.96 | 9.88 | 10.11 | - |

- The LCoE calculation for the two-WEC system disregarded the hydrodynamic interaction effect on the power performance and the fatigue damage, i.e., all the WECs were assumed to have the same power performance and mooring fatigue life as the corresponding values from the reference WaveEL 3.0 system.
- The AEP of the WECs in different systems was calculated using two different values. In the first calculation, the AEP of the WECs in different systems was calculated by assuming an installed power of 125 kW for each individual WEC, i.e., the design target from the reference concept. The calculation was chosen to isolate the change in the LCoE exclusively from the fatigue damage of the mooring lines and power cables. In the second calculation, the AEP of the WEC was calculated using the power matrix acquired from the numerical simulations together with the wave scatter diagram obtained at the Runde test site (which can be found in Paper II). For both calculations, two additional factors, $\eta_{\text{Availability}}$ and $\eta_{\text{Transmission}}$, were considered and respectively set to 0.95 and 0.2; see the detailed definitions of the two factors in Paper V. The AEP was therefore calculated to be $2.1 \times 10^5$ kWh/year in the first calculation and $4 \times 10^4$ kWh/year in the second calculation.
- The annually accumulated fatigue damages of the three mooring lines $\text{Moor}_1$, $\text{Moor}_2$, and $\text{Moor}_3$ were calculated to be $1.0 \times 10^{13}$, $2.2 \times 10^{-4}$, and $2.9 \times 10^{-6}$, respectively. Because the annual fatigue damage of $\text{Moor}_1$ was estimated to be greater than one, this specific mooring leg could potentially fail within one year. This estimated large fatigue damage is attributed to the fact that a constant and unidirectional $Dir_{\text{load}}$ was used in the current calculation; see the discussion in Section 5.4.2. Nonetheless, the estimated annual fatigue damage of the three mooring legs will result in fatigue lives of $1.0 \times 10^{-13}$, $4.5 \times 10^3$, and $3.4 \times 10^5$ years, respectively.
- Following a similar calculation principle for the mooring lines, the annual fatigue damage of the power able is estimated to be $3.7 \times 10^{-10}$, resulting in a fatigue life of $2.7 \times 10^9$ years.

- The factor directly connected to the fatigue damage estimation is the expected number of component replacements throughout the target service life of the system. For operational reasons, it was assumed that component replacement will be performed at most once per year. Therefore, according to the estimates gathered from the numerical simulations, only $Moor_1$ must be replaced annually, and no replacement is required for the other moorings and the power cable.

Finally, the LCoE of the systems can be recalculated based on the newly calculated frequency of component replacement and the AEP of the WEC; the corresponding results are presented in the second and third rows of Table 9. When only the fatigue damage was considered in the calculation, an 8% increase in the LCoE was found for the reference WaveEL 3.0 system, and a 25% increase on average was found for the 2-WEC system. No calculation was made for the 10-WEC system. Due to the large variation in the moorings' fatigue observed for this system (cf., Figure 33), it was determined that the updated LCoE calculation of this system based on all other assumptions would be too uncertain to provide a reliable estimate. Additionally, if the AEP of the WEC is also calculated using the power matrix, the LCoE values for all the configurations are further increased by a factor of 5.

Note that all the results presented in the table should be read with caution because the estimates encompass a large uncertainty in terms of both the numerical simulations (discussed in Sections 5.1-5.4) and the cost terms included in the LCoE analysis (see Paper V and Ringsberg et al. (2018)). Nonetheless, these results indicate that the estimation of the LCoE could potentially be underestimated if one disregards a detailed estimate of the components' fatigue lives as well as the WEC's power performance.

### 5.5.2 Effect of the hydrodynamic interaction between WECs in array configurations

The primary objective of Paper V was to quantify how the power performance and fatigue lives of the moorings are affected by the interaction effect between the WECs in a wave farm. As a secondary objective, Paper V presents LCoE calculations that quantify the magnitude of the contribution that the interaction effects may make to the LCoE value per installed WEC unit. A sample result for the latter objective is presented and discussed in this section, and the reader is referred to Paper V for further details.

In the LCoE calculation, two primary factors are directly associated with the influence from the hydrodynamic interaction effects: the power performance and the expected replacement of moorings due to the change in the accumulated fatigue damage. The change in the accumulated fatigue is quantified by the factor $I_F$, which is the ratio of the mooring's fatigue damage with the interaction effect to that without the interaction effect. Similarly, the change in the power performance due to the interaction effect is quantified by the factor $I_P$. The calculated LCoE including the interaction effect is hereafter referred to as $LCoE_{Interact}$, whereas the value calculated without the interaction effect is referred to as $LCoE_{Initial}$.

Figure 36 presents the results obtained from the LCoE calculations for the 10-WEC array system. Because the LCoE value is directly affected by $I_P$ and $I_F$, a large number of LCoE calculations were carried out. The $x$-axis range corresponds to the lower and upper values of $I_F$, and the $y$-axis range corresponds to the lower and upper values of $I_P$ estimated from the six

loading cases studied in Paper V. The fraction $LCoE_{Interact}/LCoE_{Initial}$ was thus calculated for a large number of combinations and plotted as contours – a value of less than one is favourable. The hydrodynamic interaction between the WECs shows a strong effect on the LCoE of the 10-WEC system; the LCoE of the system can be reduced by at most a factor of 2 or increased by a factor of 7. The results presented in Figure 36 highlight the need to investigate the effect of the interaction between the WECs for a realistic economic estimation when the WECs are to be deployed in a large array farm.

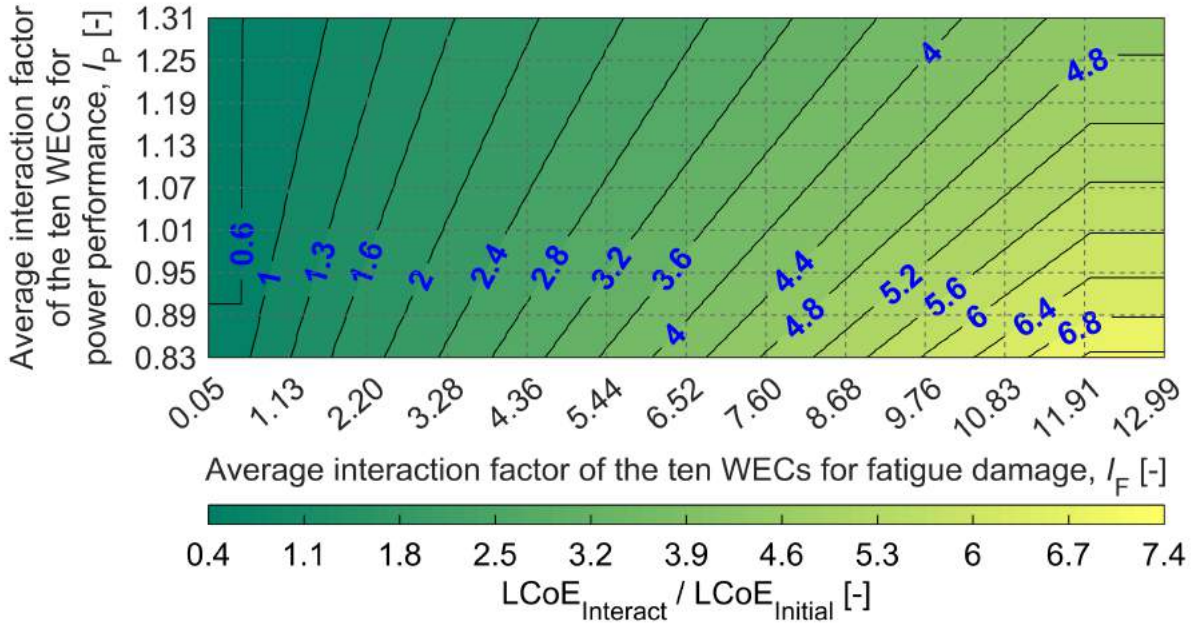


**Figure 36.** Results from LCoE calculations of the 10-WEC array system showing the changes in $LCoE_{Interact}/LCoE_{Initial}$ owing to hydrodynamic interaction effects that affect $I_F$ and $I_P$. The absolute value of $LCoE_{Initial}$ used in the current figure is 1.10 EUR/kWh. $I_F$ and $I_P$ are referred to as the interaction ratios with regard to accumulated fatigue damage and power performance, respectively. $I_F$ or $I_P$ values greater than one respectively indicate that the accumulated fatigue damage or the power performance is increased due to the hydrodynamic interaction effect between WECs.

## 5.6 Experimental analysis

The section presents sample results from two experimental analyses carried out in this thesis. Section 5.6.1 compares a WEC motion validation study of the simulation procedure with experiments carried out in a laboratory ocean basin. The study is presented in detail in Paper IV. Section 5.6.2 presents results from full-scale measurements and comparisons with results from numerical simulations of the WaveEL 3.0 WEC installed in Runde, Norway. These results have not been presented or published in the papers appended to this thesis.

### 5.6.1 Laboratory ocean basin experiments

The detailed design of the experimental WEC model and all of its components and properties are presented in Paper IV. The test programme included several combinations of sea states

(regular and irregular) and ocean current loads, divided into operational and survival conditions. Decay and mooring stiffness tests were also carried out. A 1:20 scale model was used in the operational conditions cases, while a 1:36 scale model was used for the survival conditions cases. Although both operational and survival conditions were tested in the laboratory ocean basin, the operational conditions were the focus of this thesis; see Paper IV for details.

Floating point-absorbing WEC systems should allow for large flexibility to move in the heave and surge directions (Falnes & Hals, 2012; Gao & Moan, 2009). Fitzgerald & Bergdahl (2007) and Paper I showed that the pitch motion is also important to consider, especially in comparisons between numerical simulation models and experiments. Hence, these three motions were compared between the numerical simulation model and the physical models used in the experiments. Figure 37 presents the results of WEC motion under regular and irregular wave cases, which have been reproduced from Figures 7 and 8 of Paper IV.

The motions of the WEC in the regular wave cases are presented in the form of response amplitude operators (RAOs); see Figures 37(a), 37(b), and 37(c) for the surge, heave, and pitch motions of the WEC, respectively. For each set of results, the data points from short to long wave periods and from low to high RAOs correspond to the regular wave cases Re1 to Re7, cf., Table 4. There is good agreement between the simulations and the experiments with respect to both the heave and surge motions of the WEC when the incoming wave period is far from the resonance period of the WEC, which for the physical model was 1.424 seconds; see cases Re1, Re2, Re6, and Re7. Note that the Re2 case was an exception that could not be understood based on the assessment of the experimental and numerical results. For the other cases in which good agreement was obtained, the ratios of the RAOs calculated from the numerical simulations and the RAOs estimated from the experiments were on average 0.97 and 1.05 in the surge and heave directions, respectively.

The results from the simulations and experiments deviate with respect to both surge and heave for the cases with a wave period close to resonance (namely, cases Re3, Re4, and Re5). The simulation model underestimates (by a factor of 0.76) the surge motion in the low wave height condition (Re3), while it overestimates the surge motion (by a factor of 2.11) in the high wave height condition (Re5). This result aligns with another observation made during a horizontal stiffness test; the test showed that the simulated mooring stiffness was smaller in the high-load region but larger in the low-load region; see Paper IV for details.

The taut-moored system used in the study is highly complex and includes many parts and connection points in the physical model. It was a challenge to represent the system in the simulation model as it introduced a large model uncertainty. For instance, different small steel rings were used to link floaters, wires, and springs in the experimental model, but they were represented in the numerical model as node-to-node connections due to the lack of a detailed description of these couplings in the physical model. In addition, the mooring steel wires were covered by a plastic tube. The software used did not allow for inhomogeneous cross-section modelling of the mooring lines; hence, the steel wire and the plastic tube were modelled as one slender structure with the mechanical properties of the two combined. The abovementioned issues contribute to the model uncertainty, which affects the discrepancy in the prediction of the WEC's surge motion compared with the measured surge motions using the physical model.

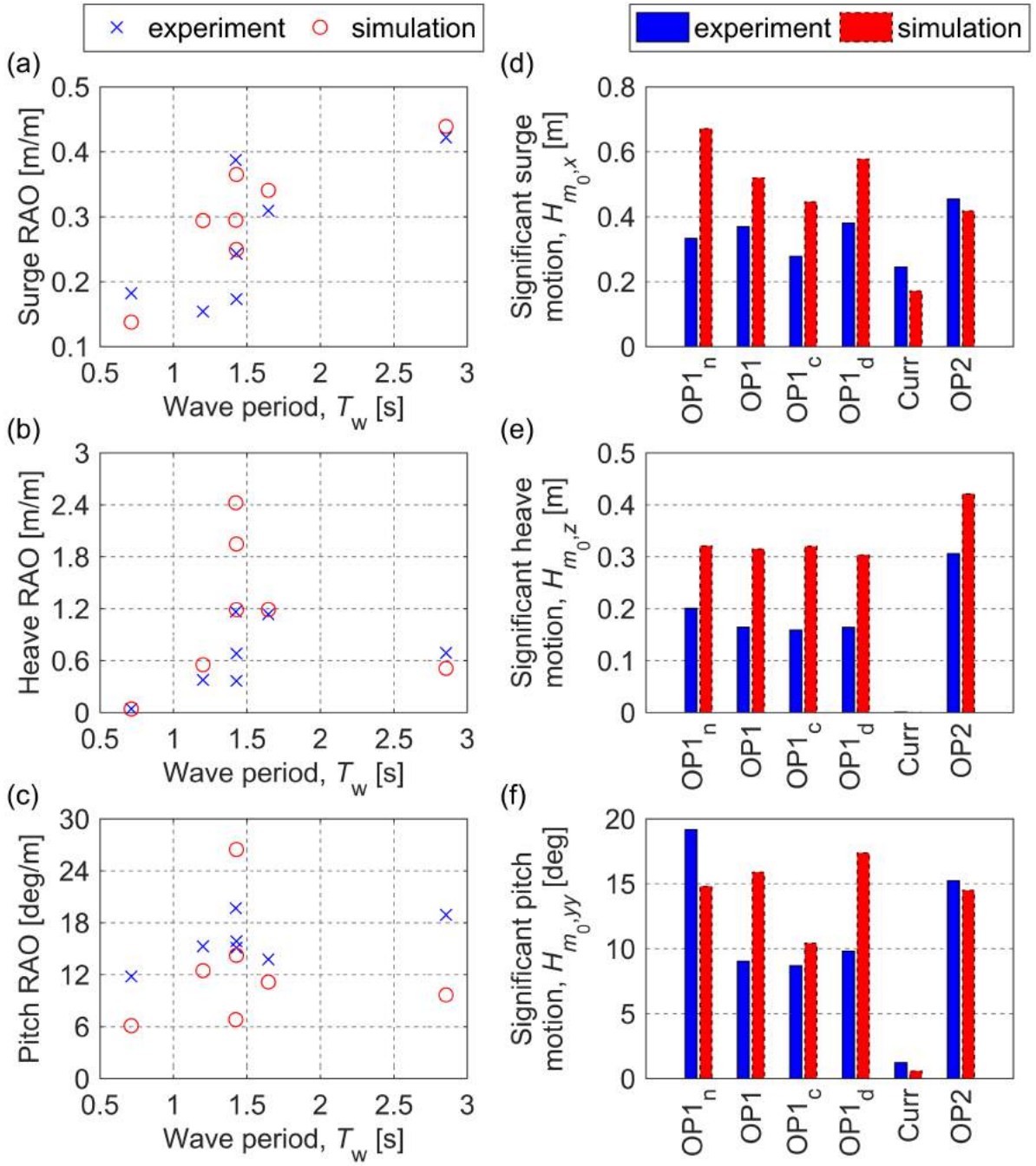


**Figure 37.** Results (from Paper IV) from experiments and numerical simulations of the WEC's motion under regular wave cases ((a) – (c)) and irregular wave cases ((d) – (f)). Three directions of WEC motion are plotted, including ((a) and (d)) surge, ((b) and (e)) heave, and ((c) and (f)) pitch motions. For each set of results presented in (a) – (c), the data points from short to long wave periods and from low to high RAOs correspond to the regular wave cases Re1 – Re7. For WEC motion under irregular wave conditions (results in (d) – (f)), the results for significant motions (namely, $H_{m0}$, or, mean of the highest third of the motion response) are plotted.

For heave motion under resonance, larger responses were consistently predicted by the simulation, where the ratio of the estimated response amplitude between the simulations and

experiments was on average 2.7 (Re3, Re4, and Re5). During the experiments, overtopping of the WEC (i.e., green water) was observed in all three cases (as well as in all the tested irregular wave cases); see Figure 38 for an example. It is known that overtopping on WECs can contribute to additional damping. The simulation model and software used can neither simulate the phenomenon nor consider its influence on the WEC's response. The observed overtopping phenomenon serves as one explanation for the overestimation in the heave motion in the resonant regular wave cases.

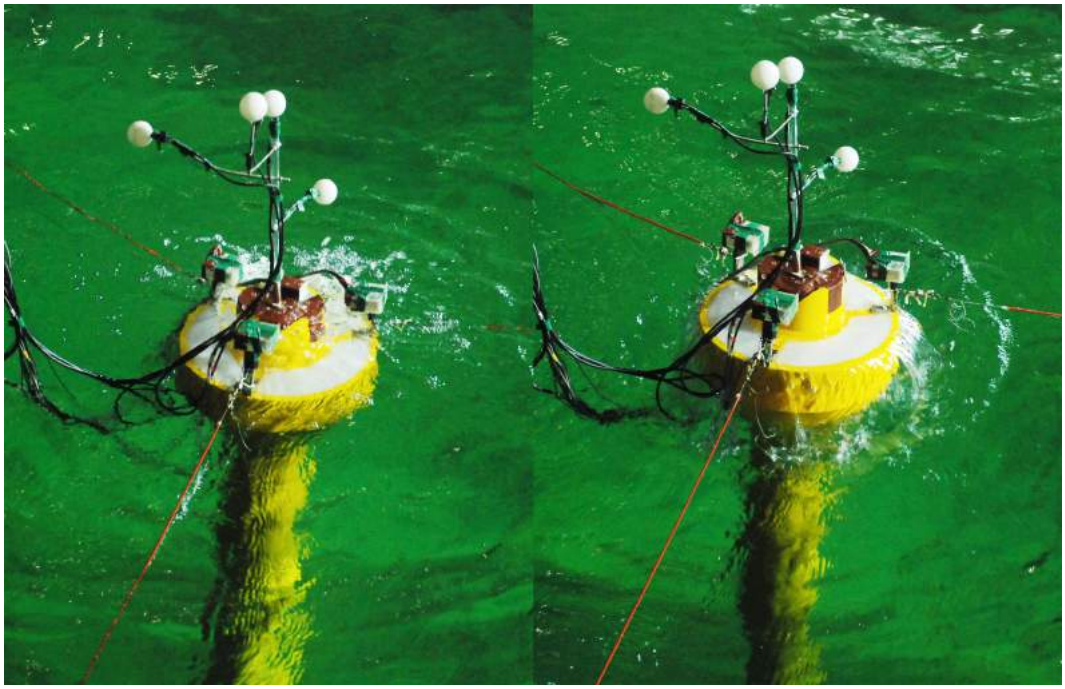

**Figure 38.** Example of observed overtopping of the WEC buoy; the photograph was obtained for the test case OP1: (left) the WEC buoy is completely submerged; (right) the WEC buoy leaves the submerged condition. The figure is reproduced from Figure 12 of Paper IV.

The comparison between the experiments and the simulations with respect to the pitch motion is also less satisfactory. The cause of the discrepancies in the pitch and heave (specifically under the resonance) is likely attributed to the uncertainty from a complex PTO installation and the modelling approach used in the numerical simulation. During the experiment, the damping effect of the heave plate was measured by a decay test through a 1-DoF spring-mass-damping system under a still-water condition. No estimation or tuning was made with regard to the PTO damping under various frequencies or to the position of the heave plate. Therefore, the frequency and position dependence of the heave plate damping was disregarded in the numerical model. In addition, for the current model implementation of the PTO system, except for the spring that was directly defined by its mechanical properties in the numerical model, the connection bar and heave plate were represented by the Morison model, which introduced only the viscous damping effect on the motion of the WEC buoy. The inertial and restoring effects of the connection bar and heave plate were considered in a different manner and included in the mass and inertia of the WEC buoy. The results shown in Figures 37(b) and 37(c) suggest that a more detailed modelling of the PTO system may be needed in future work; see discussion in Chapter 7.

Irregular waves were included in the test programme to investigate the integrated hydrodynamic characteristics of the entire WEC system. Comparisons of the experimental and simulation results for significant surge, heave, and pitch motions of the WEC for all the irregular wave cases are presented in Figures 37(d), 37(e), and 37(f), respectively, whereas a comparison in terms of the standard deviation and response spectra is presented in detail in Paper IV.

A comparison of surge motion in case Curr confirmed that the use of the current load coefficient together with the mean drift approximated by the numerical model is capable of modelling the current load effect on the WEC buoy. As suggested by DNV GL (2017a), the current load coefficient should ideally be determined by a dedicated tank test with a WEC buoy, while the numerical model for the experiment adopts an empirical formula, as suggested by Moberg (1988). The results show that the ratio of the estimated significant motions in surge between the simulation and experiment is 0.7, which is comparable to results published by others, such as Gao & Moan (2009) and Moberg (1988). Hence, the observed discrepancy in the estimated surge motion due to the current load between the experiment and simulation results was deemed acceptable.

As expected, the differences between the results obtained from the experiments and the simulations were found to be more evident when the irregular wave cases were closer to the resonance frequency (i.e., all the OP1-related cases). For these cases, the average ratios of the estimated significant motion between the simulation and experiment were 1.64, 1.85, and 1.38 in the surge, heave, and pitch of the WEC, respectively. The overestimations from the numerical simulations are believed to be due to a combination of the factors addressed above: the underestimated mooring stiffness in the high-load region, the damping effect due to overtopping, the simplified numerical model of the PTO system, and the use of a current load coefficient from an empirical formula. In general, the results suggest that a better numerical model for the PTO system must be implemented to fully capture all the damping effects present in the physical model of the WEC system.

A comparison between the experiments and the numerical simulation shows reasonable agreement for case OP2, with relative differences in the observed motion responses of 8%, 35%, and 5% for the surge, heave, and pitch directions, respectively. Together with the results presented for the regular wave cases, the numerical model was demonstrated to be useful for predicting the dynamic motion response of the WEC system under off-resonant wave conditions.

### 5.6.2 Full-scale measurement

This section compares results from numerical simulations and measurements made on the full-scale WEC installation WaveEL 3.0 over three days, June 16, 18 and 19, 2017. The section aims to present and discuss the predictability of the numerical simulation model; thus, the section focuses on presenting results. A full description of how the measurement data were post-processed and how the sea states and environmental loads to which the WEC was subjected over the three days were identified were presented by Lang et al. (2018); see Table 6 for a description of the environmental loads used in the numerical simulations. In the following, a comparison of the three translational motions of the WEC is presented, followed by a comparison of the mooring forces. Note that in this thesis, because the WEC buoy used in the full-scale installation was different from the prototype WEC used to design the ocean basin experiment, no further comparison was made between the results from the model-scale and full-scale measurements.

Figure 39 presents a spectral analysis of the WEC's motion in the heave direction based on the measurement data and the results from the numerical simulations. The figure shows reasonably good agreement in terms of the overall trend and the peak values of the spectra. However, the measurements show broader band spectra compared with the simulations. Two peaks not found in the simulation results were observed in the measurement data. The reason for this discrepancy is derived from how the environmental conditions used in the numerical simulation model were retrieved. Lang et al. (2018) indicated that the environmental conditions during the measurement campaign carried out on June 16, 18 and 19 were not monitored. A method was developed to identify which environmental conditions (i.e., stationary sea states with a duration of 3 hours) gave rise to the WEC's motions. This information was thereafter used in numerical simulations in which the sea state was assumed to be stationary for 3 hours and followed the JONSWAP spectrum with a peak enhancement factor of 2.4. The results in Figure 39 indicate that these assumptions may have been violated, as in reality, it is likely that the sea states in Runde were not stationary during the 3-hour periods on which the measurement data were based. Additionally, the wave spectrum used in the simulation model could have been represented by another model because the WEC installation is rather close to an island. Nevertheless, despite these assumptions, which contributed to the model uncertainty, the comparison of the spectral responses was considered acceptable given the objectives of this thesis.

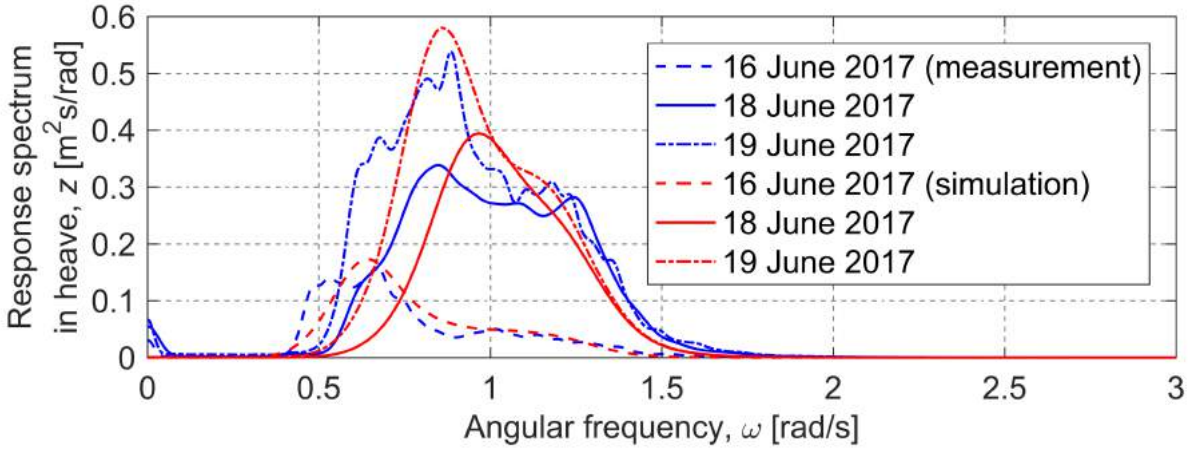


**Figure 39.** Response spectra for the heave motion of the WEC from the full-scale measurements (blue lines) and the numerical simulations (red lines).

The WEC's motions in the heave, surge, and pitch directions are presented in Figure 40 as the significant motions. The incident wave load direction during the measurements was not recorded very accurately, but it was estimated at the test site to vary between 0 and 60 degrees; this finding was also confirmed in the post-processing of the recorded measurements. Because the horizontal motion of a WEC is known to be greatly influenced by the incident wave direction ($Dir_{\text{wave}}$), see the discussion by Yang et al. (2014), the numerical simulations were carried out for three incident wave directions to assess the sensitivity to the WEC motion responses under the current environmental loading conditions.

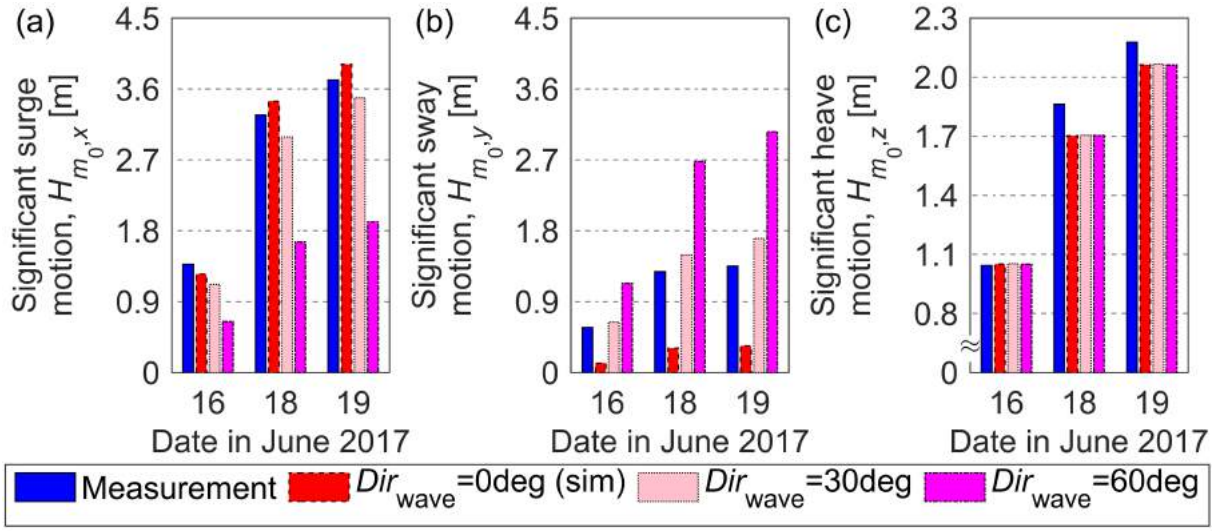


**Figure 40.** Comparison of results from measurements and numerical simulations: the significant motions for (a) surge, (b) sway, and (c) heave. Three incident wave loading directions in the numerical simulations are included ($Dir_{\text{wave}} = 0$, 30, and 60 deg).

The agreement in the heave motion responses between the measurements and simulations is good. $Dir_{\text{wave}}$ has a negligible influence on the heave response. Irrespective of $Dir_{\text{wave}}$, the ratios of the estimated significant heave motion between the simulations and the measurements were consistently 1.01, 0.92, and 0.95 on June 16, 18, and 19, respectively. The sea state on June 18 was closer to the WEC's resonance period, whereas the sea states on the other two days were further away from the resonance of the WEC. This finding could explain why the discrepancy in the heave motion was observed to be the largest on June 18.

Conversely, $Dir_{\text{wave}}$ has a stronger influence on the surge and sway motions; see Figures 40(a) and 40(b). An analysis of the measurement data showed that the 30-degree wave loading direction was the most frequent wave loading direction during the measurement campaign. Hence, the discussion of the surge and sway results will focus on this simulation case. The three-day averaged ratio of the estimated significant motion between the simulations and the measurements were 0.89 and 1.18 for the surge and sway, respectively. For the significant motion in the surge direction, the largest discrepancy was observed on June 16, when the simulated surge motion was 0.82 times greater than the measured motion. The largest discrepancy in the sway was observed on June 19, when the simulated sway motion was 1.26 times greater than the measured motion. In comparing the magnitude of these differences with what was observed in the ocean basin experiments in Paper IV, and considering the uncertainty in the environmental loading conditions of the full-scale measurement, the differences between the measurements and simulations observed in Figure 40 are within the range that could have been expected prior to the comparison.

Another important and contributing factor to the discrepancy in the horizontal motions (i.e., surge and sway) originates from wave directional spreading. In the numerical model, the wave load in a simulation had a pre-defined incident direction for which directional spreading was not accounted. It is known that ocean waves have multidirectional components that are very difficult to measure/estimate if the measurement is carried out at a single point, as was the case in Runde (McAllister et al., 2017). Figure 41 compares the WEC's horizontal motions determined from the measurements and the numerical simulations. Because of the larger motion

area in the measurement part of the figure, the results in the figure confirm that wave directional spreading should have been considered in the numerical model.

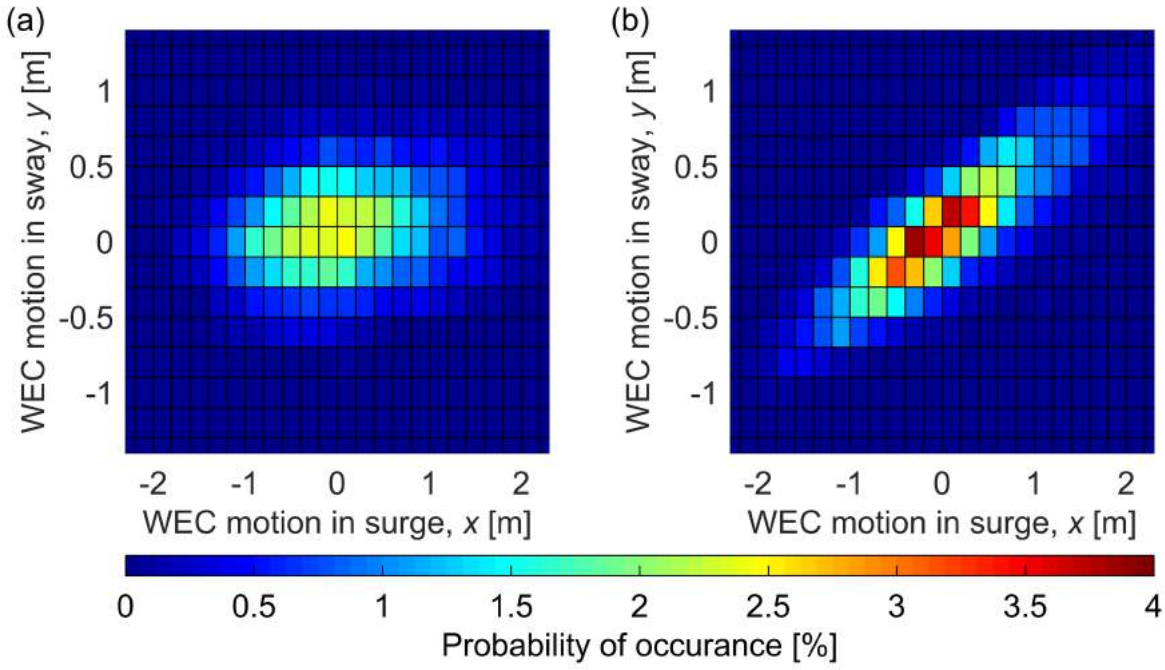


**Figure 41.** The WEC's motions in the horizontal plane determined from (a) measurements and (b) numerical simulations. The results are presented using data from the measurements performed on June 19, 2017. The numerical simulation was carried out using $Dir_{\text{wave}} = 30$ deg. The origin of each figure defines the mean position of the WEC, calculated from its full data. The colour scheme shows the probability of occurrence of the WEC present in that specific area from each of the three-hour data.

The mooring line forces are compared in Figure 42. The mooring line forces were measured by load cells at the fairlead points of the WEC; hence, the mooring line forces obtained from the numerical model were presented in the same locations. The results for mooring line $\text{Moor}_3$ were excluded from the comparison. During data processing, a malfunction in the mooring's load cell was found. In addition, the sea states during the measurement campaign were calm, and the measurement accuracy of the load cells was rather low. Therefore, only the mean values of the mooring line forces during the identified 3-hour stationary sea states are presented because other statistical properties will not be useful or reliable in the comparison under these circumstances.

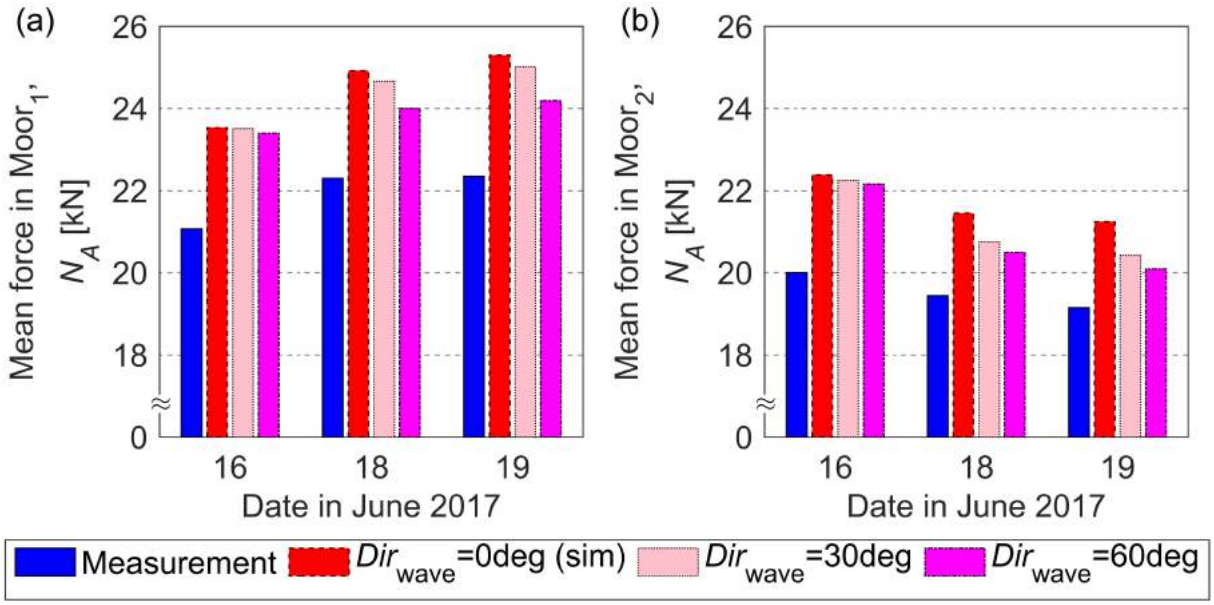


**Figure 42.** Mean force responses in (a) $Moor_1$ and (b) $Moor_2$ measured for the full-scale installation and determined by numerical simulation.

The results show that the numerical model overestimates the mooring forces relative to the results from the measurements. For the $Dir_{\text{wave}} = 30$ deg simulation case, for example, the simulations show approximately 11% and 8% higher forces in $Moor_1$ and $Moor_2$, respectively. This discrepancy between the measurements and numerical simulations must be considered acceptable, considering all of the uncertainties that exist, some of which were discussed previously in this sub-section. An additional uncertainty that must be studied is that associated with the material data of the mooring lines, i.e., the influence of the material properties of the WaveEL 3.0 polyester mooring lines under dry and soaked conditions.

The discrepancy in the motion and force responses between the measurement and simulation can also be attributed to the realisation of ocean waves in the numerical simulation. Due to the lack of exact measurement data from ocean waves, the wave loads used in the numerical simulation were sampled by the software using pseudo-random numbers (SINTEF Ocean, 2017a, 2017b). Although the statistical properties of different wave realisations are identical, the actual individual wave components for a particular wave time series can vary, which will further influence the motion and force responses predicted by the numerical simulation. Figure 43 shows one example of a comparison between the measurement data and the numerical simulation results from different wave realisations. As shown in Figure 43, one can find maximum differences of 13%, 33%, and 9% between the simulated motion responses and the measured surge, sway, and heave motions of the WEC on June 18, 2017. In contrast, due to the differences in the wave realisations, the minimum differences between the simulated responses and measurements were 0.3%, 16%, and 6% for the surge, sway, and heave motions of the WEC on the same date. The comparison for the mooring force was found to be less affected by the variation of the wave realisations. The maximum differences were found to be 10.7% and 6.9% for $Moor_1$ and $Moor_2$, respectively, whereas the minimum differences were found to be 10.5% and 6.5% for $Moor_1$ and $Moor_2$, respectively.

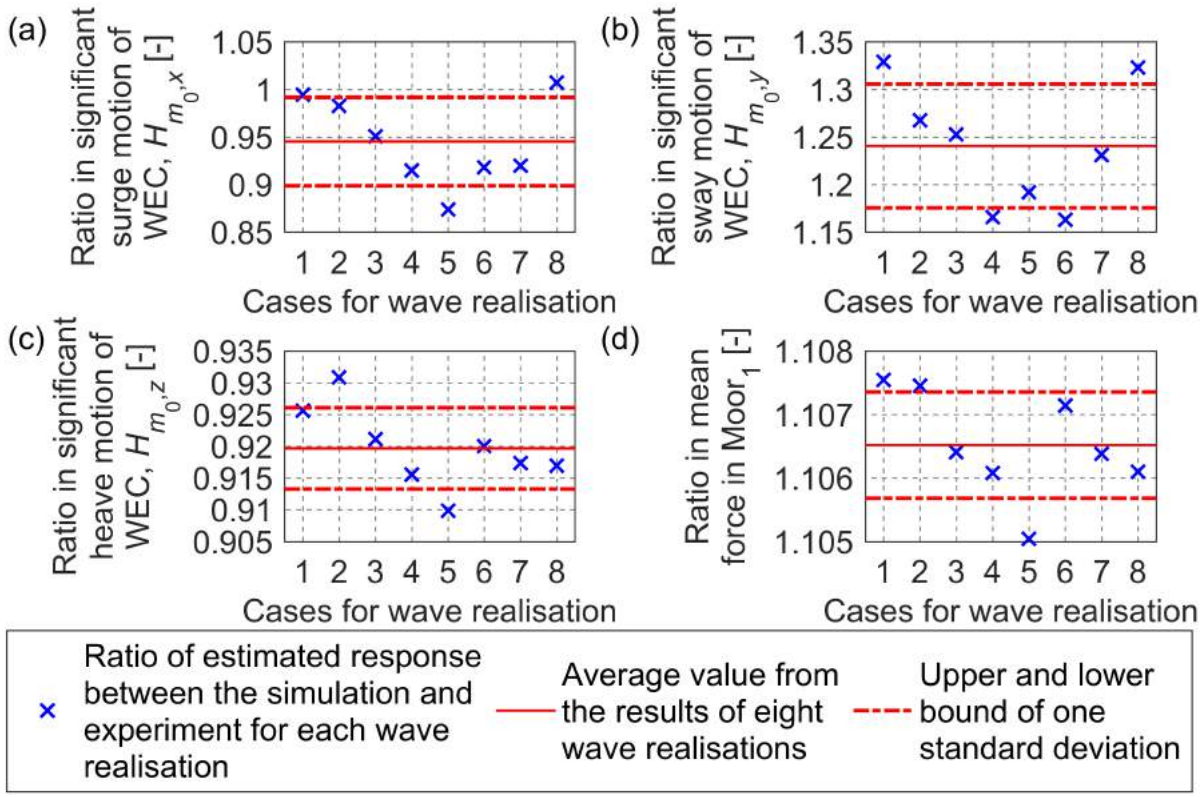


**Figure 43.** Comparison of the estimated (a) surge, (b) sway, and (c) heave motions of the WEC and (d) the mean force of $Moor_1$ using different random seeds of wave realisation. The numerical simulation was carried out for the sea states on June 18, 2017, with $Dir_{\text{wave}} = 30$ deg. All the results are normalised by the corresponding value from the measurement on the same date. The results obtained for Case 4 in the figure are the same results presented in Figures 40 and 42.

To conclude, the numerical simulation model of the WaveEL 3.0 WEC system installed in Runde shows some differences relative to the real and physical WEC system. These differences include, among others, a simplified PTO system model, a hub modelled as a stationary fixed point, and wave loading conditions that were not yet modelled in this thesis by considering wave spreading or the exact wave spectrum at the measurement site. Despite all the differences, the average ratios of the estimated significant motion between the simulation using $Dir_{\text{wave}} = 30$ deg and the measurements were 0.89, 1.18, and 0.96 for the surge, sway, and heave motions of the WEC, respectively. For the mooring forces, with reference to the $Dir_{\text{wave}} = 30$ deg simulation case, the simulations showed approximately 10% higher mean forces compared with the measured forces. A validation study of the simulation model regarding its ability to predict mooring line forces versus the laboratory ocean basin experiments is planned for future work. However, regarding the rather good agreement with the measured mooring line forces, the numerical simulation model's prediction ability can be considered good at least for rather calm sea states. It will be important to compare the numerical model's prediction ability against measurements obtained under more severe sea states in which the hydrodynamics and coupling effects are more pronounced, which may require additional revisions of the numerical model.

# 6 Conclusions

The main objective of the work presented in the thesis was to develop a complete numerical analysis procedure for the mooring lines and power cables used in WEC systems. Such an analysis should address the fatigue life assessments of the moorings and cables while providing high-level assessments of the overall performance of the WEC system, such as its power performance.

An analysis procedure was developed in the thesis project, and this thesis presents how the different parts of that procedure were developed and partly verifies and validates the method. The procedure enables the detailed fatigue life assessment of the mooring lines and power cables used in floating point-absorbing WEC systems. With the support of the analysis procedure, the thesis contributes to the understanding of how numerical and experimental analysis methods can be applied to simulate and assess the fatigue characteristics of mooring lines and power cables in a WEC system as well as the system's power performance, both of which are essential to realistic economic and feasibility assessments of a system. The novelty of this work lies in the systems perspective adopted, the large number of parameter sensitivity studies performed, and the numerical simulations and experimental analyses conducted at the model scale and at full scale, while studying the fatigue of the sub-components in a WEC system. The aim was not only to study the fatigue characteristics of the mooring and cable components but also to provide an analysis method for high-level assessments of the overall performance of the WEC system. The overall analysis methods can therefore be used to provide confidence in the cost-efficient development of wave energy applications, which is needed to reach large-scale commercialisation.

*Numerical analysis procedure*

Comparison of different simulation procedures were presented primarily in Papers I and V. Two de-coupled analysis approaches were compared with a coupled analysis approach. With regard to the main objective of this thesis, the conclusion was to recommend the coupled analysis approach because it best captured the hydrodynamic interactions between WECs in an array system; more importantly, it captured the couplings between the WEC and the mooring lines and power cable connected to it. These coupling effects and the hydrodynamic interactions were found to be of great importance in performing realistic and reliable simulations of the dynamic motions and force responses of the WEC system and, hence, in yielding a reliable estimate of the fatigue service life of the system's moorings and cables.

The power cable was consistently estimated to have a long fatigue life under all simulated conditions throughout this thesis project. The methodology employed is based on a first-principles design level and consequently does not include all the intrinsic mechanics that lead to the fatigue degradation of the cable (such as wear and fretting). Therefore, the fatigue life predicted using the methodology may be considered an upper bound. However, the investigated power cable underwent extensive fatigue rotating testing in a laboratory. Based on the test results, the power cable was able to survive more than $10^6$ rotating bending cycles and several run-outs for large curvatures (compared with a traditional offshore cable at a scale of $10^3$ fatigue cycle as the reference). Hence, although a more detailed local model of the power cable must be developed to truly capture its failure mechanics, the current simulated results of the power cable with regard to its fatigue are considered acceptable.

*Parametric and sensitivity studies*

A fatigue wave-height/wave-period matrix was designed as a visualisation tool to reflect the influence of environmental loads on the fatigue damage accumulation in the mooring lines and the power cable. The simulation results showed that the fatigue lives of the mooring lines and power cable were largely influenced by the environmental loads and their compositions. Parameter sensitivity studies were carried out and showed how the mutual directionality of wave, wind and ocean current loads affects the fatigue lives of the moorings and cables. For example, large accumulation of fatigue damage in the moorings and the cable occurs at high wave heights and near the resonant wave period of the WEC, which also represent the target operational window over which the WEC exhibits its best power performance. The presence of ocean current loads strongly enhances the accumulation of fatigue damage; thus, such must always be considered in the design of WEC systems, preferably by using values and profiles based on measurements at the planned site of operation. The fatigue lives of the moorings and cables are sensitive to the incoming loading directions. For the mooring designs studied in this thesis, the shortest fatigue lives were consistently calculated when these components were located in the upwind position of the WEC system.

Various design parameters for the mooring lines and the power cable were investigated throughout this thesis. As reported in Papers I and III, the sufficient margin in the moorings' line length with a suitable stiffness provided by the entire mooring system was found to be important in ensuring a long fatigue service life for the moorings without compromising the power performance of the WEC. The use of the shared mooring configuration in a WEC array was found to be useful and reduced the LCoE of the WECs in a large deployment; see Paper V. However, a large variation in the accumulated fatigue damage between mooring segments could potentially pose an additional challenge in maintaining the entire shared mooring system.

Paper II showed that the fatigue damage of the power cable is governed by its curvature responses, i.e., a larger curvature response often results in a larger fatigue damage of the cable. The curvature response of the cable can be decreased by increasing the cable mass, the bending stiffness, or the cable length. However, all of these approaches have certain side effects that should be studied before any specific approach is adopted. The simulation results showed that a thorough study of the system's dynamic responses in the initial phase of a WEC design project is paramount to the reliable design of mooring lines and power cables.

*Impact of biofouling*

Parameter sensitivity analyses showed that marine biofouling significantly reduces the power performance of the WEC and the fatigue life of the mooring lines. If the WEC system is assumed to operate for 25 years, the presence of biofouling can lead to a 10% reduction in absorbed power and a 20% decrease in the fatigue life of the mooring line that accumulates the most fatigue damage throughout the entire mooring system. It was concluded that marine biofouling should be considered during the early design phase of a WEC system from the perspectives of power performance and fatigue life, as it also plays an important role in the planning of the maintenance schedule of the WEC system.

*Validation study of WEC motions*

The numerical simulation model was validated against a laboratory ocean basin experiment. The experimental WEC system consisted of a WEC buoy, a unique three-leg two-segment mooring system with submerged floaters, and a PTO system designed for the experiment as a heave plate. The validation study focused on the motion responses of the WEC buoy in surge, heave, and pitch. For all the tested regular and irregular wave cases, the simulation results showed good agreement with the experiments when the wave frequency was far from the WEC's resonance; the ratios of the estimated motion responses between the simulation and experiment were on average 1.15 and 1.11 in surge and heave, respectively. The comparison with respect to the pitch motion was less satisfactory; the numerical model overestimated the motion response of the WEC under the resonant condition. The discrepancy in the latter two aspects suggest that the damping effect captured in the numerical simulation was not sufficient. A better damping model for the PTO system must be developed to capture the damping effect under various sea state conditions.

*Numerical model and simulations of a full-scale WEC system installation*

A numerical simulation model was built to simulate the full-scale WEC system WaveEL 3.0 installed in Runde, Norway. The results of numerical simulations and measurements from a measurement campaign were compared. The results agreed well; the average estimated surge, sway, and heave motion responses from the simulations were 0.89, 1.18, and 0.96 times those of the measurements, respectively. In terms of the mooring forces, the simulations showed approximately 10% higher mean forces compared with the measured forces. Overall, the agreement between the measurements and numerical simulations of the environmental conditions for the three days included in the measurement campaign was good. The numerical simulation model's prediction ability can be considered good at least for rather calm sea states. It will be important to compare the numerical model's prediction ability against measurements obtained under more severe sea states, in which the hydrodynamics and coupling effects are more pronounced, and this may require additional revisions of the numerical model.

*Hydrodynamic interaction effects and LCoE calculations*

Two 2-WEC models (with separation distances of 250 metres and 600 metres) and one 10-WEC array system were studied in Paper V with the objective of quantifying the influence of the hydrodynamic interaction between WECs with regard to the power performance of the WECs and fatigue damage of the mooring lines, among other factors. The hydrodynamic interaction had a minor influence on the power performance, with the induced difference not exceeding 5% among all the studied configurations and environmental conditions. Fatigue analyses of the mooring lines showed a strong influence of the hydrodynamic interaction: the results ranged from a 100% increase to a 60% decrease in the accumulated fatigue damage depending on the WEC configuration and the load case studied. A comparison of the 2-WEC models and the 10-WEC system showed that the hydrodynamic interaction produces a much stronger effect on the latter configuration. Based on the results presented in Paper V, it was concluded that the close proximity between the WECs and the mechanical coupling between the WECs and moorings were the sources for the stronger effect of the hydrodynamic interaction on the 10-WEC system.

The LCoE calculation of the 10-WEC array system yielded LCoE values ranging from a reduction of 40% to an increase of 60% relative to the simulations that did not consider the hydrodynamic interaction effects. It was therefore concluded that the hydrodynamic interaction must be considered in a system analysis of a full WEC system and wave farm.

# 7 Future work

The purpose of this PhD research as a whole was to develop a complete numerical analysis procedure for the mooring lines and power cables used in floating WEC systems, which will hopefully contribute to the long-term advancement of wave energy technology. The work presented in this thesis was conducted in accordance with the research framework presented in Figure 3. With an emphasis on improving the structural integrity and service lives of the moorings and cables, while also considering WEC energy harvesting performance, a number of issues have been identified as potential topics of future work to enable us to reach our long-term goals. We aim to reach those goal by providing a solution for ensuring long service lives of the mooring lines and power cables used in WEC systems.

*Validation of forces from the ocean basin test*

The ocean basin experimental data have, to date, been used to validate numerical simulations of the WECs' motions under operational conditions. The validation of the mooring line forces, force responses of the PTO system, and survival conditions was planned in the course of this thesis but has not been completed at the time of writing. In addition, nonlinear hydrodynamic phenomena, such as overtopping and vortex-induced motion, were visually observed during the experiment. An additional investigation is also needed to focus on the cases in which the nonlinear wave load plays an important role. Hence, an obvious next step is to complete the planned validation task. The accomplishment of the validation work will thus ensure the overall validity of the proposed methodology for hydrodynamic and structural response analyses of WEC systems.

*Development of the methodology for the survival conditions*

As presented in Section 5.4.1, the mooring lines can accumulate relatively large fatigue damage under harsh environmental conditions. Many of these conditions require nonlinear wave theory for numerical simulations and are not suited for simulation by the method adopted in this thesis due to the use of Airy wave theory. Hence, the development of a methodology for severe and survival loading conditions is in order to accurately assess the structural integrity and service life of mooring lines and power cables under all possible loading scenarios.

*Reliability analysis of WEC systems*

The current thesis work mainly focused on the sensitivity of components' fatigue damage accumulation with regard to various design parameters and environmental conditions. Further development is needed to quantify the uncertainty in different parameters and hence enable the reliability analysis of the overall WEC system. The knowledge gained from the reliability analysis may be used to guide product development and the operation and maintenance planning of WEC systems.

*Investigation of true nonlinear mooring material behaviour*

Several types and materials have been proposed for WEC moorings to cope with the dynamic characteristic of WEC systems; see examples in Seaflex (2018) and Thies et al. (2014). In the current thesis, we mainly studied linear elastic mooring materials, namely, steel. Although nonlinear moorings made out of polyester rope were also studied, the only nonlinear property included in the numerical model was a nonlinear and discretised relation between the load and elongation based on a monotonic stress test. As demonstrated by the test results presented by Falkenberg et al. (2018), polyester rope has viscoelastic stiffness and stretch characteristics. The tension versus stretch response of the fibre rope is nonlinear and load-path-dependent, and the length varies with the rate and duration of loading (due to elongation and contraction). This issue was recently addressed by Weller et al. (2018), who developed a time-domain analytical model to capture the time-dependent load and material response relationship that exists in various synthetic ropes, including those made of polyester. To increase the accuracy of the predicted motion and structural response of the WEC system, we would like to incorporate such a model into the current methodology. The incorporation of such a model will also ensure the usability of our developed simulation procedure and can assist the design of mooring solutions with a long service life.

*Integration of the analysis method for the local analysis of a power cable*

The results of Papers II and III highlight the importance of developing a local model to capture the intrinsic failure mechanism of the power cable. The local model was developed in a parallel research project conducted at Chalmers University of Technology. A comparison between the model used in the current thesis and the developed local model is depicted in Figure 44. However, the developed method has not yet been integrated into the overall methodology presented in the current thesis, and it is not yet known how the local model analysis will influence the fatigue assessment of the power cables. Hence, an obvious extension of the research is to integrate the local model analysis into the current analysis methodology.

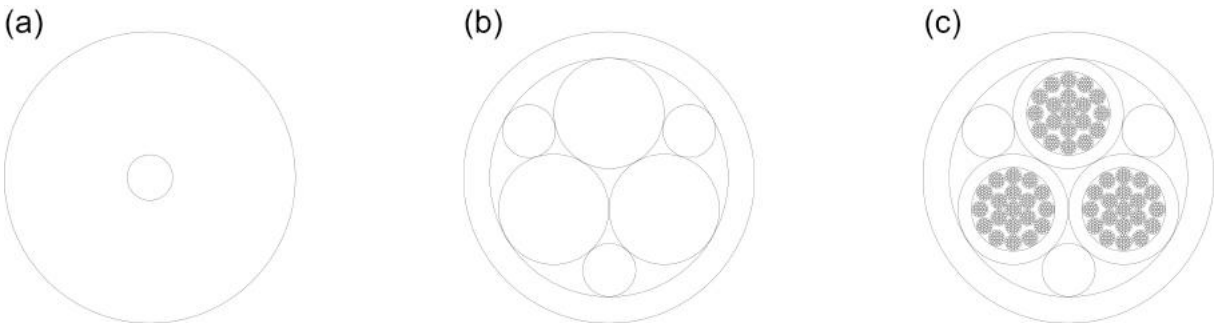


**Figure 44.** Cable models with different levels of complexity: (a) simple model used in the thesis and (b) intermediate and (c) complex models developed in a parallel research project at Chalmers University of Technology. (Courtesy of MSc. Arjoms Kuznecovs.)

*Numerical model of the WaveEL concept*

The numerical model of the WaveEL concept is subject to several simplifications and can be improved in the future. The WEC buoy from the original concept has a central hollow tube, and the tube contains a piston. The piston slides along the tube, and power absorption relies on the relative heave motion between the buoy and the water enclosed in the tube. As discussed by Falcão et al. (2012), the flow motion of the enclosed water in the tube might be important to consider to accurately estimate the hydrodynamics induced by the piston-type PTO mechanism. In addition, a study of a hydraulic PTO system similar to that used in the WaveEL concept (Henderson, 2006) showed that a numeral model of the hydraulic PTO, which allows for a simulation of its nonlinear PTO behaviour in the time domain, is necessary to maximise the power performance and improve the survivability of the PTO system. Finally, the power-collecting hub was modelled as a fixed point, consistent with the initial design assumption. However, due to the observed potential fatigue-critical response of the cable near the hub side, this assumption should also be further examined by explicitly modelling the hub as part of the WEC system.

*Assessment of additional WEC concepts*

The methodology presented in the current thesis is generally applicable to all oscillating WEC systems that require mooring lines and power cables but was applied to only one point-absorbing WEC system designed by the Swedish company Waves4Power. In future work, it would be valuable to extend the application of the proposed methodology to different WEC concepts. The purpose is to demonstrate the usability of the methodology and thereby support different wave energy companies in their concept developments.

*Implementation of a complete LCoE assessment*

The LCoE assessment performed in this thesis is limited to the cost terms related to electricity generation but not to transmission. The sources of the latter costs include, for example, subsea cables from the hub to the shore or transformers in the grid or on shore. Castro-Santos et al. (2016a, 2016b) showed that these cost terms could represent a significant portion of the LCoE. Hence, a more complete calculation must be performed to accurately predict the LCoE of the entire wave array farm. In addition, as reviewed by Dalton et al. (2015), the viability and impact of a wave energy project or a wave energy technology should not be assessed from an economic perspective alone; other assessments from social and environmental perspectives are needed to support decision making for private investment or for public development. Throughout the course of this thesis project, such discussion was initiated in Ringsberg et al. (2018) and two of the master's theses co-supervised by the author of this thesis (Jansson & Örgård, 2017; Vance 2018) and should also be developed further in the future. The complete economic assessment, together with the fatigue assessment tool presented in this thesis, can then be used to assist companies in product development and operation and maintenance planning.

# 8 References


Ambli, N., Bønke, K., Malmo, O., & Reitan, A. (1982) The Kvaerner multiresonant OWC. In: Berge, H. (ed.) Proceedings of the 2nd International Symposium on Wave Energy Utilization, 22-24 June 1982, Trondheim, Norway. pp. 275-295.

Astariz, S., Perez-Collazo, C., Abanades, J., & Iglesias, G. (2015) Co-located wave-wind farms: Economic assessment as a function of layout. Renewable Energy 83, 837-849. [Online] Available from: doi:10.1016/j.renene.2015.05.028 [Accessed 4th March 2018].

Barltrop, N., Varyani, K.S., Grant, A., Clelland, D., & Pham, X. (2006) Wave-current interactions in marine current turbines. Proceedings of the Institution of Mechanical Engineers, Part M: Journal of Engineering for the Maritime Environment 220 (4), 195-203. [Online] Available from: doi:10.1243/14750902JEME45 [Accessed 17th February 2018].

Beels, C., Troch, P., De Backer, G., Vantorre, M., & De Rouck, J. (2010) Numerical implementation and sensitivity analysis of a wave energy converter in a time-dependent mild-slope equation model. Coastal Engineering 57 (5), 471-492. [Online] Available from: doi:10.1016/j.coastaleng.2009.11.003 [Accessed 15th April 2018].

Bhinder, M.A., Karimirad, M., Weller, S., Debruyne, Y., Guérinel, M., & Sheng, W. (2015) Modelling mooring line non-linearities (material and geometric effects) for a wave energy converter using AQWA, SIMA and Orcaflex. In: Proceedings of the 11th European Wave and Tidal Energy Conference (EWTEC2015), 6-11 September 2015, Nantes, Frances. pp. 09D05-02-01—09D05-02-10. 09D5-2.

Callaghan, J., & Boud, R. (2006) Future marine energy. Results of the marine energy challenge: Cost competitiveness and growth of wave and tidal stream energy. London, UK, Carbon Trust. [Online] Available from: https://www.bchydro.com/content/dam/hydro/medialib/internet/documents/planning_regulatory/iep_ltap/ror/appx_11a_marine_energy.pdf [Accessed 15th July 2018].

Carbon Trust, & DNV (2005) Guidelines on design and operation of wave energy converters. Carbon Trust and Det Norske Veritas (DNV). [Online] Available from: https://www.scribd.com/document/57281675/DNV-Wave-Energy-Converter-Regs [Accessed 15th July 2018].

Carswell, W. (2015) Soil-structure modeling and design considerations for offshore wind turbine monopile foundations. Thesis for Doctor of Philosophy, Department of Civil and Environmental Engineering, University of Massachusetts Amherst, Amherst, MA, USA.

Casaubieilh, P., Thiebaut, F., Sheng, W., Bosma, B., Retzler, C., Shaw, M., & Letertre, Y. (2014) Performance improvements of mooring systems for wave energy converters. In: Guedes Soares, C. (ed.) Progress in Renewable Energies Offshore—Proceedings of the 1st International Conference on Renewable Energies Offshore (RENEW2014), 24-26 November 2014, Lisbon, Portugal. London, Taylor & Francis Group. pp. 897-903.

Castro-Santos, L., Martins, E., & Guedes Soares, C. (2016a) Cost assessment methodology for combined wind and wave floating offshore renewable energy systems. Renewable Energy 97, 866-880. [Online] Available from: doi:10.1016/j.renene.2016.06.016 [Accessed 14th February 2018].

Castro-Santos, L., Martins, E., & Guedes Soares, C. (2016b) Methodology to calculate the costs of a floating offshore renewable energy farm. Energies 9 (5), 324. [Online] Available from: doi:10.3390/en9050324 [Accessed 4th March 2018].

Cerveira, F., Fonseca, N., & Pascoal, R. (2013) Mooring system influence on the efficiency of wave energy converters. International Journal of Marine Energy 3–4, 65-81. [Online] Available from: doi:10.1016/j.ijome.2013.11.006 [Accessed 12th February 2018].

Chakrabarti, S.K. (1987a) Wave force on small structures, In: Hydrodynamics of offshore structures. Dorchester, Springer-Verlag. pp. 168-231.

Chakrabarti, S.K. (1987b) Wave theories, In: Hydrodynamics of offshore structures. Dorchester, Springer-Verlag. pp. 41-85.

Cheng, Z., Yang, J., Hu, Z., & Xiao, L. (2014) Frequency/time domain modeling of a direct drive point absorber wave energy converter. Science China Physics, Mechanics and Astronomy 57 (2), 311-320. [Online] Available from: doi:10.1007/s11433-013-5200-8 [Accessed 5th January 2018].

Cho, I.H., & Kim, M.H. (2017) Hydrodynamic performance evaluation of a wave energy converter with two concentric vertical cylinders by analytic solutions and model tests. Ocean Engineering 130, 498-509. [Online] Available from: doi:10.1016/ j.oceaneng.2016.11.069 [Accessed 10th February 2018].

Combourieu, A., Lawson, M., Babarit, A.l., Ruehl, K., Roy, A., Costello, R., Weywada, P.L., & Bailey, H. (2015) Wec$^3$: Wave energy converter code comparison project. In: Proceedings of the 11th European Wave and Tidal Energy Conference (EWTEC2015), 6-11 September 2015, Nantes, France. pp. 07D01-03-01—07D01-03-10. 07D1-3.

Costello, R., & Pecher, A. (2017) Economics of WECs, In: Pecher, A., and Kofoed, J.P. (eds.) Handbook of ocean wave energy, Springer International Publishing. pp. 101-138.

Dalton, G., Allan, G., Beaumont, N., Georgakaki, A., Hacking, N., Hooper, T., Kerr, S., O'Hagan, A.M., Reilly, K., Ricci, P., Sheng, W., & Stallard, T. (2015) Economic and socio-economic assessment methods for ocean renewable energy: Public and private perspectives. Renewable and Sustainable Energy Reviews 45, 850-878. [Online] Available from: doi:10.1016/j.rser.2015.01.068 [Accessed 23rd July 2018].

Davidson, J., & Ringwood, J.V. (2017) Mathematical modelling of mooring systems for wave energy converters—a review. Energies 10 (5), 666. [Online] Available from: doi:10.3390/en10050666 [Accessed 15th February 2018].

de Andres, A., Medina-Lopez, E., Crooks, D., Roberts, O., & Jeffrey, H. (2017) On the reversed LCOE calculation: Design constraints for wave energy commercialization. International Journal of Marine Energy 18, 88-108. [Online] Available from: doi:10.1016/ j.ijome.2017.03.008 [Accessed 26th June 2018].

DNV GL (2015) Offshore standard DNVGL-OS-E301 position mooring. Høvik, DNV GL AS. [Online] Available from: https://rules.dnvgl.com/docs/pdf/dnvgl/os/2015-07/DNVGL-OS-E301.pdf [Accessed 5th February 2018].

DNV GL (2017a) Recommended practice DNVGL-RP-C205 environmental conditions and environmental loads. Høvik, DNV GL AS. [Online] Available from: https://www.dnvgl.com/oilgas/download/dnvgl-rp-c205-environmental-conditions-and-environmental-loads.html [Accessed 14th March 2018].

DNV GL (2017b) Recommended practice DNVGL-RP-F205 global performance analysis of deepwater floating structures. Høvik, DNV GL AS. [Online] Available from: http://rules.dnvgl.com/docs/pdf/dnvgl/RP/2017-06/DNVGL-RP-F205.pdf [Accessed 15th February 2018].

DNV GL (2018a) DeepC. V5.2-02 ed. Høvik, DNV GL AS. [Assessed 5th January 2018].

DNV GL (2018b) Homepage of DNV GL SESAM software. DNV GL AS. [Online] Available from: https://www.dnvgl.com/services/strength-assessment-of-offshore-structures-sesam-software-1068?gclid=Cj0KCQiA_JTUBRD4ARIsAL7_VeXZx4k-Hq97sk4PDb87JPAj5DSFf_m1shg-aJJS765Zv8LwvcAi_uEaAo1VEALw_wcB [Accessed 15th February 2018].

DNV GL (2018c) HydroD. V4.9-02 ed. Høvik, DNV GL AS. [Assessed 5th January 2018].

DNV GL (2018d) WADAM. V9.3-07 ed. Høvik, DNV GL AS. [Assessed 5th January 2018].

EC (2016) EU reference scenario 2016: Energy, transport and GHG emissions trends to 2050. Luxembourg, European Commission (EC). [Online] Available from: https://ec.europa.eu/energy/en/data-analysis/energy-modelling [Accessed 19th June 2018].

EIA (2017) International energy outlook 2017. U.S. Energy Information Administration (EIA). [Online] Available from: https://www.eia.gov/outlooks/ieo/ [Accessed 12th April 2018].

Endo, T., & Morrow, J.D. (1969) Cyclic stress-strain and fatigue behavior of representative aircraft metals. Journal of Materials, JMLSA 4 (1), 159-175.

Eugster, A. (2010) Runde meteorological station: Data report for 2005 – 2009. Runde, Runde miljøsenter. [Online] Available from: http://www.rundecentre.no/wp-content/uploads/2015/02/Runde-MetStation-2005-2009-report.pdf [Accessed 15th February 2018].

Eurostat (2018) Supply, transformation and consumption of electricity - annual data. In: Eurostat (ed) [Online] Available from: http://ec.europa.eu/eurostat/web/products-datasets/-/nrg_105a [Accessed 10th February 2018].

Falcão, A.F.d.O. (2010) Wave energy utilization: A review of the technologies. Renewable and Sustainable Energy Reviews 14 (3), 899-918. [Online] Available from: doi:10.1016/j.rser.2009.11.003 [Accessed 10th February 2018].

Falcão, A.F.O., Cândido, J.J., Justino, P.A.P., & Henriques, J.C.C. (2012) Hydrodynamics of the IPS buoy wave energy converter including the effect of non-uniform acceleration tube cross section. Renewable Energy 41, 105-114. [Online] Available from: doi:10.1016/j.renene.2011.10.005 [Accessed 22th June 2018].

Falkenberg, E., Yang, L., & Åhjem, V. (2018) The Syrope method for stiffness testing of polyester ropes. In: Proceedings of the ASME 2018 37th International Conference on Ocean, Offshore and Arctic Engineering (OMAE2018), 17-22 June 2018, Madrid, Spain. New York, NY, American Society of Mechanical Engineers. OMAE2018-77944.

Falnes, J. (2002) Wave-energy absorption by oscillating bodies, In: Ocean waves and oscillating systems: Linear interactions including wave-energy extraction. Cambridge, Cambridge University Press. pp. 196-224.

Falnes, J., & Hals, J. (2012) Heaving buoys, point absorbers and arrays. Philosophical Transactions of the Royal Society A: Mathematical, Physical and Engineering Sciences 370 (1959), 246-277. [Online] Available from: doi:10.1098/rsta.2011.0249 [Accessed 3rd March 2018].

Fevåg, L.S. (2012) Influence of marine growth on support structure design for offshore wind turbines. Thesis for MSc, Department of Civil and Transport Engineering, Norwegian University of Science and Technology, Trondheim, Norway. [Online] Available from: http://urn.kb.se/resolve?urn=urn:nbn:no:ntnu:diva-18682 [Accessed 22th June 2018].

Fitzgerald, J., & Bergdahl, L. (2007) Considering mooring cables for offshore wave energy converters. In: Proceedings of 7th European Wave Tidal Energy Conference (EWTEC2007), 11-13 September 2007, Porto, Portugal.

Fitzgerald, J., & Bergdahl, L. (2008) Including moorings in the assessment of a generic offshore wave energy converter: A frequency domain approach. Marine Structures 21 (1), 23-46. [Online] Available from: doi:10.1016/j.marstruc.2007.09.004 [Accessed 12th February 2018].

Folley, M. (2016) Numerical modelling of wave energy converters: State-of-the-art techniques for single devices and arrays. London, Academic Press.

Forestier, J.-M., Holmes, B., Barrett, S., & Lewis, A.W. (2007) Value and validation of small scale physical model tests of floating wave energy converters. In: Proceedings of the 7th European Wave and Tidal Energy Conference (EWTEC2007), 11-13 September 2007, Porto, Portugal.

Fraunhofer, & ECORYS (2017) Study on lessons for ocean energy development. Luxembourg, European Union. [Online] Available from: doi:10.2777/389418 [Accessed 11th February 2018].

Frost, C., Findlay, D., Macpherson, E., Sayer, P., & Johanning, L. (2018) A model to map levelised cost of energy for wave energy projects. Ocean Engineering 149, 438-451. [Online] Available from: doi:10.1016/j.oceaneng.2017.09.063 [Accessed 20th February 2018].

Gao, Z., & Moan, T. (2009) Mooring system analysis of multiple wave energy converters in a farm configuration. In: Proceedings of the 8th European Wave and Tidal Energy Conference (EWTEC2009), 7-10 September 2009, Uppsala, Sweden. pp. 509-518.

Gross, R., Heptonstall, P., & Blyth, W. (2007) Investment in electricity generation: The role of costs, incentives and risks. London, Imperial College Centre for Energy Policy and Technology (ICEPT) for the Technology and Policy Assessment Function of the UK Energy Research Centre. [Online] Available from: http://seg.fsu.edu/Library/Investment%20in%20Electricity%20Generation_%20The%20Role%20of%20Costs,%20Incentives,%20and%20Risks.pdf [Accessed 11th February 2018].

Hall, M., Buckham, B., & Crawford, C. (2014) Evaluating the importance of mooring line model fidelity in floating offshore wind turbine simulations. Wind Energy 17 (12), 1835-1853. [Online] Available from: doi:10.1002/we.1669 [Accessed 15th April 2018].

Hals, J., Falnes, J., & Moan, T. (2010) Constrained optimal control of a heaving buoy wave-energy converter. Journal of Offshore Mechanics and Arctic Engineering 133 (1), 011401. [Online] Available from: doi:10.1115/1.4001431 [Accessed 15th February 2018].

Harnois, V.R. (2014) Analysis of highly dynamic mooring systems: Peak mooring loads in realistic sea conditions. Thesis for Doctor of Philosophy in Renewable Energy, College of Engineering, Mathematics and Physical Sciences, University of Exeter, Exeter, UK. [Online] Available from: http://hdl.handle.net/10871/17205 [Accessed 20th February 2018].

Harris, R.E., Johanning, L., & Wolfram, J. (2004) Mooring systems for wave energy converters: A review of design issues and choices. In: Proceedings of 3rd International Conference on Marine Renewable Energy (MAREC2004), 6-9 July 2004, Blyth, UK. London, Institute of Marine Engineering, Science, and Technology. pp. 180-189.

Henderson, R. (2006) Design, simulation, and testing of a novel hydraulic power take-off system for the Pelamis wave energy converter. Renewable Energy 31 (2), 271-283. [Online] Available from: doi:10.1016/j.renene.2005.08.021 [Accessed 11th July 2018].

Holmes, B. (2009) Tank testing of wave energy conversion systems: Marine renewable energy guides. London, European Marine Energy Centre. [Online] Available from: http://www.emec.org.uk/tank-testing-of-wave-energy-conversion-systems/ [Accessed 3rd February 2018].

IEA (2017a) World energy balances: Overview. International Energy Agency (IEA). [Online] Available from: http://www.iea.org/publications/freepublications/publication/WorldEnergyBalances2017Overview.pdf [Accessed 20th February 2018].

IEA (2017b) World energy outlook 2017. International Energy Agency (IEA). [Online] Available from: https://www.iea.org/weo2017/ [Accessed 20th February 2018].

IEA, & NEA (2015) Projected costs of generating electricity 2015. France, International Energy Agency (IEA) and OECD Nuclear Energy Agency (NEA). [Online] Available from: https://webstore.iea.org/projected-costs-of-generating-electricity-2015 [Accessed 30th June 2018].

IEA-OES (2015) International levelised cost of energy for ocean energy technologies: An analysis of the development pathway and levelised cost of energy trajectories of wave, tidal, and OTEC technologies. Lisbon, International Energy Agency (IEA) - Ocean Energy Systems Technology Collaboration Programme (OES). [Online] Available from: https://www.ocean-energy-systems.org/news/international-lcoe-for-ocean-energy-technology/ [Accessed 12th February 2018].

IEA-OES (2018) OES annual report 2017. Lisbon, International Energy Agency (IEA) - Ocean Energy Systems Technology Collaboration Programme (OES). [Online] Available from: https://www.ocean-energy-systems.org/publications/annual-reports/document/oes-annual-report-2017/ [Accessed 26th June 2018].

Iglesias, G., & Carballo, R. (2014) Wave farm impact: The role of farm-to-coast distance. Renewable Energy 69, 375-385. [Online] Available from: doi:10.1016/j.renene.2014.03.059 [Accessed 15th April 2018].

IRENA (2017) Renewable capacity statistics 2017. International Renewable Energy Agency (IRENA). [Online] Available from: http://www.irena.org/publications/2017/Mar/Renewable-Capacity-Statistics-2017 [Accessed 15th April 2018].

IRENA (2018) Renewable capacity statistics 2018. International Renewable Energy Agency (IRENA). [Online] Available from: http://www.irena.org/publications/2018/Mar/Renewable-Capacity-Statistics-2018 [Accessed 15th April 2018].

Isaacson, M., & Nwogu, O. (1987) Wave loads and motions of long structures in directional seas. Journal of Offshore Mechanics and Arctic Engineering 109 (2), 126-132. [Online] Available from: doi:10.1115/1.3257000 [Accessed 15th June 2018].

ITTC (2014) ITTC – recommended guidelines: Wave energy converter model test experiments. International Towing Tank Conference (ITTC). [Online] Available from: https://ittc.info/media/4168/75-02-07-037.pdf [Accessed 3rd March 2018].

Jansson, H., & Örgård, M. (2017) Design of mooring system for point absorbing wave energy devices in an array system. Thesis for Master's degree, Department of Mechanics and Maritime Sciences, Chalmers university of Technology, Gothenburg, Sweden.

Johanning, L., Smith, G.H., & Wolfram, J. (2006) Mooring design approach for wave energy converters. Proceedings of the Institution of Mechanical Engineers, Part M: Journal of Engineering for the Maritime Environment 220 (4), 159-174. [Online] Available from: doi:10.1243/14750902JEME54 [Accessed 20th February 2018].

Johanning, L., Smith, G.H., & Wolfram, J. (2007) Measurements of static and dynamic mooring line damping and their importance for floating WEC devices. Ocean Engineering 34 (14–15), 1918-1934. [Online] Available from: doi:10.1016/j.oceaneng.2007.04.002 [Accessed 17th February 2018].

Karlsen, S. (2010) Fatigue of copper conductors for dynamic subsea power cables. In: Proceedings of the ASME 2010 29th International Conference on Ocean, Offshore and Arctic Engineering (OMAE2010), 6-11 June 2010, Shanghai, China. New York, NY, American Society of Mechanical Engineers. pp. 275-281. OMAE2010-21017.

Karlsen, S., Slora, R., Heide, K., Lund, S., Eggertsen, F., & Osborg, P.A. (2009) Dynamic deep water power cables. In: Proceedings of the 9th International Conference and Exhibition for Oil and Gas Resources Development of the Russian Arctic and CIS Continental Shelf (RAO/CIS Offshore 2009), 15-18 September 2009, Saint-Petersburg, Russia. pp. 194-203.

Kempener, R., & Neumann, F. (2014) Wave energy technology brief. International Renewable Energy Agency (IRENA). [Online] Available from: http://www.irena.org/documentdownloads/publications/wave-energy_v4_web.pdf [Accessed 5th February 2018].

Kingsbury, R.W.S.M. (1981) Marine fouling of North Sea installations. In: Marine Fouling of Offshore Structures, 19-20 May 1981, London, UK. London, Society for Underwater Technology.

Korde, U.A., Robinett, R.D., & Wilson, D.G. (2016) Wave-by-wave control in irregular waves for a wave energy converter with approximate parameters. Journal of Ocean Engineering and Marine Energy 2 (4), 501-519. [Online] Available from: doi:10.1007/s40722-016-0068-0 [Accessed 11th February 2018].

LaBonte, A., O'Connor, P., Fitzpatrick, C., Hallett, K., & Li, Y. (2013) Standardized cost and performance reporting for marine and hydrokinetic technologies. In: Proceedings of the 1st Marine Energy Technology Symposium (METS13), 10-11 April 2013, Washington, D.C., USA.

Lang, X., Yang, S.-H., Ringsberg, J.W., Johnson, E., Guedes Soares, C., & Rahm, M. (2018) Comparison between full-scale measurements and numerical simulations of mooring forces in a floating point-absorbing WEC system. In: 3rd International Conference on Renewable Energies Offshore (RENEW2018), 8-10 October 2018, Lisbon, Portugal. (Accepted for presentation)

Langhamer, O. (2012) Artificial reef effect in relation to offshore renewable energy conversion: State of the art. The Scientific World Journal 2012, 386713. [Online] Available from: doi:10.1100/2012/386713 [Accessed 3rd March 2018].

Langhamer, O., Wilhelmsson, D., & Engström, J. (2009) Artificial reef effect and fouling impacts on offshore wave power foundations and buoys – a pilot study. Estuarine, Coastal and Shelf Science 82 (3), 426-432. [Online] Available from: doi:10.1016/j.ecss.2009.02.009 [Accessed 15th February 2018].

Law, J., & Rennie, R. (2015) Interaction. In: Law, J., and Rennie, R. (eds.) A Dictionary of Physics, 7 ed. Oxford University Press. [Online] Available from: doi:10.1093/acref/9780198714743.001.0001 [Accessed 15th April 2018].

Lewis, A., Estefen, S., Huckerby, J., Lee, K.S., Musial, W., Pontes, T., & Torres-Martinez, J. (2011) Ocean energy. Cambridge, United Kingdom and New York, NY, USA, Cambridge University Press. [Online] Available from: http://srren.ipcc-wg3.de/report/IPCC_SRREN_Ch06.pdf [Accessed 15th February 2018].

Li, Y., & Yu, Y.-H. (2012) A synthesis of numerical methods for modeling wave energy converter-point absorbers. Renewable and Sustainable Energy Reviews 16 (6), 4352-4364. [Online] Available from: doi:10.1016/j.rser.2011.11.008 [Accessed 15th February 2018].

MacGillivray, A., Jeffrey, H., Hanmer, C., Magagna, D., Raventos, A., & Badcock-Broe, A. (2013) Ocean energy technology: Gaps and barriers. SI Ocean. [Online] Available from: http://www.policyandinnovationedinburgh.org/ocean-energy-technology-gaps-and-barriers.html [Accessed 24th February 2018].

Mazarakos, T.P., & Mavrakos, S.A. (2013) Wave–current interaction on a vertical truncated cylinder floating in finite-depth waters. Proceedings of the Institution of Mechanical Engineers, Part M: Journal of Engineering for the Maritime Environment 227 (3), 243-255. [Online] Available from: doi:10.1177/1475090212454096 [Accessed 17th February 2018].

McAllister, M.L., Venugopal, V., & Borthwick, A.G.L. (2017) Wave directional spreading from point field measurements. Proceedings of the Royal Society A: Mathematical, Physical & Engineering Sciences 473 (2200), 20160781. [Online] Available from: doi:10.1098/rspa.2016.0781 [Accessed 15th April 2018].

McCombes, T., Johnstone, C., Holmes, B., Myers, L.E., Bahaj, A.S., & Kofoed, J.P. (2010) Best practice for tank testing of small marine energy devices. EquiMar: Equitable testing and evaluation of marine energy extraction devices in terms of performance, cost and environmental impact. European Commission. [Online] Available from: https://www.wiki.ed.ac.uk/display/EquiMarwiki/EquiMar [Accessed 15th February 2018].

Michailides, C., Gao, Z., & Moan, T. (2016) Experimental and numerical study of the response of the offshore combined wind/wave energy concept SFC in extreme environmental conditions. Marine Structures 50, 35-54. [Online] Available from: doi:10.1016/j.marstruc.2016.06.005 [Accessed 16th April 2018].

Millar, D.L., Smith, H.C.M., & Reeve, D.E. (2007) Modelling analysis of the sensitivity of shoreline change to a wave farm. Ocean Engineering 34 (5–6), 884-901. [Online] Available from: doi:10.1016/j.oceaneng.2005.12.014 [Accessed 16th April 2018].

Moberg, G. (1988) Wave forces on a vertical slender cylinder. Thesis for Doctor of Philosophy, School of Civil Engineering, Chalmers University of Technology, Gothenburg, Sweden.

Mofor, L., Goldsmith, J., & Jones, F. (2014) Ocean energy: Technology readiness, patents, deployment status and outlook. Abu Dhabi, International Renewable Energy Agency (IRENA). [Online] Available from: http://www.irena.org/publications/2014/Aug/Ocean-Energy-Technologies-Patents-Deployment-Status-and-Outlook [Accessed 12th February 2018].

Muliawan, M.J., Gao, Z., Moan, T., & Babarit, A. (2013) Analysis of a two-body floating wave energy converter with particular focus on the effects of power take-off and mooring systems on energy capture. Journal of Offshore Mechanics and Arctic Engineering 135 (3), 031902. [Online] Available from: doi:10.1115/1.4023796 [Accessed 15th April 2018].

Nasution, F.P., Sævik, S., Gjøsteen, J.K.Ø., & Berge, S. (2013) Experimental and finite element analysis of fatigue performance of copper power conductors. International Journal of Fatigue 47, 244-258. [Online] Available from: doi:10.1016/j.ijfatigue.2012.09.006 [Accessed 15th February 2018].

NORSOK (2007) NORSOK standard N-003 actions and action effects. Lysaker, NORSOK. [Online] Available from: http://www.ivt.ntnu.no/imt/courses/tmr4195/literature/Standards%20and%20Recommendations/N-003e2.pdf [Accessed 3rd March 2018].

Ocean Energy Europe (2018) Europe needs ocean energy. Ocean Energy Europe. [Online] Available from: https://www.oceanenergy-europe.eu/ocean-energy/ [Accessed 19th June 2018].

Ocean Energy Forum (2016) Ocean energy strategic roadmap 2016, building ocean energy for Europe. Ocean Energy Forum. [Online] Available from: https://webgate.ec.europa.eu/maritimeforum/en/frontpage/1036 [Accessed 4th March 2018].

Palm, J., Eskilsson, C., & Bergdahl, L. (2017) An *hp*-adaptive discontinuous Galerkin method for modelling snap loads in mooring cables. Ocean Engineering 144, 266-276. [Online] Available from: doi:10.1016/j.oceaneng.2017.08.041 [Accessed 15th June 2018].

Palm, J., Eskilsson, C., Paredes, G.M., & Bergdahl, L. (2013) CFD simulation of a moored floating wave energy converter. In: Frigaard, P., Kofoed, J.P., Bahaj, A.S., Bergdahl, L., Clément, A., Conley, D., Falcão, A.F.O., Johnstone, C.M., Margheritini, L., Masters, I., Sarmento, A.J., and Vicinanza, D. (eds.) Proceedings of the 10th European Wave and Tidal Energy Conference (EWTEC2013), 2-5 September 2013, Aalborg, Denmark. Aalborg, European Wave and Tidal Energy Conference.

Palm, J., Eskilsson, C., Paredes, G.M., & Bergdahl, L. (2016) Coupled mooring analysis for floating wave energy converters using CFD: Formulation and validation. International Journal of Marine Energy 16, 83-99. [Online] Available from: doi:10.1016/j.ijome.2016.05.003 [Accessed 3rd February 2018].

Paredes, G.M., Bergdahl, L., Palm, J., Eskilsson, C., & Pinto, F.T. (2013) Station keeping design for floating wave energy devices compared to floating offshore oil and gas platforms. In: Frigaard, P., Kofoed, J.P., Bahaj, A.S., Bergdahl, L., Clément, A., Conley, D., Falcão, A.F.O., Johnstone, C.M., Margheritini, L., Masters, I., Sarmento, A.J., and Vicinanza, D. (eds.) Proceedings of the 10th European Wave and Tidal Energy Conference (EWTEC2013), 2013, Aalborg, Denmark. Aalborg, European Wave and Tidal Energy Conference.

Paredes, G.M., Palm, J., Eskilsson, C., Bergdahl, L., & Taveira-Pinto, F. (2016) Experimental investigation of mooring configurations for wave energy converters. International Journal of Marine Energy 15, 56-67. [Online] Available from: doi:10.1016/j.ijome.2016.04.009 [Accessed 16th February 2018].

Payne, G.S., Taylor, J.R.M., & Ingram, D. (2009) Best practice guidelines for tank testing of wave energy converters. The Journal of Ocean Technology 4 (4), 38-70. [Online] Available from: https://strathprints.strath.ac.uk/id/eprint/61396 [Accessed 16th February 2018].

Pecher, A. (2017) Experimental testing and evaluation of WECs, In: Pecher, A., and Kofoed, J.P. (eds.) Handbook of ocean wave energy, Springer International Publishing. pp. 221-260.

Piscopo, V., Benassai, G., Della Morte, R., & Scamardella, A. (2017) Towards a cost-based design of heaving point absorbers. International Journal of Marine Energy 18, 15-29. [Online] Available from: doi:10.1016/j.ijome.2017.03.005 [Accessed 22th June 2018].

Ransley, E.J. (2015) Survivability of wave energy converter and mooring coupled system using CFD. Thesis for Doctor of Philosophy, School of Marine Science and Engineering, University of Plymouth, Plymouth, UK. [Online] Available from: http://hdl.handle.net/10026.1/3503 [Accessed 22th June 2018].

REN21 (2017) Renewables 2017 global status report. Paris, Renewable Energy Policy Network for the 21st Century (REN21). [Online] Available from: http://www.ren21.net/gsr-2017/ [Accessed 15th February 2018].

Ringsberg, J.W., Jansson, H., Örgård, M., Yang, S.-H., & Johnson, E. (2018) Comparison of mooring solutions and array systems for point absorbing wave energy devices. In: Proceedings of the ASME 2018 37th International Conference on Ocean, Offshore and Arctic Engineering (OMAE2018), 17-22 June 2018, Madrid, Spain. New York, NY, American Society of Mechanical Engineers.

Sarmento, A., & Thomas, G. (2008) Guidelines for laboratory testing of WECs, In: Cruz, J. (ed.) Ocean wave energy: Current status and future perspectives. Heidelberg, Springer-Verlag. pp. 160-169.

Saruwatari, A., Ingram, D.M., & Cradden, L. (2013) Wave–current interaction effects on marine energy converters. Ocean Engineering 73, 106-118. [Online] Available from: doi:10.1016/j.oceaneng.2013.09.002 [Accessed 10th February 2018].

Seaflex (2018) Homepage of Seaflex. Seaflex AB. [Online] Available from: http://www.seaflex.net/products/seaflex-mooring-system/ [Accessed 22th May 2018].

Sheng, W., Alcorn, R., & Lewis, T. (2014) Physical modelling of wave energy converters. Ocean Engineering 84, 29-36. [Online] Available from: doi:10.1016/j.oceaneng.2014.03.019 [Accessed 10th February 2018].

SI Ocean (2012) Ocean energy: State of the art. SI Ocean. [Online] Available from: https://elearning.umj.ac.id/pluginfile.php?file=%2F10144%2Fcourse%2Foverviewfiles%2FMateri_MKE%20gelombang%20laut.pdf&amp%3Bforcedownload=1 [Accessed 12th February 2018].

SI Ocean (2013) Ocean energy: Cost of energy and cost reduction opportunities. SI Ocean. [Online] Available from: https://energiatalgud.ee/img_auth.php/1/10/SI_OCEAN._Ocean_Energy_-_Cost_of_Energy_and_Cost_Reduction._2013.pdf [Accessed 14th February 2018].

Sidenmark, M., Rashid, A., Ghodrati, A., & Hultgren, A. (2015) Modelling and simulation of a collector hub system combining core technologies. In: Proceedings of the 11th European Wave and Tidal Energy Conference (EWTEC2015), 6-11 September 2015, Nantes, France. pp. 07B04-04-01–07B04-04-10. 07B4-4.

Sims, R.E.H., Schock, R.N., Adegbululgbe, A., Fenhann, J., Konstantinaviciute, I., Moomaw, W., Nimir, H.B., Schlamadinger, B., Torres-Martínez, J., Turner, C., Uchiyama, Y., Vuori, S.J.V., Wamukonya, N., & Zhang, X. (2007) Energy supply, In: Metz, B., Davidson, O.R., Bosch, P.R., Dave, R., and Meyer, L.A. (eds.) Climate change 2007: Migration of climate change. Contribution of working group III to the fourth assessment report of the Intergovernmental Panel on Climate Change (IPCC), 2007. Cambridge, UK and New York, NY, USA, Cambridge University Press. pp. 251-322.

SINTEF Ocean (2017a) RIFLEX 4.10.3 theory manual. Trondheim, SINTEF Ocean. [Online] Available from: [Accessed 5th January 2018].

SINTEF Ocean (2017b) SIMO 4.10.3 theory manual. Trondheim, SINTEF Ocean. [Online] Available from: [Accessed 5th January 2018].

SINTEF Ocean (2018a) RIFLEX. V4.10-03 ed. Trondheim, SINTEF Ocean. [Assessed 5th January 2018].

SINTEF Ocean (2018b) SIMA. V3.4-01 ed. Trondheim, SINTEF Ocean. [Assessed 5th January 2018].

SINTEF Ocean (2018c) SIMO. V4.10-03 ed. Trondheim, SINTEF Ocean. [Assessed 5th January 2018].

SJTU (2018) State Key Laboratory of Ocean Engineering. Shanghai Jiao Tong University (SJTU). [Online] Available from: http://en.sjtu.edu.cn/research/centers-labs/state-key-laboratory-of-ocean-engineering [Accessed 20th April 2018].

The MathWorks Inc. (2016) MATLAB. R2016b ed. Natick, MA, USA, The MathWorks Inc. [Assessed 5th January, 2018].

Thies, P.R., Johanning, L., & McEvoy, P. (2014) A novel mooring tether for peak load mitigation: Initial performance and service simulation testing. International Journal of Marine Energy 7, 43-56. [Online] Available from: doi:10.1016/j.ijome.2014.06.001 [Accessed 22th May 2018].

Thies, P.R., Johanning, L., & Smith, G.H. (2011) Assessing loading regimes and failure modes of marine power cables in marine energy applications. In: Proceedings of the 19th Advances in Risk and Reliability Technology Symposium (AR2TS), 12-14 April 2011, Stratford-upon-Avon, UK. pp. 237-251.

Thies, P.R., Johanning, L., & Smith, G.H. (2012) Assessing mechanical loading regimes and fatigue life of marine power cables in marine energy applications. Proceedings of the Institution of Mechanical Engineers, Part O: Journal of Risk and Reliability 226 (1), 18-32. [Online] Available from: doi:10.1177/1748006X11413533 [Accessed 14th February 2018].

Thomsen, J.B., Ferri, F., & Kofoed, J.P. (2017) Screening of available tools for dynamic mooring analysis of wave energy converters. Energies 10 (7), 853. [Online] Available from: doi:10.3390/en10070853 [Accessed 14th February 2018].

Tiron, R., Mallon, F., Dias, F., & Reynaud, E.G. (2015) The challenging life of wave energy devices at sea: A few points to consider. Renewable and Sustainable Energy Reviews 43, 1263-1272. [Online] Available from: doi:10.1016/j.rser.2014.11.105 [Accessed 3rd March 2018].

Tiron, R., Pinck, C., Reynaud, E.G., & Dias, F. (2012) Is biofouling a critical issue for wave energy converters? In: Proceedings of the 22nd International Offshore and Polar Engineering Conference (ISOPE2012), 17-22 June 2012, Rhodes, Greece. International Society of Offshore and Polar Engineers (ISOPE). pp. 669-679. ISOPE-I-12-159.

Titah-Benbouzid, H., & Benbouzid, M. (2015) Marine renewable energy converters and biofouling: A review on impacts and prevention. In: Proceeding of the 11th European Wave and Tidal Energy Conference (EWTEC2015), 6-11 September 2015, Nantes, France. pp. 09P01-04-01–09P04-04-08. 09P1-4.

Tokat, P. (2018) Performance evaluation and life cycle cost analysis of the electrical generation unit of a wave energy converter. Thesis for Doctor of Philosophy, Department of Electrical Engineering, Chalmers University of Technology, Gothenburg, Sweden. [Online] Available from: https://research.chalmers.se/publication/500823 [Accessed 3rd April 2018].

UN (2018) Sustainable development goals. United Nations (UN). [Online] Available from: https://www.un.org/sustainabledevelopment/sustainable-development-goals/ [Accessed 20th February 2018].

Vance, C. (2018) Efficient point absorbing wave energy converter configurations: Influence of environment and array design. Thesis for Master's degree, Department of Mechanics and Maritime Sciences, Chalmers University of Technology, Gothenburg, Sweden.

Vicente, P.C., Falcão, A.F.d.O., Gato, L.M.C., & Justino, P.A.P. (2009) Dynamics of arrays of floating point-absorber wave energy converters with inter-body and bottom slack-mooring connections. Applied Ocean Research 31 (4), 267-281. [Online] Available from: doi:10.1016/j.apor.2009.09.002 [Accessed 20th February 2018].

Vicente, P.C., Falcão, A.F.O., & Justino, P.A.P. (2013) Nonlinear dynamics of a tightly moored point-absorber wave energy converter. Ocean Engineering 59, 20-36. [Online] Available from: doi:10.1016/j.oceaneng.2012.12.008 [Accessed 15th April 2018].

Vickers, A.W. (2012) Improve the understanding of uncertainties in numerical analysis of moored floating wave energy converters. Thesis for Doctor of Philosophy in Earth Resources, University of Exeter, Exeter, UK. [Online] Available from: http:// hdl.handle.net/10871/12142 [Accessed 3rd February 2018].

WAFO Group (2011) WAFO. V2.5 ed. Lund, Mathematical Statistics, Lund University. [Assessed 3rd September 2017].

Wan, L., Gao, Z., & Moan, T. (2015) Experimental and numerical study of hydrodynamic responses of a combined wind and wave energy converter concept in survival modes. Coastal Engineering 104, 151-169. [Online] Available from: doi:10.1016/ j.coastaleng.2015.07.001 [Accessed 24th February 2018].

Wang, L., Isberg, J., & Tedeschi, E. (2018) Review of control strategies for wave energy conversion systems and their validation: The wave-to-wire approach. Renewable and Sustainable Energy Reviews 81, 366-379. [Online] Available from: doi:10.1016/ j.rser.2017.06.074 [Accessed 12th February 2018].

Waves4Power (2018a) Waves4power - the solution. Waves4Power AB. [Online] Available from: https://www.waves4power.com/waves4power-the-solution/ [Accessed 22th April 2018].

Waves4Power (2018b) WaveEL: Demonstration site at Runde, Norway. Waves4Power AB. [Online] Available from: https://www.waves4power.com/demo-runde/ [Accessed 14th February 2018].

Weller, S.D., Banfield, S.J., & Canedo, J. (2018) Parameter estimation for synthetic rope models. In: Proceedings of the ASME 2018 37th International Conference on Ocean, Offshore and Arctic Engineering (OMAE2018), 17-22 June 2018, Madrid, Spain. New York, NY, American Society of Mechanical Engineers. OMAE2018-78606.

Westgate, Z.J., & DeJong, J.T. (2005) Geotechnical considerations for offshore wind turbines. [Online] Available from: https://pdfs.semanticscholar.org/25e8/f7178ed1ccd039818ca1a15406458cab12f1.pdf [Accessed 19th June 2018].

Wolgamot, H.A., & Fitzgerald, C.J. (2015) Nonlinear hydrodynamic and real fluid effects on wave energy converters. Proceedings of the Institution of Mechanical Engineers, Part A: Journal of Power and Energy 229 (7), 772-794. [Online] Available from: doi:10.1177/0957650915570351 [Accessed 22th June 2018].

Worzyk, T. (2009) Submarine power cables: Design, installation, repair, environmental aspects. Heidelberg, Springer-Verlag.

Yang, S.-H., Ringsberg, J.W., & Johnson, E. (2014) Analysis of mooring lines for wave energy converters - a comparison of de-coupled and coupled simulation procedures. In: Proceedings of the ASME 2014 33rd International Conference on Ocean, Offshore and Arctic Engineering (OMAE2014), 8-13 June 2014, San Francisco, California, USA. New York, NY, American Society of Mechanical Engineers. OMAE2014-23377.

Yr (2017) Date search for Runde, Herøy. Yr. [Online] Available from: https://www.yr.no/place/Norway/Møre_og_Romsdal/Herøy/Runde/almanakk.html?dato=2017-06-19 [Accessed 14th February 2018].

Yu, Y., & Li, Y. (2011) Preliminary results of a RANS simulation for a floating point absorber wave energy system under extreme wave conditions. In: Proceedings of the ASME 2011 30th International Conference on Ocean, Offshore and Arctic Engineering (OMAE2011), 19-24 June 2011, Rotterdam, The Netherlands. Golden, CO, National Renewable Energy Lab (NREL).